

**PALM-BASED LIQUID CRYSTALS CONTAINING SCHIFF BASE
ESTER LINKING GROUP: SYNTHESIS AND STRUCTURE-
MESOMORPHIC PROPERTIES**

LEE WENG NAM

**FACULTY OF SCIENCE
UIVERSITI MALAYA
KUALA LUMPUR
2023**

**PALM-BASED LIQUID CRYSTALS
CONTAINING SCHIFF BASE ESTER LINKING
GROUP:
SYNTHESIS AND STRUCTURE-MESOMORPHIC
PROPERTIES**

LEE WENG NAM

**THESIS SUBMITTED IN FULFILMENT OF THE
REQUIREMENTS FOR THE DEGREE OF
DOCTOR PHILOSOPHY**

**DEPARTMENT OF CHEMISTRY
FACULTY OF SCIENCE
UNIVERSITI MALAYA
KUALA LUMPUR**

2023

UNIVERSITY OF MALAYA
ORIGINAL LITERARY WORK DECLARATION

Name of Candidate: **LEE WENG NAM**

Matric No: **17043503/1**

Name of Degree: **DOCTOR OF PHILOSOPHY**

Title of Thesis (“this Work”):

PALM-BASED LIQUID CRYSTALS CONTAINING SCHIFF BASE ESTER LINKING GROUP: SYNTHESIS AND STRUCTURE-MESOMORPHIC PROPERTIES.

Field of Study: **MATERIAL CHEMISTRY**

I do solemnly and sincerely declare that:

- (1) I am the sole author/writer of this Work;
- (2) This Work is original;
- (3) Any use of any work in which copyright exists was done by way of fair dealing and for permitted purposes and any excerpt or extract from, or reference to or reproduction of any copyright work has been disclosed expressly and sufficiently and the title of the Work and its authorship have been acknowledged in this Work;
- (4) I do not have any actual knowledge nor do I ought reasonably to know that the making of this work constitutes an infringement of any copyright work;
- (5) I hereby assign all and every rights in the copyright to this Work to the University of Malaya (“UM”), who henceforth shall be owner of the copyright in this Work and that any reproduction or use in any form or by any means whatsoever is prohibited without the written consent of UM having been first had and obtained;
- (6) I am fully aware that if in the course of making this Work I have infringed any copyright whether intentionally or otherwise, I may be subject to legal action or any other action as may be determined by UM.

Candidate’s Signature

Date: 21 Mac 2023

Subscribed and solemnly declared before,

Witness’s Signature

Date: 21 Mac 2023

Name:

Designation:

**PALM-BASED LIQUID CRYSTALS CONTAINING SCHIFF BASE ESTER
LINKING GROUP: SYNTHESIS AND STRUCTURE-MESOMORPHIC
PROPERTIES**

ABSTRACT

In the present study, one of the five basic building blocks of oleochemicals, palm fatty acid, was chosen as flexible moiety in the synthesis of liquid crystals (LCs) due to its good reactivity for chemical modifications and non-toxicity. Three new series of palm-based liquid crystals (PBLCs), namely, **PB1 – PB3**, **PB4 – PB6** and **PB7 – PB9** consisting of Schiff base ester-based mesogenic core have been successfully synthesized. The chemical structure of all synthesized PBLCs was characterized and confirmed by Fourier Transform Infrared Spectroscopy (FT-IR), ¹H and ¹³C Nuclear Magnetic Resonance (NMR). Polarizing Optical Microscopy (POM) revealed that the synthesized PBLCs were monomorphic and enantiotropic in nature exhibiting only smectic A phase upon heating and cooling except for **PB9** in which smectic A phase can only be seen in the cooling cycle (monotropic). The phase transition temperatures observed under POM were found to be in good agreement with the Differential Scanning Calorimetry (DSC) thermograms obtained. The mesophase texture of smectic A phase was further verified by Small Angle X-ray Scattering (SAXS). The presence of a three-ring Schiff base ester-based mesogenic core with a terminal bromo group within the series of **PB1 – PB3** has led to higher molecular linearity and polarizability which eventually resulted in a stable mesophase range. As for the unsubstituted analogues of **PB4 – PB6** series, the mesophase range was found to be narrower due to lower molecular polarizability with the absence of bromo group as terminal substituent. **PB7 – PB9** series is composed of a mesogenic core with one less phenyl ring and an ester group. Therefore, owing to its lower molecular linearity and polarizability, **PB7 – PB9** exhibited the least stable smectic A phase. As far as thermal stability is concerned, all synthesized PBLCs were found to be thermally stable above

300°C except for **PB3** (decomposed with 5% weight loss at 281.66°C), **PB4** and **PB5** (decomposed with 5% weight loss at 201°C).

Keywords: Flexible alkyl chain, palm fatty acids, Schiff base, smectic, green chemistry.

Universiti Malaya

**HABLUR CECAIR BERASASKAN MINYAK SAWIT YANG TERDIRI
DARIPADA ESTER ASAS SCHIFF BASE: SINTESIS DAN SIFAT
MESOMORFIK STRUKTUR**

ABSTRAK

Dalam kajian ini, salah satu daripada lima bahan oleokimia asas asid lemak dari minyak sawit, telah dipilih sebagai rantaian fleksibel dalam sintesis hablur cecair disebabkan oleh kereaktifannya yang baik untuk pengubahsuaian kimia dan tidak beracun. Tiga siri hablur cecair berasaskan minyak sawit (PBLC), iaitu, **PB1 – PB3**, **PB4 – PB6** dan **PB7 – PB9** yang terdiri daripada teras mesogenik berasaskan ester asas Schiff telah berjaya disintesis. Struktur kimia semua PBLC yang disintesis telah disahkan melalui teknik spektroskopi seperti spektroskopi inframerah transformasi Fourier (FT-IR), resonans magnetik nuklear ^1H dan ^{13}C (NMR) dan analisis unsur. Mikroskop optik berkutub (POM) menunjukkan bahawa semua PBLC bersifat monomorfik dan enantiotropik, iaitu hanya mempamerkan mesofasa smektik A semasa pemanasan dan penyejukan kecuali **PB9** di mana mesofasa smektik A hanya dapat dilihat dalam kitaran penyejukan (monotropik). Suhu peralihan fasa yang diperhatikan di bawah POM didapati selaras dengan termogram kalorimetri imbasan perbezaan (DSC). Tekstur mesofasa smektik A disahkan lagi dengan menggunakan serakan sinar-X bersudut kecil (SAXS). Kehadiran teras mesogenik berasaskan ester asas Schiff dengan tiga cincin fenil dan kumpulan bromo terminal dalam siri **PB1 – PB3** telah membawa kepada kelinearan dan kebolehpolaran molekul yang lebih tinggi yang menghasilkan mesofasa yang stabil. Bagi analog yang tiada kumpulan penukarganti iaitu siri **PB4 – PB6**, julat mesofasa didapati lebih sempit kerana kebolehpolaran molekul yang lebih rendah dengan ketiadaan kumpulan bromo terminal. Siri **PB7 – PB9** terdiri daripada teras mesogenik dengan hanya dua cincin fenil dan kekurangan satu kumpulan ester. Oleh itu, kelinearan dan kebolehpolaran molekulnya adalah dijangka lebih rendah. Disebabkan ini, **PB7 – PB9**

menunjukkan fasa smektik A yang kurang stabil. Berdasarkan kestabilan terma, semua PBLC yang telah disintesis didapati stabil secara terma melebihi 300°C kecuali **PB3** (kehilangan berat sebanyak 5% pada 281.66°C), **PB4** dan **PB5** (kehilangan berat sebanyak 5% pada 201°C).

Kata kunci: Rantai alkil fleksibel acid lemak, asas Schiff, smektik, kimia hijau.

Universiti Malaya

ACKNOWLEDGEMENT

First and foremost, I would like to express my sincere gratitude to my supervisors, Associate Professor Dr. Cheng Sit Foon and Dr. Noordini binti Mohamad Salleh, for giving me the opportunity to conduct this research and providing invaluable guidance throughout the study. They have taught me the methodology to carry out the research and to present the research works as clearly as possible. Their vision and motivations have deeply inspired me. It was a great privilege and honour to work and study under my supervisors.

Next, I am very thankful to my wife and my family for their understanding, love and continuing support to complete my research work. Also, I would like to thank Dr. Noor Idayu, Mr. Fateh, Ms. Fiona, Ms. Lela and Ms. Azlin for their technical lab support and constructive comments.

Finally, I would like to thank the Department of Chemistry, Universiti Malaya and Heriot-Watt University Malaysia for providing me with a conducive environment in conducting my research.

TABLE OF CONTENTS

ORIGINAL LITERACY WORK DECLARATION	ii
ABSTRACT	iii
ABSTRAK	v
ACKNOWLEDGEMENT	vii
TABLE OF CONTENTS	viii
LIST OF FIGURES	xi
LIST OF TABLES	xv
LIST OF SCHEMES	xvi
LIST OF SYMBOLS AND ABBREVIATIONS	xvii
LIST OF APPENDICES	xviii
CHAPTER 1: INTRODUCTION	1
1.1 Background of study	1
1.2 Motivation and research objectives	5
1.3 Thesis outline	6
CHAPTER 2: LITERATURE REVIEW	7
2.1 Liquid crystal	7
2.2 Classification of liquid crystals	8
2.3 Calamitic liquid crystals	10
2.3.1 Nematic phase	12
2.3.2 Smectic phase	13
2.4 Synthesis approach of liquid crystals	15
2.4.1 Condensation	16
2.4.2 Azo coupling	17
2.4.3 Esterification	18

2.5	Schiff base liquid crystals	20
2.6	Schiff base ester-based liquid crystals	23
2.7	Structure-mesomorphic properties relationship	25
2.7.1	Structure of mesogenic core unit	26
2.7.2	Compact terminal substituent	30
2.7.3	Flexible alkyl chain length	33
2.8	Applications of liquid crystals	37
CHAPTER 3: METHODOLOGY		40
3.1	Materials	40
3.2	Synthesis of palm-based liquid crystals	40
3.2.1	Synthesis of Schiff base	41
3.2.2	Synthesis of palm-based spacer	42
3.2.3	Synthesis of PB1-PB3	45
3.2.4	Synthesis of PB4-PB6	48
3.2.5	Synthesis of PB7-PB9	51
3.3	Characterization and instrumentation	54
3.3.1	Fourier Transform Infrared Spectroscopy (FT-IR)	54
3.3.2	Nuclear Magnetic Resonance (NMR)	55
3.3.3	CHN Elemental Analysis	55
3.3.4	Differential Scanning Calorimetry (DSC)	55
3.3.5	Polarized Optical Microscopy (POM)	55
3.3.6	Small Angle X-ray Scattering (SAXS)	56
3.3.7	Thermogravimetric Analysis (TGA)	56
CHAPTER 4: RESULTS AND DISCUSSION		57
4.1	Design of palm-based liquid crystals	57
4.2	Synthesis of palm-based liquid crystals	60

4.3	Structural determination	67
4.3.1	Fourier Transform Infrared spectroscopy (FT-IR)	67
4.3.2	¹ H NMR spectra	69
4.3.3	¹³ C NMR spectra	74
4.4	Thermal degradation of palm-based liquid crystals	77
4.5	Mesomorphic behaviour of palm-based liquid crystals	83
4.6	Structure-mesomorphic property of palm-based liquid crystals	97
4.6.1	Effect of flexible palm fatty acid chain	99
4.6.2	Effect of compact terminal substituent	101
4.6.3	Effect of mesogenic core	102
4.7	Potential applications of palm-based liquid crystals	108
CHAPTER 5: CONCLUSIONS AND FUTURE STUDIES		110
5.1	Conclusions	110
5.2	Future studies	113
REFERENCES		115
LIST OF PUBLICATIONS AND PAPERS PRESENTED		136
LIST OF APPENDICES		137

LIST OF FIGURES

Figure 2.1	: Molecular ordering of solid crystal, liquid crystal and isotropic liquid.....	8
Figure 2.2	: The classification of liquid crystals.....	10
Figure 2.3	: General structure of calamitic liquid crystal molecule.....	11
Figure 2.4	: Schematic representation of molecular order in nematic phase and isotropic liquid.....	13
Figure 2.5	: POM image of thread-like texture of nematic phase (Andrienko, 2018).....	13
Figure 2.6	: Schematic representation of molecular order in Smectic A and Smectic C phases.....	14
Figure 2.7	: POM textures of (a) focal-conic fan texture of SmA phase (Cook <i>et al.</i> , 2012b) (b) schlieren texture of SmC phase (Majumdar <i>et al.</i> , 2006).....	15
Figure 2.8	: The mechanism of condensation reaction between aromatics amines and aldehydes derivatives.....	17
Figure 2.9	: The mechanism of diazotization and azo coupling reactions.....	18
Figure 2.10	: The mechanism of Steglich esterification (Xu <i>et al.</i> , 2005).....	19
Figure 2.11	: The mechanism of esterification using thionyl chloride as activating agent.....	19
Figure 2.12	: Liquid crystal compounds containing [1,2,3]-triazole ring (Wang <i>et al.</i> , 2019).....	27
Figure 2.13	: A series of liquid crystal compounds with 1,2,4-oxadiazole as part of mesogenic core (Ali & Tomi, 2018).....	28
Figure 2.14	: Liquid crystal compounds containing different mesogenic core (Yang <i>et al.</i> , 2018).....	29
Figure 2.15	: Molecular structure of 4-[[pyridine-4-yl)methylidene]amino]phenyl-4-alkoxy-benzoates (Ong <i>et al.</i> , 2018).....	30
Figure 2.16	: A series of three-ring Schiff base-ester based liquid crystal molecules with variations in alkoxy chain length and terminal substituents (Hagar <i>et al.</i> , 2018).....	31

Figure 2.17	: A series four-ring azo ester-based liquid crystal molecules with variations in alkoxy chain length and terminal substituents (Saad <i>et al.</i> , 2019).....	32
Figure 2.18	: A series of three-ring azo ester-based liquid crystal molecules with different terminal substituents (Sardon <i>et al.</i> , 2021).....	33
Figure 2.19	: A series of heterocyclic Schiff base ester-based liquid crystal molecules with different alkanoyloxy chain length (Chong <i>et al.</i> , 2016).....	34
Figure 2.20	: A series of laterally substituted ester-based liquid crystal molecule with different alkoxy chain length (Seou <i>et al.</i> , 2017).....	35
Figure 2.21	: A series of Schiff base ester-based liquid crystal molecule with dialkoxy chain at both terminal with different chain length (Ahmad <i>et al.</i> , 2019b).....	36
Figure 4.1	: The mechanism of condensation reaction between 4-hydroxybenzaldehydes and aniline forming Schiff base linked mesogenic core.....	61
Figure 4.2	: The mechanism for the activation of lauric acid using oxalyl chloride.....	63
Figure 4.3	: The mechanism for the activation of lauric-based spacer using oxalyl chloride.....	64
Figure 4.4	: The mechanism for the esterification between activated lauric acid and compound 1	65
Figure 4.5	: The mechanism for the esterification between activated lauric acid and 4-hydroxybenzoic acid.....	66
Figure 4.6	: The mechanism for the esterification between activated lauric-based spacer and compound 1	67
Figure 4.7	: FT-IR spectra of (a) compound 1 , (b) lauric based spacer, (c) PB1	69
Figure 4.8	: ¹ H NMR spectrum of compound 1	70
Figure 4.9	: ¹ H NMR spectrum of compound 2	70
Figure 4.10	: ¹ H NMR spectrum of lauric-based spacer.....	71
Figure 4.11	: ¹ H NMR spectrum for PB1	72
Figure 4.12	: ¹ H NMR spectrum for PB4	73

Figure 4.13	:	^1H NMR spectrum for PB7	74
Figure 4.14	:	^{13}C NMR spectrum for PB1	75
Figure 4.15	:	^{13}C NMR spectrum for PB4	76
Figure 4.16	:	^{13}C NMR spectrum for PB7	77
Figure 4.17	:	TGA scans for PBLCs.....	78
Figure 4.18	:	DTG curves for PBLCs.....	79
Figure 4.19	:	DSC thermograms for PBLCs.....	86
Figure 4.20	:	POM textures of PB2 upon cooling: (a) smectic A phase with focal conic fan-shaped and homeotropic textures at 201°C, (b) smectic A with focal conic fan-shaped texture at 196°C, (c) transition from smectic A phase to crystalline structure of smectic A at 90°C, (d) crystalline structure of smectic A at 85°C.....	88
Figure 4.21	:	POM textures of PB1 upon heating: focal conic fan-shaped of smectic A phase at (a) 254°C, (b) 224°C.....	89
Figure 4.22	:	POM textures of PB3 upon cooling: (a) focal conic fan-shaped of smectic A phase at 203°C, (b) crystalline structure of smectic A phase at 50°C.....	89
Figure 4.23	:	POM textures of PB5 upon cooling: (a) batonnets at 147°C, (b) smectic A with focal conic fan-shaped at 138°C, (c) crystalline structure of smectic A at 97°C, (d) crystalline structure of smectic A at 86°C.....	90
Figure 4.24	:	POM textures of PB4 upon cooling: smectic droplets at (a) 162°C, (b) 224°C.....	91
Figure 4.25	:	POM textures of PB6 upon cooling: (a) focal conic fan-shaped of smectic A phase at 144°C, (b) crystalline structure of smectic A phase at 75°C.....	91
Figure 4.26	:	POM textures upon cooling: (a) focal conic fan-shaped of PB7 at 101°C, (b) transition of smectic A phase to crystalline structure of PB7 at 90°C, (c) focal conic fan-shaped of PB8 at 90°C, (d) focal conic fan-shaped of PB9 at 104°C.....	94
Figure 4.27	:	SAXS pattern of PB1 – PB3 at 180°C confirming smectic A phase.....	95
Figure 4.28	:	Schematic representation of singular molecular layers and bilayer structure.....	96

Figure 4.29	: Chemical structures, phase transition temperatures and mesophase range of PBLCs.....	98
Figure 4.30	: Plot of transition temperatures of PB1 – PB3 against the number of carbon atoms in flexible alkyl chain during the heating cycle.....	100

Universiti Malaya

LIST OF TABLES

Table 4.1	: Molecular structure and percentage yield of PBLCs.....	59
Table 4.2	: TGA data for PBLCs.....	82
Table 4.3	: Phase transition temperatures and associated enthalpy changes of PBLCs on heating and cooling runs at a scan of $10^{\circ}\text{C min}^{-1}$ by DSC. The phase identity was determined from POM.....	84
Table 4.4	: Layer spacing and estimated molecular length of PBLCs.....	96
Table 4.5	: Polarizability value for PBLCs calculated from ACD/Chemsketch software.....	102
Table 4.6	: Mesomorphic data of structurally related compounds.....	107

LIST OF SCHEMES

Scheme 3.1	: Synthetic route of compound 1 and 2	41
Scheme 3.2	: Synthetic route of palm-based spacer.....	43
Scheme 3.3	: Synthetic route for PB1 – PB3	45
Scheme 3.4	: Synthetic route for PB4 – PB6	49
Scheme 3.5	: Synthetic route for PB7 – PB9	52

Universiti Malaya

LIST OF SYMBOLS AND ABBREVIATIONS

<i>ATR</i>	:	Attenuated Total Reflectance
<i>CDCl₃</i>	:	Deuterated chloroform
<i>DCC</i>	:	Dicyclohexylcarbodiimide
<i>DCU</i>	:	Dicyclohexylurea
<i>DMAP</i>	:	Dimethylaminopyridine
<i>DMF</i>	:	Dimethylformamide
<i>DMSO-d₆</i>	:	Deuterated dimethyl sulfoxide
<i>DSC</i>	:	Differential Scanning Calorimetry
<i>DTG</i>	:	Derivative Thermogravimetric
<i>FT-IR</i>	:	Fourier Transform Infrared Spectroscopy
<i>LC</i>	:	Liquid crystal
<i>NMR</i>	:	Nuclear Magnetic Resonance Spectroscopy
<i>PBLCs</i>	:	Palm-based liquid crystals
<i>POM</i>	:	Polarizing Optical Microscopy
<i>SAXS</i>	:	Small Angle X-ray Scattering
<i>THF</i>	:	Tetrahydrofuran
<i>T_d 5%</i>	:	Thermal decomposition temperature correspond to 5 % weight loss
<i>T_d 50%</i>	:	Thermal decomposition temperature correspond to 50 % weight loss
<i>TGA</i>	:	Thermogravimetric Analysis

LIST OF APPENDICES

Appendix A	: FT-IR Figures.....	41
Appendix B	: ^1H NMR Figures.....	43
Appendix C	: ^{13}C NMR Figures.....	45
Appendix D	: SAXS Figures.....	49

Universiti Malaya

CHAPTER 1: INTRODUCTION

1.1 Background of study

The research and development on downstream activities of palm oil industry is established based on a three-pronged approach, one of which is to add value to palm oil by expanding its application in various uses. About 72.27 million tonnes of palm oil being produced in year 2020 and 80% was utilized in food industry as cooking oil, margarine, vitamins and supplements (Mat Dian, 2018), while the remaining 20% has been diversified in non-food applications such as surfactants, polyurethanes, polyols, lubricants, biofuel, cosmetics and pharmaceutical products (Adam *et al.*, 2020; Aguiéiras *et al.*, 2019; Aziz *et al.*, 2014; Kalustian, 1985). Being successfully used commercially even in non-food application, palm oil has been proven as an economical and a versatile raw material. The potential of palm oil and palm oil products are enormous and worthy of further scientific investigation. Besides being in-line with the effort of exploring new applications for palm oil, the application of palm oil for value-added downstream products also fulfils one of the 12 principles of green chemistry by incorporating renewable feedstocks in organic synthesis due to its non-toxicity and abundance.

Liquid crystal-based technology is a valuable and an emerging research field following the discovery of materials with 'double melting points' made by Friedrich Reinitzer in year 1888 (Reinitzer, 1888). Liquid crystals (LCs) are materials that composed of unique characteristics between crystalline solid and isotropic liquid such as the ability to flow like a liquid while maintaining certain molecular orientation (Ganicz & Stańczyk, 2009). This distinctive state of matter is commonly known as mesophase. By virtue of the fluidity, rotational and translational periodicity of mesophase, LC materials are readily stimulated by temperature, electrical and magnetic fields, lights, mechanical shear,

pressure and chemical analytes into different molecular arrangements (Esteves *et al.*, 2020; Selvarasu & Kannan, 2016). On that account, synthesis of LC materials has been established as a centre of attention for various fields of research other than information displays. These include optoelectronics, photovoltaic materials, semiconductors, organic electronics and sensing technologies (Cook *et al.*, 2012a; Gao *et al.*, 2012; Gupta *et al.*, 2016; Luan *et al.*, 2020; Setia *et al.*, 2016). The mesophase behaviour of LC materials is highly dependent on its molecular architecture. Therefore, the fundamental approach to systematically design LC materials for specific applications is the appropriate selection of rigid mesogenic core with suitable linking group (Goodby, 2017; Karuppusamy *et al.*, 2017; Yuksel *et al.*, 2007) along with other chemical moieties such as compact terminal substituents (Ahmed *et al.*, 2018; Tiong *et al.*, 2010) and flexible alkyl chain (Chen *et al.*, 2010; Hu *et al.*, 2012; Muniprasad *et al.*, 2012).

There are vast variety of mesogenic core structures with various linking groups to consider depending on the required type of mesophase as well as its stability, out of which 1,4-disubstituted aromatic rings with either azo or Schiff base linking group are the most commonly employed core structure in LC synthesis. The utilization of 1,4-disubstituted aromatic rings as core is widespread as it promotes linearity which is one of the noteworthy features to ease the formation of mesophase (Goodby, 2011). Much effort has been done in synthesizing LC materials with azo group due to their encouraging optical and thermal properties (Kamal *et al.*, 2021; Karim *et al.*, 2014; Selvarasu & Kannan, 2017; Thakor *et al.*, 2021). Nevertheless, the presence of Schiff base linking group has devoted significant attention owing to the fact that it enhances mesophase stability and the ease of synthesis as compared to azo linked LC compounds (Hagar *et al.*, 2018; Sastry *et al.*, 2016). In addition to Schiff base group, ester linkage appeared to be another promising linking group in LC due to its polarizable nature of the carbonyl group which in turn elevates overall molecular polarizability and promotes relatively stable mesophase

(Collings, 1997). Hence, it is convinced that the combination of Schiff base and ester groups as central linkages could lead to the formation LC with stable and wider mesophase range (Mohiuddin *et al.*, 2017).

It is unquestionable that the formation of stable mesophase is highly dependent on the polarizability of the LC molecules. Therefore, the incorporation of terminal substituent in the mesogenic core could potentially be an effective way to obtain a specific type of mesophase for targeted applications (Dixit & Intwala, 2016). The polarity of different terminal substituents is acknowledged to either enhance or suppress liquid crystallinity. For instance, polar substituents such as halogens with strong dipole moment are able to increase molecular polarizability and hence stronger intermolecular attraction which in return stabilize molecular orientation in the mesophase (Hagar *et al.*, 2019c; Sardon *et al.*, 2021). In spite of that, research show that among halogens, the one with larger atomic radius tends to be polarized at ease due to their valence electrons are not strongly held to the nucleus (Yeap *et al.*, 2006a). Furthermore, owing to the fact that highly asymmetrical molecules favour the formation of wider mesophase range (Mieczkowski *et al.*, 2003), halogens with greater atomic radii are capable of promoting steric hindrance which make asymmetrical characteristic of the mesogenic core system more intense. Interestingly, some studies reported the opposite trend wherein fluoro terminated mesogenic core exhibited higher mesophase stability as compared to chloro and bromo groups (Karim *et al.*, 2016). Therefore, the effect of terminal polar substituent on mesophase behaviour is worthy of research attention owing to the inconclusive findings in the literature so far.

In the attempt of enhancing accessibility to LC phase, the balance between the flexible unit and the rigid mesogenic core of a LC molecule is undeniably important. Microphase segregation between these incompatible portions of the molecule would result in various types of mesophase (Yuvaraj *et al.*, 2021). Thus, in order to acquire knowledge in designing a chemical compound with specific mesophase and functionality, it is crucial

to study the effect of flexible alkyl chain length on mesophase behaviour. A considerable number of studies have shown that varying the length of flexible alkyl chain in LC materials would have a twofold effect. First, with increasing alkyl chain length, it gives rise to an increase in anisotropic properties of a LC molecule which subsequently enhances mesophase stability. Second, when the alkyl chain length increases, it tends to dilute the rigidity of the mesogenic core and consequently a shorter mesophase range is expected (Luo *et al.*, 2017; Srinivasa, 2019). In extension to this, the flexible alkyl chain length was found to exhibit prominent odd-even effect on mesophase behaviour. Even number of carbon atoms in the flexible alkyl chain tends to induce stronger intermolecular forces between LC molecules due to higher linearity of molecular conformation as compared to odd number of carbons (Chong *et al.*, 2016).

In adding value to LCs as functional materials that potentially solve technological challenges such as maintaining mesomorphic character over a broad range of working temperatures, faster switching time, optical rotational power near ambient temperature and mesophase type, a more sustainable synthesis approach by using renewable resources as building blocks rather than exhausting our limited and non-renewable petroleum resources, is much desirable. In material science, it is not uncommon that renewable resources like cholesterol being used as chemical feedstock for the synthesis of functional LCs (Hu *et al.*, 2003; Marcelis *et al.*, 2003; Yeap *et al.*, 2004). However, the utilization of palm fatty acids in the synthesis LC materials remains unexplored and scarcely discussed in the literature.

1.2 Motivation and research objectives

The functionality of LCs covers a wide range of applications, which is undoubtedly depends on their unique characteristics of mesophase. As mentioned in Section 1.1, the mesophase behaviour of a LC molecule can be enhanced by altering its chemical moieties such as the rigid mesogenic core structure, linking groups, length of flexible alkyl chain (including odd-even effect) as well as its compact terminal substituent. Moreover, in line with an increasing demand for a renewable and non-toxic raw material in organic synthesis, it is vital to explore greener alternatives for a better sustainability in the field of LCs. Palm fatty acids are natural occurring carboxylic acids from palm oil that consist of an even number of medium to long unbranched (from 8 carbons onwards) and flexible aliphatic carbon chain, thus making it a safer alternative to non-renewable petrochemicals as the flexible unit in LC molecule.

Based on the above considerations, this research work attempted to synthesize 3 series of Schiff base ester-based LC molecules with palm fatty acids as flexible alkyl chain. In order to study the structure-mesomorphic property relationship, these palm-based liquid crystals (PBLCs) were designed in such a way that they differ in terms of mesogenic core structure (2 or 3 aromatic rings), flexible alkyl chain length (lauric acid (C12), palmitic acid (C16) and stearic acid (C18)) and terminal substituent on the mesogenic core (-Br substituent or the unsubstituted analogues). Despite the fact that Schiff base ester-based LCs have been widely studied but the exploitation of palm fatty acids as flexible alkyl chain has not been reported widely in the literature.

Following the motivation stated above, the research objectives can be summarized as:

1. To synthesize three (3) series of palm-based LCs (PBLCs) containing Schiff base ester as linking group and fatty acids from palm oil, namely, lauric acid, palmitic acid and stearic acid as the flexible alkyl chain

2. To characterize the synthesized PBLCs using Fourier Transform Infra-Red spectroscopy (FT-IR), Nuclear Magnetic Resonance spectroscopy (NMR), Differential Scanning Calorimetry (DSC), Polarized Optical Microscopy (POM), Small Angle X-ray Scattering (SAXS) and Thermal Gravimetric Analysis (TGA)
3. To investigate the effect of mesogenic core structure, terminal substituent and flexible alkyl chain length on mesophase behaviour.

1.3 Thesis outline

This thesis is composed of five (5) chapters. Chapter 1 (Introduction) presents the background of study, motivation and research objectives. Review of relevant literature such as types of liquid crystals (LCs), types of mesophases and synthesis approach are presented in Chapter 2 (Literature Review). Chapter 3 (Methodology) consists of material preparations, experimental procedures for the synthesis of palm-based liquid crystals and characterization methods using suitable instruments. Chapter 4 (Results and Discussion) provides the results and discussion on synthesis approach, structural characterization which includes assignment of peaks from FT-IR, ^1H and ^{13}C NMR spectroscopies, thermal stability, structure-mesomorphic property relationship and dielectric properties of PBLCs. Last but not least, Chapter 5 (Conclusion and Future Studies) presents the conclusion derived from the research findings and proposes future studies to fill gaps in the present work.

CHAPTER 2: LITERATURE REVIEW

2.1 Liquid crystals

Following the unusual state of matter discovered by Reinitzer in 1888 wherein a material exhibits the ability to diffuse freely like a liquid while maintaining some characteristic features of solid crystalline (Stephen & Straley, 1974), a term 'liquid crystals' was introduced and used by Lehmann to denote this interesting new phase (Stegemeyer, 1989). Molecules that arranged in a long-range positional order and repeated periodically throughout the entire system is certainly observed in solid crystalline state. As temperature increases, the kinetic energy of the molecules is expected to rise causing the loss of some positional orders due to more vigorous movements, while retaining the full orientational order of molecules. This signifies an intermediate state between the anisotropic solid and the isotropic liquid, known as liquid crystals (LCs) (An *et al.*, 2016). Molecules in an isotropic liquid state, however, have gained sufficient amount of energy to break free from any positional and orientational orders which allow them to disperse randomly in all directions and promote fluidity (Kumar, 2014). The molecular ordering of solid crystal, liquid crystal and isotropic liquid is illustrated in Figure 2.1.

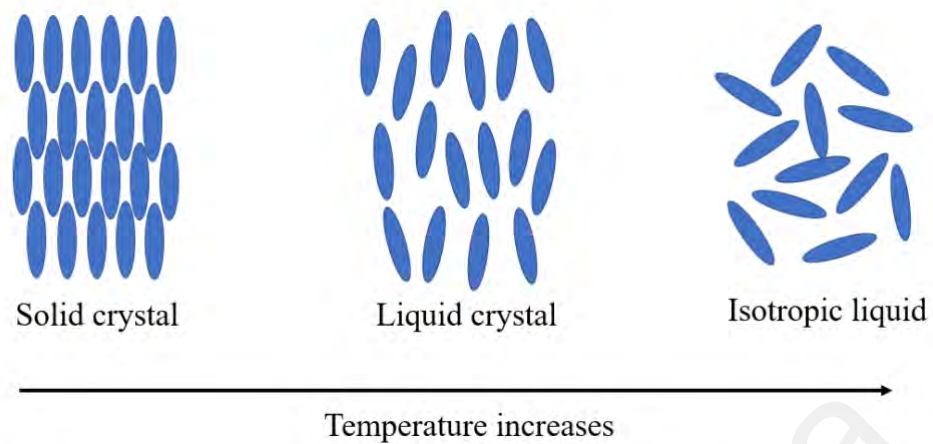


Figure 2.1: Molecular ordering of solid crystal, liquid crystal and isotropic liquid

Owing to their intermediate nature, LCs are also known as mesophase wherein the prefix “meso” originates from a Greek word “mesos” which denotes middle or intermediate (Meier, 1975). The existence of orientation order coupled with the typical thin and long molecular shape, LCs tend to arrange in order but not as rigid as solid crystalline, which consequently manifest the anisotropic properties. Therefore, LCs exhibit unique optical and mechanical properties that are incomparable with those in solid and liquid states. Furthermore, with certain degree of flexibility in molecular movement and the ability to flow, LCs are highly responsive to external stimuli such as temperature, pressure, lights, electrical and magnetic fields which could result in molecular orientation changes and thus showing a vast variety of LC phases (Dierking, 2018). This has led to the formation of the basis for the classification of LCs.

2.2 Classification of liquid crystals

Generally, an organized method for classification of liquid crystals (LCs) has been adopted. Sequentially, LCs are classified according to (i) how a mesophase is obtained; (ii) whether it is a high or low molecular mass LC molecule; and finally (iii) the molecular shape.

The formation of mesophases can be manipulated by temperature or concentration of a solvent at a particular temperature. The former is classified as thermotropic LCs whereas the latter is known as lyotropic LCs (Garidel *et al.*, 2015). In order to access lyotropic LC phases, amphiphilic molecules are dissolved in a solvent forming a solution at a fixed temperature. Different mesophases can be acquired by varying the concentration of the mixture or adding different types of solvents (Bubnov *et al.*, 2013). On the other hand, thermotropic LC molecules demonstrate mesophase within the range of temperature between the melting point and the clearing point (Popov *et al.*, 2017). Melting point is the temperature at which solid crystalline transits into mesophase whereas clearing temperature denotes the onset temperature of mesophase dissolving into an isotropic liquid. A LC molecule is classified as enantiotropic when mesophase is observed during both heating and cooling processes. While on the contrary, it will be determined as monotropic in nature if mesophase is observed only during the cooling cycle (Niezgoda *et al.*, 2014).

In comparison, thermotropic LC materials are deemed more practical from the point of application as their mesophase as a function of temperature without the need of solvent (Fleischmann & Zentel, 2013; Petsch *et al.*, 2014; Popov *et al.*, 2018). Therefore, only thermotropic LC materials will be further discussed in this thesis.

Thermotropic LC molecules can be subdivided into two categories based on molecular mass. High molecular mass LC molecules are known as LC polymers whereas LC materials with low molecular mass are further classified by their molecular shape, into three main types, namely, calamitic LCs, discotic LCs and bent-shaped LCs (Chandrasekhar *et al.*, 1977; Goodby, 1998; Niori *et al.*, 1996). Manipulating the architecture of each molecular shape could result in different mesophases such as nematic and smectic phases. Nematic phase refers to a molecular arrangement with only long range orientational order whereas smectic phase exhibits both orientational and positional

order. Figure 2.2 shows the classification of LCs according to the aforementioned classification.

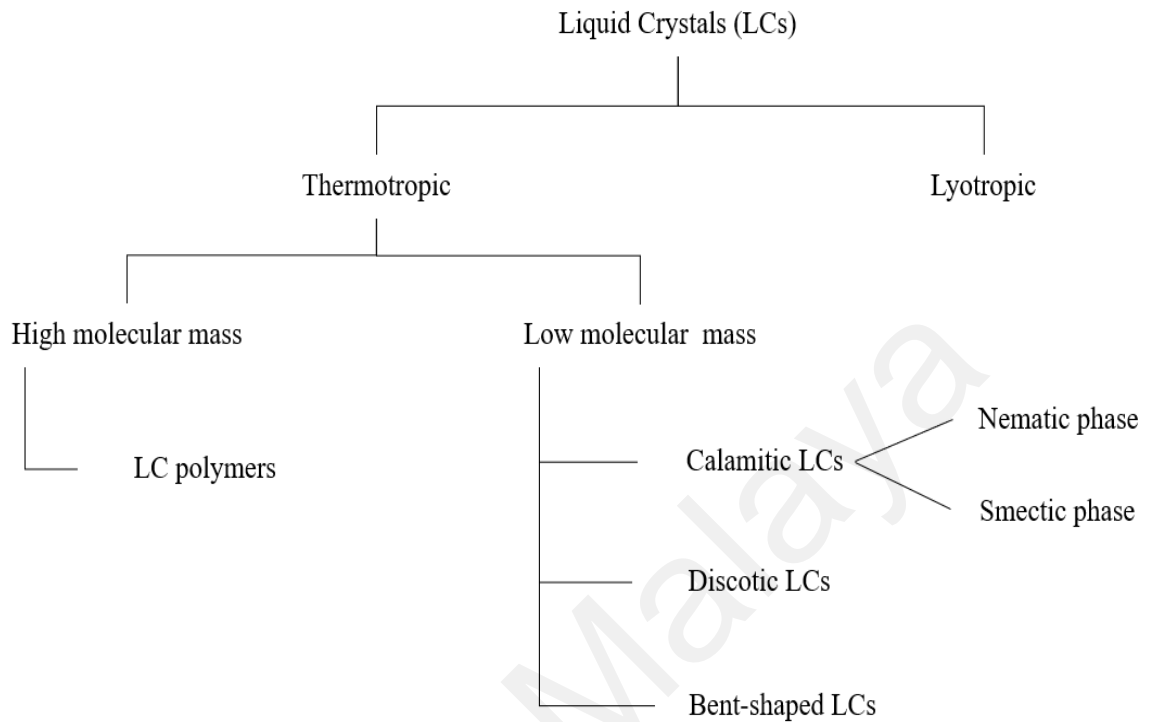


Figure 2.2: The classification of liquid crystals

2.3 Calamitic liquid crystals

Molecules that display mesophase, either enantiotropic or monotropic, within a temperature range are typically consists of an anisotropy rod-like structure in which its molecular length is remarkably higher than its molecular breath are known as calamitic liquid crystals (LCs). The anisotropic properties of rod-like molecules have always been one of the pre-requisites for the formation of thermotropic mesophase (Ha *et al.*, 2010). This may be attributed to the overall molecular orientation stability achieved by the elongated molecules that favour steric packing and resulting in less chances for collision with each other. Figure 2.3 shows the general structure of calamitic LC molecule.

chain or an alkoxy chain is indispensable for an ideal calamitic LC molecule. Subject to the molecular architecture and arrangement, calamitic LC molecules tend to exhibit two types of mesophases; nematic and smectic phases (Luan *et al.*, 2020).

2.3.1 Nematic phase

Nematic phase possesses molecules with only long-range orientational order along the long-molecular axis which shape a parallel arrangement of molecules with a common axis called the director, $\hat{\mathbf{n}}$ (Bruce *et al.*, 2007). The order parameter, S , can be used to define the degree of molecular alignment along the director as shown in Eq 2.1 (Fakruddin *et al.*, 2009).

$$S = \frac{1}{2} \langle 3 \cos^2 \theta - 1 \rangle \quad (2.1)$$

Where θ is the angle between the long axis of a LC molecule and the director, $\hat{\mathbf{n}}$. The value within the angular brackets is an average value measured over all molecular orientations. When $S = 1$, molecules are aligned in a perfect order which indicates a crystalline solid whereas a zero would reflect an isotropic liquid. A nematic phase has a typical range of S between 0.4 and 0.7. Moreover, S is mesophase specific and temperature dependent.

Nematic phase has the least ordered molecular arrangement which is in close proximity to an isotropic liquid as shown in Figure 2.4. Therefore, owing to its high level of fluidity, the reorientation of nematic LC molecules can be readily induced by electric and magnetic fields (Bury *et al.*, 2020) which subsequently changes their optical properties for desired applications such as information display (Camley *et al.*, 2018), waveguides for optofluidic (d'Alessandro *et al.*, 2015), 3D active glasses (Mazur *et al.*, 2017), microstrip patch antennas (Srilekha *et al.*, 2020) and broadband tetrahertz (THz) applications (Li *et al.*, 2016a). The name “nematic” originates from a Greek word for “thread” which can be

associated with the typical thread-like texture of nematic phase under polarizing optical microscopy (POM) as presented in Figure 2.5.

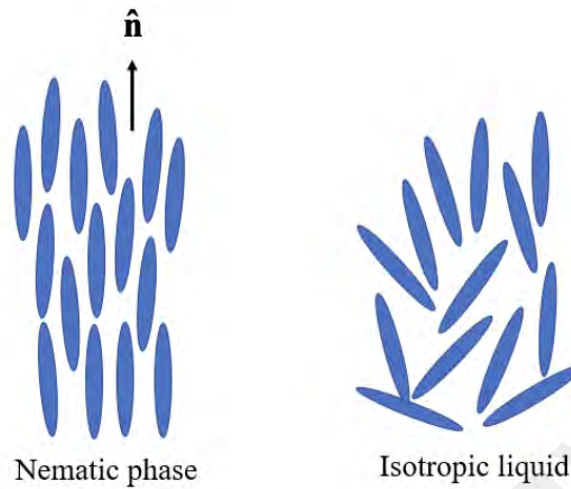


Figure 2.4: Schematic representation of molecular order in nematic phase and isotropic liquid

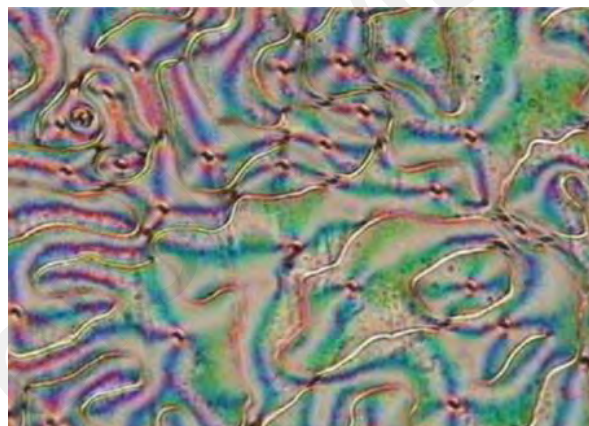


Figure 2.5: POM image of thread-like texture of nematic phase (Andrienko, 2018)

2.3.2 Smectic phase

As opposed to nematic phase, smectic phase LC molecules are arranged in a lamellar ordering which involves both orientational and positional orders in each layer (Bailly-Reyre & Diep, 2020). Owing to its higher order arrangement, smectic phase ordinarily emerges at lower temperature. Nevertheless, the LC molecules are still having some degree of mobility due to the weaker interlayer attractions as compared to the attraction forces along the short axes of the molecules within a layer. The freedom of movement

among LC molecules has led to the formation of different smectic phases such as smectic A, B, C, F and I. These phases are characterized by the orientation of the long molecular axis within and between the layers. Smectic A (SmA) and smectic C (SmC) are the mesophases that regularly reported in the literature.

SmA molecules are oriented in such a way that their long molecular axes are perpendicular to the layer planes and pointing to the same direction (the director, \hat{n}) as the layer normal, z . In SmC phase, however, molecules are arranged in layers with the director, \hat{n} , tilted at an angle with respect to the layer normal, z , and this angle is known to be temperature dependent. The molecular arrangement of SmA and SmC is illustrated in Figure 2.6. Under POM, the texture of SmA phase appears as focal-conic fan shape whereas SmC emerges as schlieren texture as shown in Figure 2.7.

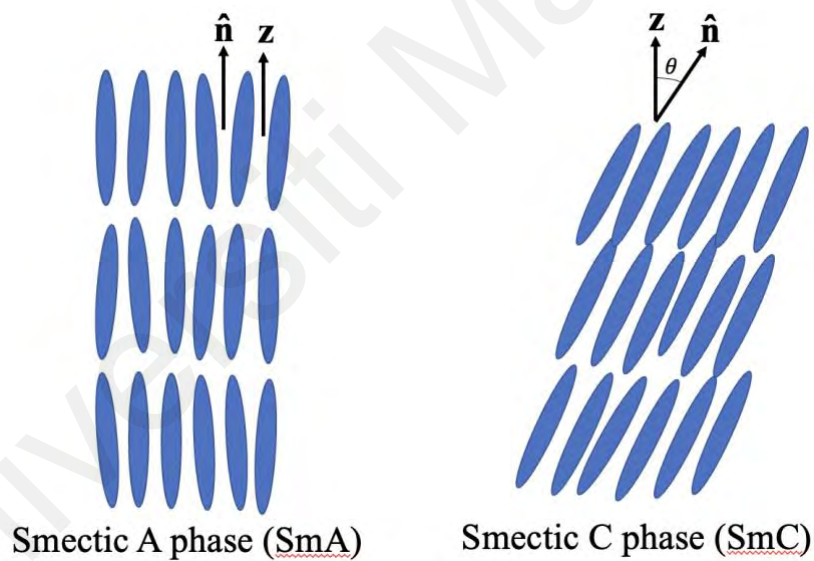


Figure 2.6: Schematic representation of molecular order in SmA and SmC phases

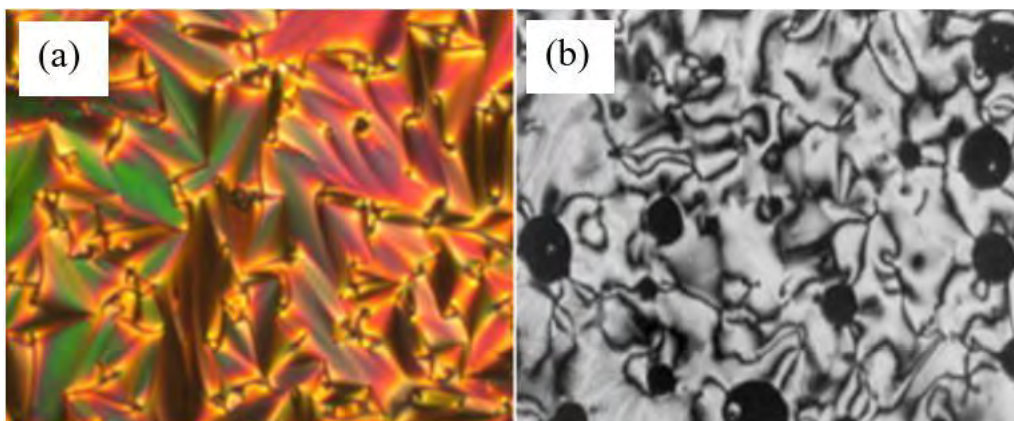


Figure 2.7: POM textures of (a) focal-conic fan texture of SmA phase (Cook *et al.*, 2012b) (b) schlieren texture of SmC phase (Majumdar *et al.*, 2006)

The high viscosity of smectic phases coupled with fluid behaviour has allowed them to show a broad range of interesting topologies, morphologies and defects. On that account, smectic LC materials are of great interest in a number of potential applications. For instance, defects formed by SmA phase, also known as focal-conic domains have been acknowledged as a promising material for building blocks in micro lens arrays, functional surfaces and photo mask (Kim & Yoon, 2018; Preusse *et al.*, 2020). In addition, owing to its reconfigurable curvatures or lamellar structures, smectic phases can be directed into different alignments with an external stimulus such as interfacial layers leading to distinctive optical response. This unique responsive nature makes smectic LC a remarkable material for sensor industry (Prakash *et al.*, 2020).

2.4 Synthesis approach of liquid crystals

As mentioned in Section 2.3, a small change in molecular architecture can lead to a substantial change in mesophase behaviour such as the type and stability of the mesophase formed. Therefore, the incorporation of different mesogenic core units and terminal substituents are the requisite specifications (Elmalı Gülbaşı *et al.*, 2014). Aromatic rings are the common core units used in the synthesis of calamitic LCs owing to the ease of synthesis. A considerable amount of calamitic LCs consist of at least two or three

aromatic rings bridged *via* ester, azo and Schiff base linkages (Ahmed *et al.*, 2020b; Huang *et al.*, 2014; Thakor *et al.*, 2021; Veerabhadraswamy *et al.*, 2018). The introduction of different linking groups in LC molecule plays an important role in determining overall molecular polarizability which eventually affects the stability of the mesophase. For that, there are many choices of versatile organic reactions that can be applied for the synthesis of potential LC, for example, condensation, azo coupling and esterification reactions.

2.4.1 Condensation

LC molecules that comprised of Schiff base or imine as linking unit for mesogenic core or terminal group have been studied to a great extent owing to their interesting mesophase behaviour (Nafee *et al.*, 2020). Schiff base linkage within the mesogenic core provides a stepped core structure which preserves molecular linearity and this in turn enhances mesophase stability (Patel *et al.*, 2010). Generally, Schiff base group can be synthesized through condensation reaction between aromatic amines and aldehydes or ketones derivatives. The reaction mechanism is shown in Figure 2.8. Zakaria *et al.* (2021) have synthesized a series of Schiff base LC molecules through condensation reaction between formyl derivatives and 4-arylamines in ethanol under reflux with relatively high yield (more than 90%). Similar reaction conditions were reported for the synthesis of Schiff base in a plethora of studies involving a vast variety of substituted aromatic amines as well as aldehydes derivatives (Ahmed *et al.*, 2020a; Alamro *et al.*, 2021; Nakum *et al.*, 2019).

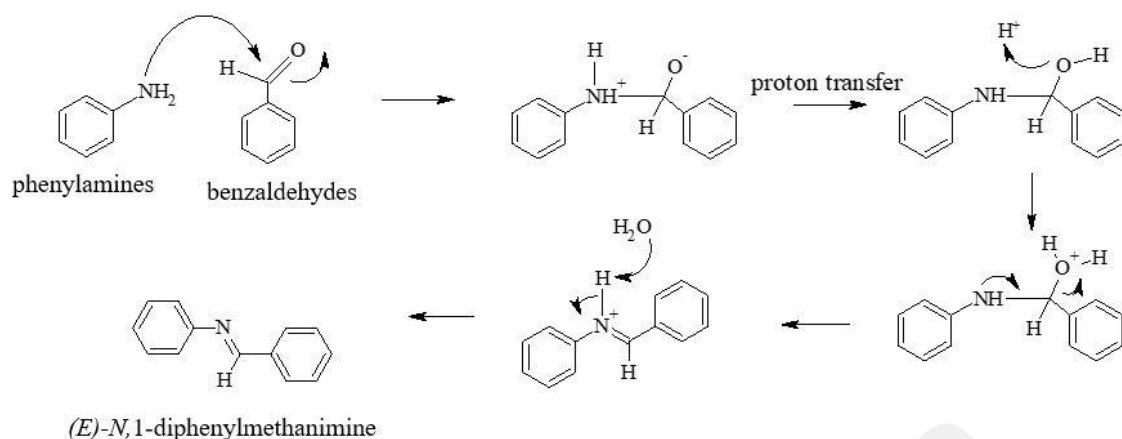


Figure 2.8: The mechanism of condensation reaction between aromatic amines and aldehydes derivatives

2.4.2 Azo coupling

Numerous studies have been conducted on the synthesis of LC materials containing azo linking group due to their unique mechanical and optical properties (Al-Hamdani *et al.*, 2010; Wang *et al.*, 2020; Zhu *et al.*, 2017). Azobenzene, one of the widely used chemical moieties in azo-based LC molecules, is capable of undergoing photoisomerization under various electromagnetic radiations such as UV and visible lights with high thermal stability (Liu *et al.*, 2019; Sperner *et al.*, 2019). Hence, some studies show that the presence of azo linking group is far superior to Schiff base and ester linkages in terms of photochemical properties (Nagaveni *et al.*, 2010; Trišović *et al.*, 2015). Naoum *et al.* (2015a) conducted an azo coupling reaction between ethyl-4-amino benzoate that dissolved in concentrated hydrochloric acid with sodium nitrite added dropwise and 3-(or 2-) methylphenol in sodium hydroxide solution at 0°C. This typical azo coupling reaction was also reported in other relevant studies that were intended to synthesize azo-based LC materials (Jadeja *et al.*, 2016; Jadeja *et al.*, 2019; Kamal *et al.*, 2021). Generally, the reaction mechanism for the formation of azo linkage can be divided into a 2-stage reaction, namely, diazotization (between suitable phenyl amines with

sodium nitrite that dissolved in concentrated hydrochloric acid) followed by azo coupling reaction with phenol or its derivatives as shown in Figure 2.9.

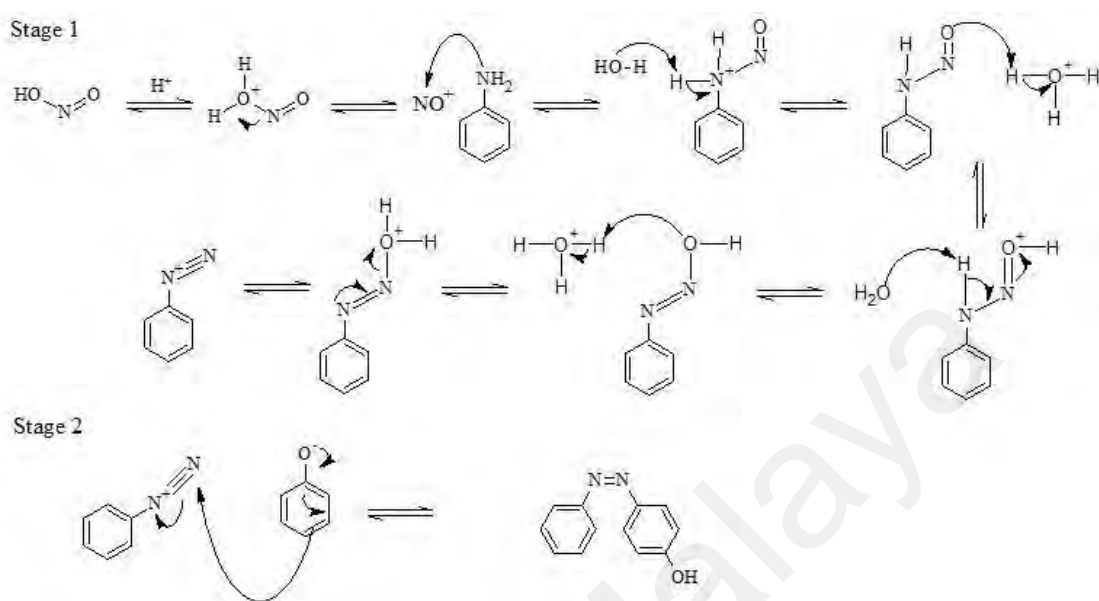


Figure 2.9: The mechanism of diazotization and azo coupling reactions

2.4.3 Esterification

LC molecules with ester linkage tend to have lower melting point but higher molecular stability and polarizability (Collings, 1997). Additionally, ester bond not only can be used to connect aromatic cores but also to bridge terminal flexible alkyl chain. As a result, esterification has been extensively used in the synthesis of LC materials especially Steglich esterification (Alnoman *et al.*, 2019; Lim *et al.*, 2017; Ong *et al.*, 2018; Sharma *et al.*, 2017). Figure 2.10 shows the mechanism of Steglich esterification. It is a mild reaction that uses dicyclohexylcarbodiimide (DCC) as a coupling agent and dimethylaminopyridine (DMAP) as a catalyst. However, there are some noticeable drawbacks which include long reaction time, the formation of dicyclohexylurea (DCU) from DCC wherein the purification process made difficult, and lack of chemoselectivity when phenolic hydroxy substituted aromatic carboxylic acids are involved (Hosangadi & Dave, 1996). On that account, some researchers reported the use of thionyl chloride as an

activating reagent to convert aromatic carboxylic acids into more reactive acyl chlorides (with a better leaving group than -OH) in order to ease the subsequent esterification reaction with shorter reaction time and higher yield (Arrieta *et al.*, 1982; Ha *et al.*, 2009; Selvarasu & Kannan, 2016; Yeap *et al.*, 2006a). The reaction mechanism is presented in Figure 2.11.

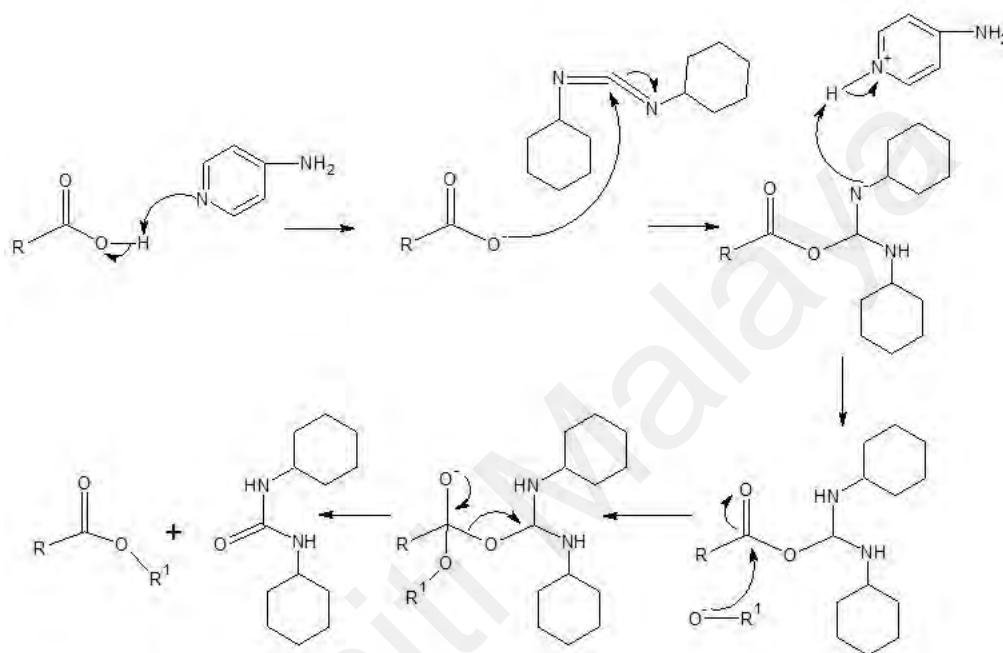


Figure 2.10: The mechanism of Steglich esterification (Xu *et al.*, 2005)

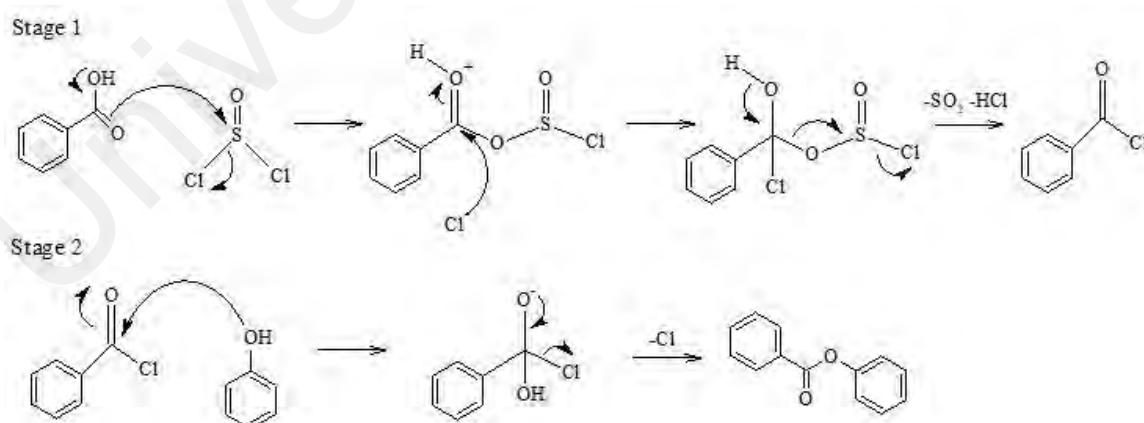


Figure 2.11: The mechanism of esterification using thionyl chloride as activating agent

2.5 Schiff base liquid crystals

A tremendous number of studies have been conducted on the exploitation of Schiff base linkage as part of the mesogenic core of a LC molecule following the breakthrough discovery of LC molecules showing mesophase at room temperature (Kelker & Scheurle, 1969). This type of LC molecules is conveniently known as Schiff base LCs. Although the use of azo linking group within mesogenic core is well known for its unique mechanical and optical properties (Wang *et al.*, 2020; Zhu *et al.*, 2017), yet Schiff base linkage promotes high molecular linearity which enable the formation of mesophase at lower transition temperature (Thaker *et al.*, 2010). Low melting point LC is of great interest as it provides optimum temperature range for device applications. In recent studies, it is manifested that the presence of Schiff base linking group has the tendency to form smectic mesophase and leading to the uncovering of new smectic phases (Abberley *et al.*, 2018; Salamończyk *et al.*, 2019). Therefore, apart from azo coupling, condensation reaction has become increasingly important in the synthetic route of LCs.

Nafee *et al.* (2020) have successfully synthesized a new series of two-ring Schiff base LC molecules, N-arylidene-4-(hexyloxy)benzenamines, with variations in terminal polar substituents. It was reported the mesophase stability was highly dependent on the polarity and the size of the terminal substituents. Results revealed that electron-withdrawing group as terminal substituent resulted in a considerable range of mesophase stability. Only smectic phase observed for both CN and F as terminal substituent whereas Cl substituted two-ring Schiff base LC molecule exhibited smectic and nematic phases. On the other hand, an electron-donating group substituted Schiff base molecule led to a shorter range of mesophase which could be attributed to a decrease in polar anisotropy.

Owing to the curiosity on the effect of multiple Schiff base linkages, the LC properties of hexasubstituted cyclotriphosphazene molecules with two Schiff base linkages was investigated by Jamain *et al.* (2020). All synthesized compounds exhibited mesophase

except compound with NH_2 terminal group was found to be non-mesomorphic. Results from POM and DSC showed that compounds with longer terminal alkoxy chain length possessed enantiotropic smectic phase. This can be ascribed to the long terminal alkoxy chain (C9, C10, C12 and C14) that favours the formation of lamellar arrangement, whereas, compound with shorter alkoxy chain length (C7) exhibited both smectic and nematic phases. As for compounds with small terminal group such as -OH group, -COOH group, Cl group and -NO₂ group were nematogenic in nature. Authors explained that compound with terminal NH_2 group was non-mesomorphic could probably be due to the electron-donating effect of NH_2 which enhances the repulsion forces between mesogenic cores. The additional Schiff base linkage was intended to increase the linearity of the molecule which provides higher mesophase stability.

The use of natural fatty acids with different length and degrees of unsaturation coupled with Schiff base mesogen for the synthesis of LC materials has been studied by Alnoman *et al.* (2019). It was reported that the presence of Schiff base mesogen provides different optical transition phases with higher thermal stability as compared to their corresponding azo-based LC molecules. All synthesized fatty acid-based LC molecules were smectogenic in nature under polarized light. From DSC analysis, it was reported that the stability of SmC phase for molecule with palmitic acid as terminal chain was the lowest whereas molecule with oleic acid and linoleic acid as terminal chain exhibited a longer SmC range. Moreover, it was observed that molecule with the longest unsaturated chain length (linoleic acid) showed not only SmC but SmA phase. The formation of only smectic phases could be ascribed to the long fatty acid chain length which favours lamellar packing of molecules. Therefore, it was concluded that the stability and type of the observed mesophases were dependent on terminal chain length, types of linking group as well as the degrees of unsaturation.

There was another study conducted by Bhat *et al.* (2018) on the synthesis of self-assembled LC molecules using fatty acids with a Schiff base linkage. Two new series of self-assembled LC molecules were prepared using fatty acids, namely, nonanoic acid, capric acid, undecanoic acid, tridecanoic acid, myristic acid, palmitic acid and stearic acid as proton donor (C_m ; $m = 9, 10, 11, 13, 14, 16$ and 18) and (4-pyridyl)-benzylidene-p-n-alkylanilines (**PyBnA**; $n = 12$ and 16) as proton acceptor. The intermolecular hydrogen bonded complexes, **PyB12A:C_m** and **PyB16A:C_m** were affirmed to exhibit smectic phase under POM. Monotropic nature was identified for the two series of hydrogen bonded complexes as mesophase only observed during cooling cycle. The relationship between fatty acid chain length and mesophase range was found to show odd-even effect. Fatty acid moieties that consist of an odd number of carbon atoms possess a shorter mesophase range as compared to even number of carbons of fatty acid chain. This phenomenon can be attributed to the greater surface area of the long fatty acid chain which consequently increased the intermolecular attractions between molecules.

Ha and Lee (2014) have synthesized two series of fluorinated Schiff base LC molecules, 4-alkanoyloxybenzylidene-4'-fluoroaniline (**nABFA**; $n = 8$ and 12) and 4-fluorobenzylidene-4'-n-alkanoyloxyaniline (**nFBAA**; $n = 8$ and 12). From both POM and DSC analyses, it was apparent that the **nABFA** series showed focal conic fan shape texture, typical of smectic A phase and was found to be monotropic in nature. On the flip side, the **nFBAA** series was verified to be non-mesomorphic. Hence, it revealed the importance of the position of Schiff base linkage which can either facilitate or suppress the formation of mesophase. It was also reported that the melting point showed a decreasing trend as the alkyl chain increased from 8 to 12 carbons. Besides, when compared with other structural related compounds, it was manifested that the enhanced mesophase stability can be achieved by incorporating a larger and thus more polarizable halogen atom.

2.6 Schiff base ester-based liquid crystals

Achieving a wide and stable mesophase range has always been an essential criterion to consider in the synthesis of LC materials. The integration of different linking groups within the mesogenic core is one of the fundamental approaches to elevate mesophase stability for various applications (Šmahel *et al.*, 2020). A Schiff base ester-based mesogenic core is a prominent core unit in providing high molecular linearity which enables the formation of stable mesophase (Naoum *et al.*, 2015b). A substantial number of studies have also been carried out to evaluate the effect of having both ester and Schiff base linkages in mesogenic core unit on mesomorphic behaviour (Abberley *et al.*, 2018; Ahmed *et al.*, 2019a; Collings, 1997; Nandi *et al.*, 2017).

Hamad and Salih (2017) synthesized a new series of LC molecules with two ester linkages in addition to a Schiff base linked mesogen to investigate their corresponding mesomorphic properties. The series of molecules composed of 10 members with variations in alkoxy chain length (**DC9A_n**; n = 1-10). Only nematogenic behaviour was observed for **DC9A₁₋₃** whereas for **DC9A₈₋₁₀** only smectic phase was seen. As for the intermediate homologous, **DC9A₄₋₇**, a dimorphic behaviour was detected showing both smectic and nematic phases. It was apparent that the differences in mesomorphic properties can be attributed to the increased alkoxy chain length which subsequently affects the molecular packing from only orientational order (nematic) to a combination orientational order with some degree of positional order (smectic).

As a continuous effort in exploring the beneficial impact of ester linkage in addition to Schiff base mesogen, Karanlık *et al.* (2019) have conducted a study on the effect of orientation of ester linking group as well as terminal substituent on mesophase behaviour. Authors have successfully synthesized two series of three-ring Schiff base ester-based LC compounds, **7a, b** and **8a, b** (**a** = 12 carbons terminal alkyl chain; **b** = 12 carbons terminal

alkoxy chain). The only difference between the two series was the orientation of ester group. For the series of **7a** – **7b**, the carbonyl of the ester unit was in conjugation with imine unit whereas for **8a** – **8b** series, the ether oxygen of the ester group was in conjugation with imine group. During the cooling scan, it was noted that all synthesized compounds were showing multiple mesophases in a similar sequence of blue phase nematic to SmC phase and to smectic X. Indeed, the reversed of ester linking group has caused a decline on mesophase transition temperatures of **8a** – **8b** but not the type and sequence of the mesophase formed. It was reported that the replacement of alkyl chain with alkoxy chain has greatly enhanced the mesophase range by 30°C.

Owing to the interest and curiosity on the effect of multiple linkages within mesogenic core on mesophase behaviour, Abdulnabi *et al.* (2021) managed to synthesize and characterize a new series of Schiff base ester-based LC molecules bearing furan moiety with variations in different alkoxy chain length at one terminal and a polar nitro group at the other. The synthesized LC molecules were labelled as **C_a**-**C_k** in which the alkoxy chain length varied from C1 to C10 and C12, respectively. Results from DSC analysis revealed that all molecules were found to be enantiotropic except **C_a**, **C_e** and **C_f** wherein their mesophase only observed during cooling scan. As for their optical behaviour properties, authors reported that all LC molecules exhibited variety of nematic phases such as nematic droplets, Schlieren, marble and thread-like textures. Molecule **C_k**, on the other hand, demonstrated dimorphic behaviour in which both nematic and smectic A phases were spotted. This could probably be due to its longer alkoxy chain length (12 carbons) which resulted in an increase in intermolecular attraction between methylene carbons and therefore favouring layered molecular packing. Authors also emphasized that the mesophase range of all synthesized Schiff base ester-based molecules were relatively stable (44.05 – 101.80°C). However, due to the presence of furan moiety, the overall

molecular linearity tends to reduce which eventually led to a shorter mesophase range for molecule **C_f** as compared with structurally related LC molecule.

In the same year, another group of researchers, Al-Obaidy *et al.* (2021) reported a study on LC compounds with ester linkage as central core in addition to double Schiff bases linked mesogen. A total of 12 homologues double Schiff base-ester based LC molecules were synthesized with different alkoxy chain length at one terminal ($\text{OC}_n\text{H}_{2n+1}$, $n = 3, 4, 6, 7, 9$ and 12) while on the other terminal, either bromo (**E_n** series) or methoxy substituent (**D_n** series). Results from POM demonstrated that **D_n** series was monomorphic (nematogenic) in nature. On the other hand, due to the highly polarizable terminal bromo group, the enhanced intermolecular interactions between molecules have given rise to the appearance of smectic phase and thus **E_n** series, was found to exhibit smectic phase in addition to nematic phase. Both series of LC compounds showed a wide and stable range of mesophase, from $162.91 - 255.88^\circ\text{C}$. There was no doubt that the presence of Schiff base and ester linkages contributed to this wide mesophase range, however, the incorporation of bulky methoxy group and polarizable bromo group as terminal substituent, has played an important role in establishing a thermally stable mesophase range.

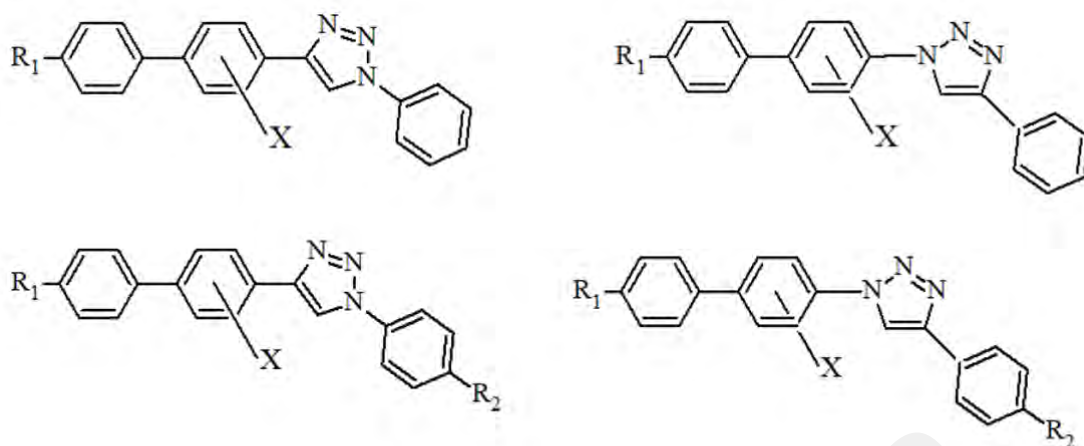
2.7 Structure-mesomorphic properties relationship for calamitic liquid crystals

As elaborated in Sections 2.4 – 2.6, the formation and the type of mesophase as well as its stability is highly dependent on the structural constitution of a calamitic LC molecule. Generally, a calamitic LC molecule consists of three (3) main components, which include a rigid mesogenic core unit, a flexible alkyl chain and a compact terminal substituent. A minor modification on each structural features could result in a substantial change in its anisotropic properties which could potentially deduce the type of mesophases and improve the stability of the mesophase formed (Chothani *et al.*, 2016;

Dixit & Intwala, 2016; Sai *et al.*, 2015). Therefore, it is vital to have insights on the structure-mesomorphic properties relationship of LC molecules in order to synthesize application-driven LC materials.

2.7.1 Structure of mesogenic core unit

As reported by most of the researchers, the mesogenic core unit of a calamitic LC molecule usually composed of two or more 1,4-disubstituted benzene rings owing to their linear molecular conformation (Goodby, 2011). In spite of that, there is an increasing number of researchers divert their interest and attention to heterocyclic rings as part of mesogenic core (Matharu & Chambers-Asman, 2007). This could probably be due to the presence of heteroatoms that may strongly influence the mesophase behaviour (Seed & Sampson, 2017). Wang *et al.* (2019) were aiming to synthesize LC compounds with broader nematic phase. As such, a five-membered ring, [1,2,3]-triazole was used as part of the mesogenic core as this heterocycle containing LC molecules were reported to exhibit unique mesophases (Benbayer *et al.*, 2013; Giroto *et al.*, 2015). Two groups of [1,2,3]-triazoyl-based LC compounds were successfully synthesized. Group 1 composed of 1,4-dialkyl-1-phenyl-4-biphenyl-[1,2,3]-triazole-based (compounds **1-1** to **1-15b**) and group 2 composed of 1,4-monoalkyldiaryl-[1,2,3]-triazoyl-based (compounds **2-1b** to **2-21**) as shown Figure 2.12. Results showed that group 1 compounds, **1-2c** to **1-5d**, **1-6b** and **1-9b**; group 2 compounds, **2-4b**, **2-5b**, **2-7b**, **2-11** to **2-14** and **2-21** were found to be enantiotropic in nature exhibited broader nematic phase as compared with those structurally similar LC molecules reported in the literature. Authors also emphasized that compounds **2-6b**, **2-9** and **2-17** were monotropic nematogenic with transition temperatures close to room temperature due to the presence laterally substituted chlorine atom.



Group 1: Compounds **1-1** to **1-15b** (R_1 and R_2 = H, alkyl, alkoxy, CN, Cl, F).

Group 2: Compounds **2-1b** to **2-21** (X = H, Cl, F).

Figure 2.12: Liquid crystal compounds containing [1,2,3]-triazole ring (Wang *et al.*, 2019)

There is another five-membered ring heterocycle, 1,2,4-oxadiazole (containing two nitrogen atoms and one oxygen atom) that received much attention in LC field as part of the rigid mesogenic core. This can be attributed to its non-linearity that result in a change in molecular polarizability which in turn alters the mesomorphic properties (Gallardo *et al.*, 2011; Subrao *et al.*, 2015). On account of the relevant literatures, Ali and his co-workers (Ali & Tomi, 2018) synthesized and investigated a new series of 1,2,4-oxadiazole-based LC molecules with variations in terminal alkoxy chain length (G_n ; n = C1 to C11). All synthesized molecules exhibited nematic phases during both cooling heating cycles under polarized light and this was consistent with data shown by DSC. The various textures observed from POM were schlieren, marble, droplets and thread-like of nematic. Interestingly, it was found that the mesophase range was independent of alkoxy chain length except for G_1 , the molecule with the shortest alkoxy chain length, showed the greatest stability (134.6°C). Authors did a comparison between G_n series with other reported compounds synthesized by Girdziunaite *et al.* (1991) in which the only structural difference was the heterocyclic ring, 1,3,4-oxadiazole rather than 1,2,4-oxadiazole.

Authors explained that 1,2,4-oxadiazole possessed higher linearity than 1,3,4-oxadiazole and hence resulted in the appearance of mesophase at a higher temperature range in G_n series. The general structure of G_n series is shown Figure 2.13.

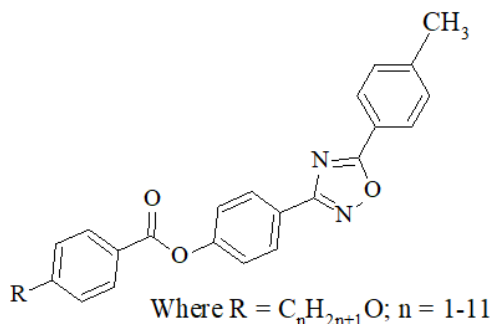


Figure 2.13: A series of liquid crystal compounds with 1,2,4-oxadiazole as part of mesogenic core (Ali & Tomi, 2018)

Other than information display, the exploitation of LC materials in tunable filters, tunable modulators and laser beam steering devices is not uncommon (Jesacher *et al.*, 2008). High birefringence LC compounds are especially important for these applications as it helps to deliver faster response time by decreasing the cell thickness (Catanescu *et al.*, 2004). Birefringence is a phenomenon in which different refractive indexes can be measured with either along or perpendicular to the director of LC molecules. For this reason, some researchers are actively searching for core structures that could enhance birefringence. A five-membered ring thiophene-based mesogenic core found to be a promising rigid core in producing high birefringence LC materials (Kovářová *et al.*, 2014). However, due to its low linearity, the resulted mesophase is known to be unstable. To overcome this challenge, Yang *et al.* (2018) managed to synthesize isothiocyanato (NCS)-based LC molecules with thieno[3,2-b]thiophene as central core (**A1-A6**) and di-substituted with fluoro atoms at 2 and 5 positions to improve linearity. For comparison purposes, the analogous biphenyl compounds (**B4-B6**) as well as thiophene-phenyl

compound (**C5**) were synthesized. The chemical structures of all synthesized molecules are shown in Figure 2.14.

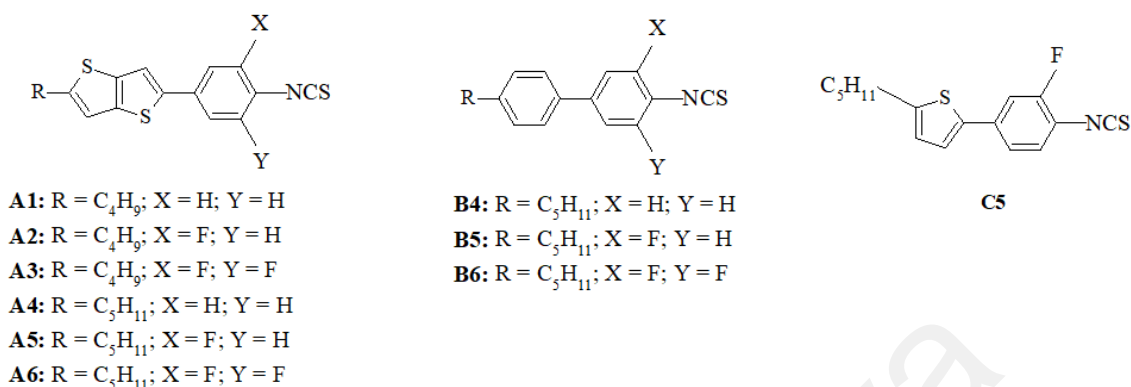
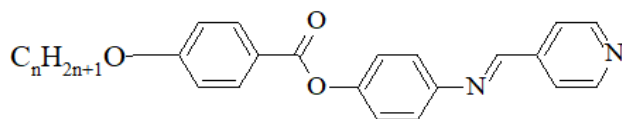


Figure 2.14: Liquid crystal compounds containing different mesogenic core (Yang *et al.*, 2018)

From the results obtained, it was evident that the lateral substituted ring tends to have lower melting point with broadened mesophase range. Furthermore, as compared with their corresponding biphenyl and thiophene-based analogues, the thieno[3,2-*b*]thiophene-based LC molecules exhibited stable mesophase range. For instance, compound **A5** demonstrated a mesophase range of 60°C whereas compound **B5** showed only 11°C of nematic phase and it was found to be monotropic. Authors explained that the wider range of mesophase was probably owing to the effect of di-substitution which in turn improved the molecular length to width ratio. Last but not least, it was manifested that the incorporation of thieno[3,2-*b*]thiophene as central core helped to enhance birefringence (> 0.34) as compared to biphenyl and thiophene cores.

Considering heterocyclic ring as mesogenic core may reduce molecular linearity which eventually suppress mesophase stability, (Ong *et al.*, 2018) believed that pyridine could be a suitable candidate as core system due to its planar structure only slightly distorted from benzene in the presence of N atom. This was followed by the synthesis of a new series of calamitic LC molecules, **nBA4MP** (n = 2, 4, 6, 8, 10, 12, 14, 16 and 18)

with pyridine as part of mesogenic core. The molecular structure of **nBA4MP** is shown in Figure 2.15.



Where $n = 2, 4, 6, 8, 10, 12, 14, 16, 18$

Figure 2.15: Molecular structure of 4-[(pyridin-4-yl)methylidene]amino]phenyl 4-alkoxy-benzoates (Ong *et al.*, 2018)

According to DSC thermograms, molecules of **nBA4MP** exhibited mesophase during both heating and cooling cycles. A monomorphic nematic phase was observed for molecules with $n = 2, 4$ and 6 while compounds **8BA4MP** and **10BA4MP** exhibited smectic A phase in addition to nematic. For molecules with longer chain length, $n = 12-18$, they were found to be smectogenic in nature. Compound **14BA4MP** was compared with structurally related compound **C** with three ester linked phenyl rings which was synthesized by Sakurai *et al.* (1989). It was noted that compound **14BA4MP** with pyridine ring demonstrated a lower melting point and wider mesophase range as compared with a pure phenyl rings system in compound **C**.

2.7.2 Compact terminal substituent

With the aim of producing multifunctional LC materials with anticipated mesophase behaviour, a considerable number of researchers have been focusing on not only the impact of different mesogenic core units but also on the effect of compact terminal substituent (Naoum *et al.*, 2014; Yeap *et al.*, 2015). The variation in polarity of a small and compact terminal substituent is generally known to either suppress or enhance mesophase stability (Alaasar *et al.*, 2013; Nath *et al.*, 2012). This is by virtue of the electronic interactions between terminal substituent and the mesogenic core system which subsequently affect overall molecular polarizability (Begum *et al.*, 2013). As one of the

basic approaches in designing calamitic LC molecule, Hagar *et al.* (2018) have started an investigation on a series of terminally substituted three-ring Schiff base ester-based LC molecules with various compact terminal groups (-OCH₃, -CH₃, -H and -Cl). Figure 2.16 shows the molecular structure of three-ring Schiff base ester-based LC molecule with variations in terminal substituents. Results from POM and DSC showed that Schiff base ester-based LC molecules **I6_{a-d}** and **I12_a** were found to be monomorphic exhibiting nematic phase whereas compound **I12_a** demonstrated only SmA phase. The rest of the synthesized LC molecules were all dimorphic, showing both nematic and smectic phases. The inductive effect of terminal substituents was regarded as important determinant in mesophase stability. In comparison with unsubstituted analogues, both electron-donating and electron-withdrawing groups were ascertained to enhance mesophase stability. This could be attributed to the increased polarity or overall polarizability of the LC molecules which subsequently stabilised molecular packing within mesophase. In spite of that, authors revealed that both -CH₃ and -OCH₃ (electron-donating) substituted molecules exhibited a wider nematic range as compared with those substituted with Cl (electron-withdrawing). This has led to a conclusion that electron-donating group favoured the formation of nematic rather than smectic phase.

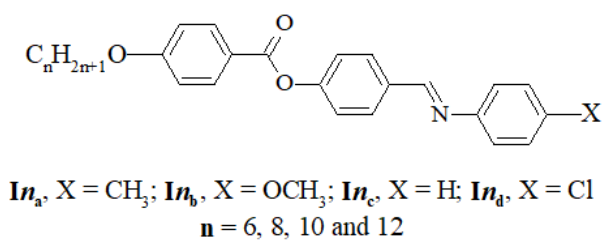


Figure 2.16: A series of three-ring Schiff base ester-based liquid crystal molecules with variations in alkoxy chain length and terminal substituents (Hagar *et al.*, 2018)

In the following year, Saad *et al.* (2019) continued the effort of Hagar and his collaborators to gain further understanding on the effect of compact terminal polar groups on the mesomorphic behaviour of a four-ring azo ester-based LC molecules. The chemical

structure is presented in Figure 2.17 with various alkoxy chain length and different terminal polar groups.

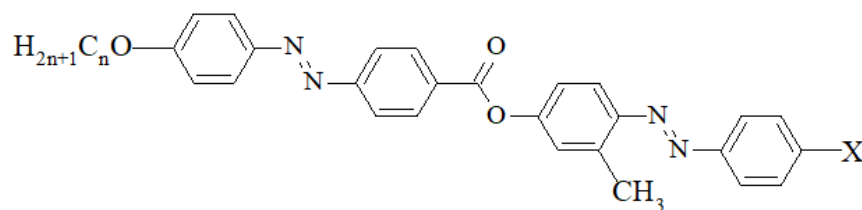


Figure 2.17: A series of four-ring azo ester-based liquid crystal molecules with variations in alkoxy chain length and terminal substituents (Saad *et al.*, 2019). $\text{II}n_x$, $X = \text{CH}_3\text{O}, \text{CH}_3, \text{H}, \text{Br}$ and NO_2 ; $n = 6, 8, 10, 14$ and 16

The mesomorphic behaviour of the studied compounds, $\text{II}n_x$ were found to be chain length and terminal group dependent. For unsubstituted derivatives, $X = \text{H}$, molecules $\text{II}6_x$, $\text{II}8_x$ and $\text{II}10_x$ exhibited only nematic phase, while the rest showed smectic phase in addition to nematic phase. As for derivatives with electron-donating group, $-\text{CH}_3\text{O}$ and $-\text{CH}_3$, regardless of alkoxy chain length, only nematic phase was observed. In contrast, the bromo substituted derivatives demonstrated dimorphic properties, showing both nematic and smectic phases except for $\text{II}6_x$ which was ascertained to be purely nematogenic. Similar trend was noted for another electron-withdrawing group, $-\text{NO}_2$ as terminal substituent. Based on the results obtained, it was apparent that the polarity of terminal substituent was the main factor governing the type of mesophase as well as mesophase stability rather than the size of the substituent. This can be further supported by the fact that both nitro and methoxy substituted derivatives showed the highest mesophase stability as compared to the rest.

With a common goal as other researchers in LC field, that is to synthesize LC molecules with encouraging mesophase behaviour and thermal stability for various applications, Sardon *et al.* (2021) have conducted another research on the relationship between different terminal polar groups substituted azo ester-based LC molecules, **M1-**

M4 and their corresponding mesophase behaviour. The molecular structure of the synthesized LC compounds is shown in Figure 2.18. It was evident that compound **M1-M4** showed purely nematic phase with different transition temperatures. Authors emphasized that overall molecular polarizability was a determining factor in facilitating and improving mesophase stability and this was in agreement with the results obtained. The unsubstituted molecule, **M1** exhibited a mesophase range of only 10°C whereas for **M2-M4** which were terminally substituted by highly polarizing Cl, Br and CN groups, respectively, demonstrated wider mesophase range (ranging from 21 – 32°C).

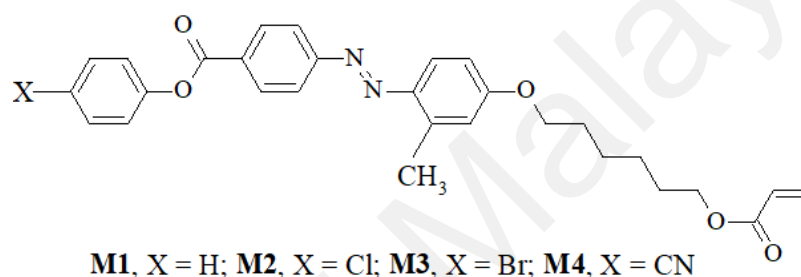
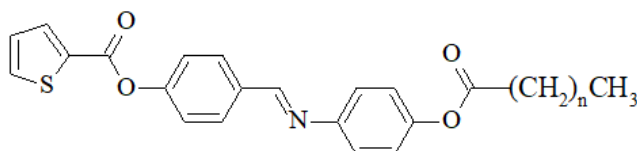


Figure 2.18: A series of three-ring azo ester-based liquid crystal molecules with different terminal substituents (Sardon *et al.*, 2021)

2.7.3 Flexible alkyl chain length

It is established that calamitic LC molecules with a rod-like structure will have high tendency to pack closely with each other to minimise free volume and hence stabilizing molecular packing and consequently enhance mesophase stability (Goodby *et al.*, 2015). However, LC molecules with high rigidity are gravitate toward high phase transition temperatures (melting and clearing) and this may limit their potentiality in various applications (Carlton *et al.*, 2013; Hagar *et al.*, 2019a). On that account, researchers have been incorporating flexible alkyl or alkoxy chain with different length at one terminal of the mesogenic core in order to dilute the rigidity so that the mesophase range can be adjusted for certain applications (Lim *et al.*, 2017). Perhaps that is also the reason why many reported studies involved the effect of flexible alkyl chain length along with other structural changes on mesomorphic behaviour. For instance, in a study conducted by

Chong *et al.* (2016), the effect of alkanoyloxy chain length coupled with the incorporation of thiophene as mesogenic core on mesomorphic properties was being investigated. The chemical structure of the heterocyclic Schiff base ester-based LC is illustrated in Figure 2.19.

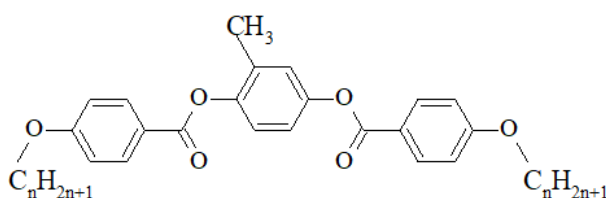


3a (n = 4), **3b** (n = 6), **3c** (n = 8), **3d** (n = 10), **3e** (n = 12), **3f** (n = 14) and **3g** (n = 16)

Figure 2.19: A series of heterocyclic Schiff base ester-based liquid crystal molecules with different alkanoyloxy chain length (Chong *et al.*, 2016)

Compound **3a** to **3e** were enantiotropic nematogen while compound **3f** and **3g** showed smectic C phase in addition to nematic phase under POM. With increasing alkanoyloxy chain length, the melting and clearing temperatures were found to show an ascending and a descending order, respectively. Authors explained that longer chain length induced stronger attraction forces between molecules which eventually led to higher melting temperature. Nevertheless, higher number of carbon atoms in the alkanoyloxy chain also implied that the rigidity of the mesogenic core has been compromised and this has led to lower mesophase stability. Authors also reiterated odd-even effect wherein even number of alkanoyloxy chain could lead to stronger intermolecular force of attraction and hence promoting stable mesophase.

Due to increasing demand for low melting point LC materials, Seou *et al.* (2017) have investigated another series of laterally substituted LC molecules with different alkoxy chain length at both terminals. The molecular structure of the synthesized molecule is shown in Figure 2.20.

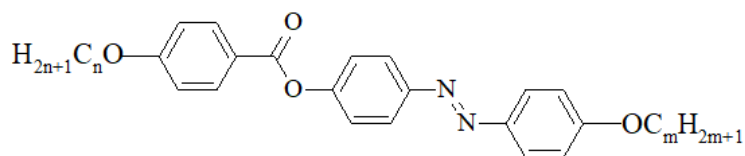


DA5Cn ($n = 2, 10, 12, 14, 16$ and 18)

Figure 2.20: A series of laterally substituted ester-based liquid crystal molecule with different alkoxy chain length (Seou *et al.*, 2017)

Under polarized light microscope, it was observed that all synthesized molecules were enantiotropic in nature. Generally, molecules with shorter chain length (**DA5C2** – **DA5C10**) exhibited only nematic phase whereas **DA5C12**, **DA5C14**, **DA5C16** and **DA5C18** demonstrated dimorphic behaviour, showing both nematic and smectic phases. The appearance of smectic phase in addition to nematic could be due to the longer alkoxy chain length which facilitate lamellar molecular packing. DSC thermograms suggested that molecules with shorter chain length possessed higher transition temperatures and this could be explained with the enhanced rigidity. As for those dimorphic derivatives, higher number of methylene units resulted in a wider range of smectic phase but on the other hand suppressed the nematic phase. Authors concluded that the length of alkoxy chain was the main determinant for mesophase range stability of the studied compounds.

Following the studies by Seou and his collaborators on ester-based LC compounds, it is well acknowledged that manipulating flexible terminal alkoxy chain would not affect the overall polarizability of a LC molecule and this has encouraged (Ahmed *et al.*, 2019b) to conduct a study on the effect of dialkoxy chain length on the mesophase behaviour of a series of Schiff base ester-based LC molecules. A new series of non-symmetrical Schiff base ester-based LC molecules that composed of two alkoxy chains that varied in length at both terminals was synthesized and characterized. The molecular structure of the synthesized compound is presented in Figure 2.21.



I*m/n*, *m* = 6 and 8; *n* = 6, 8, 10 and 12

Figure 2.21: A series of Schiff base ester-based liquid crystal molecule with dialkoxy chain at both terminal with different length (Ahmed *et al.*, 2019b)

Ahmed *et al.* (2019b) disclosed that all compounds exhibited smectic and nematic phases during both heating and cooling cycles. The stability of each phase (nematic or smectic) was highly dependent on the length of both alkoxy chain. It was noted that nematic phase range showed a declining trend with increasing chain length. The opposite trend was observed for smectic phase. This finding was consistent with the literature (Imrie & Taylor, 1989). There was a noteworthy feature of having two terminal alkoxy chains, compounds **I6/n** demonstrated a wider range of mesophase than compounds **I8/n**. The same was not observed in the comparison between **I***m*/8 and **I***m*/6. This implied that alkoxy chain that attached to phenylimino group, *m* was more effective in stabilizing mesophase as compared to alkoxy chain that bonded to the benzoate group of the core, *n*.

Owing to the invaluable findings from Ahmed and team, it is also worth mentioning that other than petrochemical derived alkyl and alkoxy chains, fatty acids have also been used as flexible moiety in LC synthesis as discussed in Section 2.5 (Alnoman *et al.*, 2019; Bhat *et al.*, 2018). Based on the research outcomes, they have concluded that the type of mesophase formed, and its stability was found to be flexible chain length dependent.

2.8 Application of liquid crystals

A continuous effort has been made to synthesize various types of LC molecules as well as to gain in-depth understanding on their structure-mesomorphic properties relationship in order to customize LCs with targeted application. LC materials have a great number of applications other than information display and light-emitting diode. These include but

not limited to superhydrophobic surfaces, LC-based sensors, drug delivery and actuator devices.

In recent years, curvatures of soft materials have been identified as a promising material in biological field, optoelectronic devices as well as polymer science (Kim & Yoon, 2018). Nevertheless, due to limited control towards bulk curvatures and their complicated morphogenesis mechanisms, low molar mass LC molecules with lamellar packing (smectic phase) have been suggested as an alternative. This is owing to their instant response with respect to external stimulations that leads to various smectic curvatures (Fong *et al.*, 2012; Kleman & Lavrentovich, 2009). Superhydrophobic self-cleaning surfaces can be one of best representative application that make use of smectic curvatures. Kim *et al.* (2013) conducted a study on self-assembled hydrophobic surface from a smectogenic LC molecule. Authors disclosed that a dual-scale roughness surface mimicking lotus leave can be made by adding smectic phase LC molecules at its clearing point onto micro-pillar patterned substrates followed by a slow cooling process to its mesophase giving rise to the formation of toric focal conic domain arrays (TFCDs). Next, the sample was further cooled generating another smectic phase (hexatic smectic B4) which subsequently preserved by a nanometre-sized helical nanofilament. The dual-scale surface formed was found to possess high contact angle value.

LC-based sensor technologies are fabricated based on the responsiveness of LC molecules in the form of molecular orientations and birefringence towards biological and chemical molecules (Esteves *et al.*, 2020; Popov *et al.*, 2016). Niu *et al.* (2016) have developed a fast-sensing device for cholic acid (CA) with the exploitation of 5CB LC droplets that dissolved in phosphate buffer saline solution. The LC molecules were in radial configuration due to the presence of SDS surfactant. With the addition of CA, competition occurred between SDS and CA molecules for adsorption onto the surface of

5CB droplets which resulted in a changed in configuration from radial to bipolar structure and this can be evaluated by analysing the images formed under POM.

Owing to the unique molecular orientation of mesophases particularly hexagonal and cubic phases, LC molecules have received significant attention in drug delivery system (Negrini *et al.*, 2015; Spillmann *et al.*, 2014). Potassium 4-methoxosalicylate (**4-MSK**) and 3-O-ethyl-ascorbic acid (**EA**) are two common active ingredients in skin-whitening cream. However due to high solubility in water, both compounds are unlikely to permeate through stratum corneum into epidermis. As such, Li *et al.* (2016b) have carried out a study with its aim to enhance skin retention of both **EA** and **4-MSK** through lamellar liquid crystal (**LLC**) cream and the results obtained was compared with the common o/w (**COW**) cream *via* in vitro permeation and in vivo drug distribution experiments. Authors reported that **LLC** cream showed an improved drug permeability, and this can be ascribed to the interactions between the LC molecules and the intercellular lipids within stratum corneum. Authors also emphasized that the chemical structure of lamellar LC molecule was similar to that of lipid bilayer in cell membrane which in turn facilitate drugs permeation into epidermis.

LC materials are well known for their anisotropic properties in which dielectric constant, elastic constant and refractive index are highly dependent on molecular orientation. Other than those anticipated applications in optic field, LC materials have proven track record in the production of smart materials such as artificial muscles, pumps and actuators (de Gennes, 1997; Fernández, 2013; Xie & Zhang, 2005). A study on the development of LC-based microactuator was conducted by Zhou *et al.* (2016). A nematic phase LC, 4-cyano-4'-pentyl biphenyl, was sandwiched between two parallel plates with the upper one a moveable plate. With a rectangular wave voltage applied, molecules within nematic phase rotate and induced a backflow with S-shape profile. This shear force was found to drive the upper plate to move horizontally with a maximum speed of 120

$\mu\text{m/s}$ at frequency not more than 175 Hz. In addition, authors proposed that the movement direction of the upper plate can be manipulated by treating the plate surface with certain pattern.

In summary, all literature review so far has pointed out the importance of good understanding on the mesomorphic properties-applications relationship to ultimately, tailor-make LC molecules for targeted applications. In line with that, the present study aims to fill some gaps in the structure-mesomorphic properties for LC containing Schiff base ester linking group.

Universiti Malaya

CHAPTER 3: METHODOLOGY

3.1 Materials

Syntheses work in the present study used aniline (Merck, 99.5%) 4-bromoaniline (Merck, 98%), 4-hydroxybenzaldehydes (Merck, 98%), 4-hydroxybenzoic acid (Merck, 98%), glacial ethanoic acid (Merck, 99%), Oxalyl chloride (Acros Organic, 98%), lauric acids (Emery Olechemicals, 99%), palmitic acids (Emery Olechemicals, 98%), stearic acids (Emery Olechemicals, 98%). All chemicals and reagents were used without further treatment.

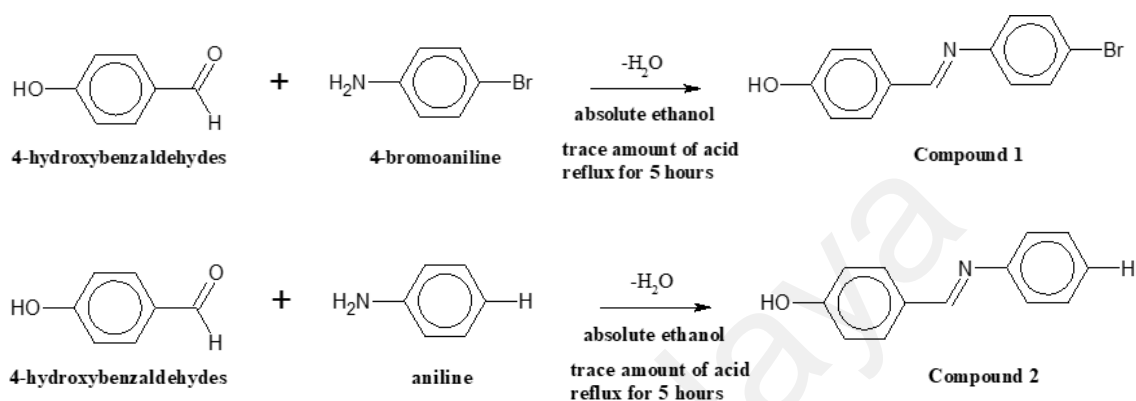
All solvents used were of reagent grade, namely, absolute ethanol (99.8%) and chloroform (99%) were purchased from System Chemicals, whereas dichloromethane (DCM), *N,N*-dimethylformamide (DMF), ethyl acetate (EA), tetrahydrofuran (THF), triethylamine (TEA) (99%), deuterated chloroform (CDCl₃) (99.8%) and deuterated dimethyl sulfoxide (DMSO-d₆) (99.8%) were acquired from Merck.

3.2 Synthesis of palm-based liquid crystals

Palm fatty acids, namely, lauric acid, palmitic acid and stearic acid were used to synthesize three different series of palm-based liquid crystals (PBLCs) with variations in flexible alkyl chain length, mesogen core and terminal substituents. The detailed procedure, route of synthesis and structural determination by Fourier Transform Infrared Spectroscopy (FT-IR), ¹H and ¹³C Nuclear Magnetic Resonance (NMR) for all synthesized liquid crystals and their intermediates are presented in the following sections.

3.2.1 Synthesis of Schiff base

Schiff bases (compound **1** and **2**) were synthesized by condensation reaction between selected starting materials as shown in Scheme 3.1.



Scheme 3.1: Synthetic route of compound 1 and 2

Synthesis of N-(4-hydroxybenzylidene)-4-bromoaniline (1)

A 0.005 mol of 4-hydroxybenzaldehyde was measured and dissolved in 60 mL of absolute ethanol in a round-bottom flask. The solution was refluxed for an hour followed by the addition of 0.005 mol of 4-bromoaniline in the presence of 20 mL absolute ethanol. Catalytic amount of glacial ethanoic acid was added to the reaction mixture. Then, the mixture was further refluxed for another 4 hours. After the completion of the reaction, the solvent as well as the water formed was removed by vacuum drying. The yellowish solid obtained was then re-dissolved in absolute ethanol followed by the addition of small water droplets until the formation of crystals was observed. The yellowish crystals obtained was vacuum filtered and dried in the oven at 40°C until a constant mass was obtained. This is to ensure both compound **1** and compound **2** are free from water, the co-product (Scheme 3.1). The crude product was purified by repeated recrystallization using absolute ethanol. The percentage yield for compound **1** was 78%.

FT-IR (ν_{\max} , cm⁻¹): 1571 (C=C aromatic ring), 1612 (C=N), 3436 (O-H). ¹H NMR (400 MHz, DMSO-d₆): δ /ppm 6.88 (2H, d, J = 8.2 Hz, 1.4 Hz, 0.5 Hz, Ar-H), 7.16 (2H, d, J

= 8.1 Hz, 1.6 Hz, 0.6 Hz, Ar-H), 7.55 (2H, d, J = 8.1 Hz, 1.6 Hz, 0.6 Hz, Ar-H), 7.77 (2H, d, J = 8.2 Hz, 1.8 Hz, 0.5 Hz, Ar-H), 8.45 (1H, s, -CH=N-), 10.16 (1H, s, -OH). ^{13}C NMR (100 MHz, DMSO- d_6): δ /ppm 116.15, 118.21, 123.58, 127.75, 131.32, 132.42, 151.63, 161.33 for aromatic carbons, 161.24 (-CH=N-).

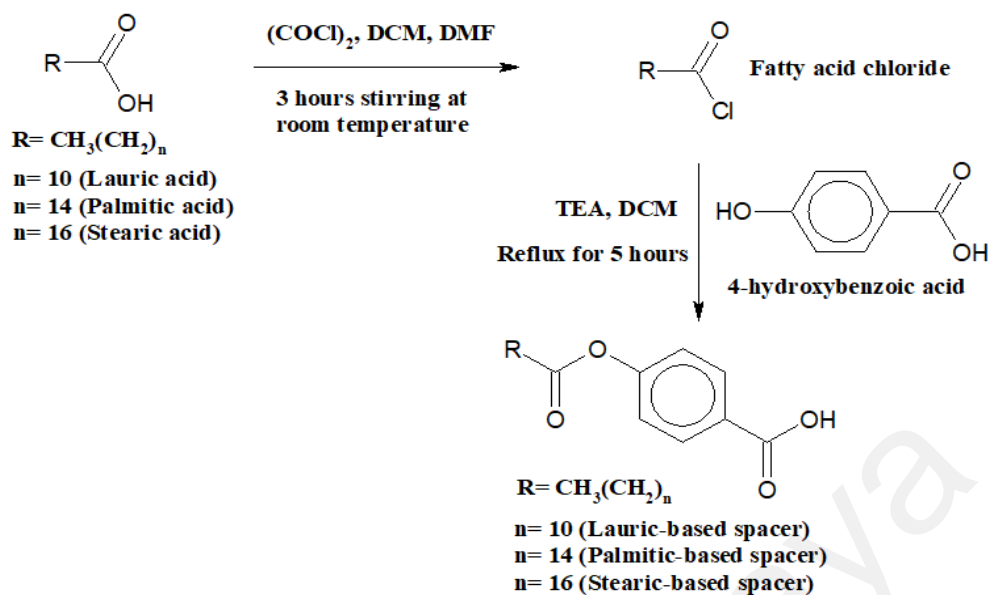
Synthesis of *N*-(4-hydroxybenzylidene)aniline (**2**)

Compound **2** was synthesized from 0.005 mol 4-hydroxybenzaldehyde and 0.005 mol of bromoaniline in the same manner as compound **1**. The percentage yield for compound **2** was 86%.

FT-IR (ν_{max} , cm^{-1}): 1571 (C=C aromatic ring), 1612 (C=N), 3436 (O-H). ^1H NMR (400 MHz, DMSO- d_6): δ /ppm 6.89 (2H, d, J = 8.2 Hz, 1.0 Hz, 0.4 Hz, Ar-H), 7.16 (1H, m, J = 7.8 Hz, 1.4 Hz, Ar-H), 7.34 (4H, m, J = 8.2 Hz, 7.8 Hz, 1.4 Hz, 0.5 Hz, Ar-H), 7.74 (2H, d, J = 8.2 Hz, 1.8 Hz, 0.4 Hz, Ar-H), 8.45 (1H, s, -CH=N-), 10.09 (1H, s, -OH). ^{13}C NMR (100 MHz, DMSO- d_6): δ /ppm 116.16, 121.39, 125.86, 128.03, 129.66, 131.21, 152.52, 160.56 for aromatic carbons, 161.15 (-CH=N-).

3.2.2 Synthesis of palm-based spacer

Palm-based spacers with varying alkyl chain were synthesized using palm fatty acids using the synthetic route depicted in Scheme 3.2.



Scheme 3.2: Synthetic route of palm-based spacer

Synthesis of 4-(dodecanoyloxy)benzoic acid (lauric-based spacer)

A 0.0075 mol of oxalyl chloride was added to 0.005 mol of lauric acid in 40 mL of dichloromethane with four drops of *N,N*-dimethylformamide (DMF) and the mixture was then stirred for 3 hours at room temperature to produce lauric acid chloride. Next, the solution was allowed to dry under reduced pressure and the resulting solid was dissolved in 10 mL of dichloromethane. To this solution, 0.0065 mol of 4-hydroxybenzoic acid that dissolved in 40 mL of dichloromethane was added followed by the addition of 8 mL triethylamine. The mixture was then heated under reflux for 5 hours. Finally, the reaction mixture was filtered, and the solvent was removed under reduced pressure. The solid obtained was further purified by recrystallization using mixture of chloroform to ethyl acetate (1:1). The percentage yield of lauric-based spacer was 33.5%.

FT-IR (ν_{max} , cm^{-1}): 1605 and 1681 (C=C aromatic ring), 1745 (C=O), 2850 and 2919 (C-H stretching). ¹H NMR (400 MHz, CDCl₃): δ /ppm 0.86 (3H, t, $J = 7.2$ Hz, -CH₃), 1.25-1.40 (16H, m, $J = 7.0$ Hz, -CH₂-), 1.75 (2H, m, $J = 7.6$ Hz, 7.4 Hz, -CH₂-), 2.58 (2H, t, $J = 7.3$ Hz, -CH₂-), 7.18 (2H, d, $J = 8.5$ Hz, 1.4 Hz, 0.5 Hz, Ar-H), 8.16 (2H, d, $J = 8.5$

Hz, 1.4 Hz, 0.5 Hz, Ar-H). ^{13}C NMR (400 MHz, CDCl_3): δ/ppm 14.21 (- CH_3), 22.77, 24.92, 29.42, 31.99, 34.49 (- CH_2 -), 121.83 (aromatic C-COOH), 126.93 (aromatic C ortho to -OC=O-), 131.88 (aromatic C ortho to -COO-), 155.11 (aromatic C-OC=O-), 170.77 (-COOH), 171.88 (-COO-).

Synthesis of 4-(hexadecanoyloxy)benzoic acid (palmitic-based spacer)

A 0.0075 mol of oxalyl chloride was added to 0.005 mol of palmitic acid in 40 mL of dichloromethane with four drops of DMF and the mixture was then stirred for 3 hours at room temperature to produce palmitic acid chloride. The subsequent steps were identical to the one described in the synthesis of lauric-based spacer. The percentage of yield of palmitic-based spacer was 40.8%.

FT-IR (ν_{max} , cm^{-1}): 1605 and 1681 (C=C aromatic ring), 1755 (C=O), 2849 and 2917 (C-H stretching). ^1H NMR (400 MHz, CDCl_3): δ/ppm 0.86 (3H, t, $J = 7.2$ Hz - CH_3), 1.24-1.40 (24H, m, $J = 7.0$, - CH_2 -), 1.74 (2H, m, $J = 7.6$ Hz, 7.4 Hz, - CH_2 -), 2.57 (2H, t, $J = 7.3$ Hz, - CH_2 -), 7.17 (2H, d, $J = 8.5$ Hz, 1.3 Hz, 0.5 Hz, Ar-H), 8.11 (2H, d, $J = 8.5$ Hz, 1.4 Hz, 0.5 Hz, Ar-H). ^{13}C NMR (400 MHz, CDCl_3): δ/ppm 14.21 (- CH_3), 22.77, 24.92, 29.42, 31.99, 34.49 (- CH_2 -), 121.83 (aromatic C-COOH), 126.93 (aromatic C ortho to -OC=O-), 131.88 (aromatic C ortho to -COO-), 155.11 (aromatic C-OC=O-), 170.77 (-COOH), 171.88 (-COO-).

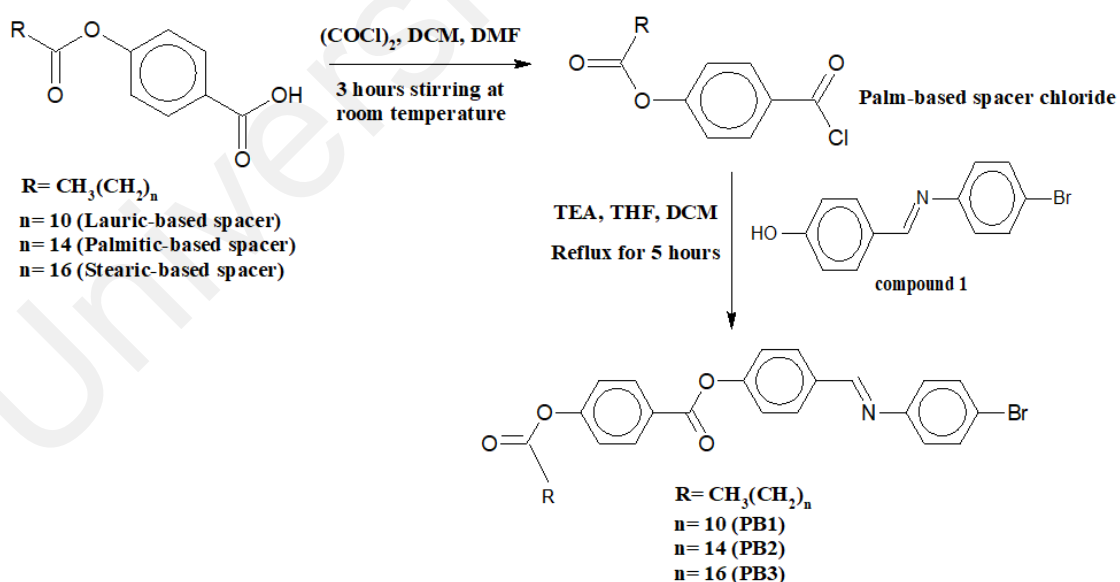
Synthesis of 4-(octadecanoyloxy)benzoic acid (stearic-based spacer)

A 0.0075 mol of oxalyl chloride was added to 0.005 mol of stearic acid in 40 mL of dichloromethane with four drops of DMF and the mixture was then stirred for 3 hours at room temperature to produce stearic acid chloride. The subsequent steps were as described in the synthesis of lauric-based spacer. The percentage yield of stearic-based spacer was 38.9%.

FT-IR (ν_{\max} , cm^{-1}): 1605 and 1681 (C=C aromatic ring), 1755 (C=O), 2849 and 2917 (C-H stretching). ^1H NMR (400 MHz, CDCl_3): δ/ppm 0.86 (3H, t, $J = 7.2$ Hz, $-\text{CH}_3$), 1.25-1.40 (28H, m, $J = 7.0$ Hz $-\text{CH}_2-$), 1.74 (2H, m, $J = 7.6$ Hz, 7.4 Hz, $-\text{CH}_2-$), 2.58 (2H, t, $J = 7.3$ Hz, $-\text{CH}_2-$), 7.18 (2H, d, $J = 8.5$ Hz, 1.3 Hz, 0.5 Hz, Ar-H), 8.16 (2H, d, $J = 8.5$ Hz, 1.4 Hz, 0.5 Hz, Ar-H). ^{13}C NMR (400 MHz, CDCl_3): δ/ppm 14.21 ($-\text{CH}_3$), 22.77, 24.92, 29.42, 31.99, 34.49 ($-\text{CH}_2-$), 121.83 (aromatic C-COOH), 126.93 (aromatic C ortho to $-\text{OC}=\text{O}-$), 131.88 (aromatic C ortho to $-\text{COO}-$), 155.11 (aromatic C-OC=O-), 170.77 ($-\text{COOH}$), 171.88 ($-\text{COO}-$).

3.2.3 Synthesis of 3-ring Schiff based ester-based LCs with terminal -Br group (PB1 – PB3).

The first series of compounds (PB1 – PB3) were synthesized through esterification between the respective activated palm-based spacer with compound 1 synthesized previously according to Scheme 3.3.



Scheme 3.3: Synthetic route for PB1 – PB3

Synthesis of *N*-4-[4-(4-dodecanoyloxybenzoyloxy)benzylidene]bromoaniline (**PB1**)

A 0.0075 mol of oxalyl chloride was added to 0.005 mol of lauric-based spacer with 4 drops of DMF and 3 mL of triethylamine. The resulted solution was stirred for 3 hours at room temperature. Then, the solution was evaporated to dryness under reduced pressure and the solid obtained was dissolved in 40 mL of dichloromethane followed by the addition of 8 mL of triethylamine. To this solution, 0.0065 mol of compound **1** that dissolved in minimum amount of THF was added. The resulting mixture was heated under reflux for 5 hours followed by a filtration. The solvent was removed by evaporation. The remaining solid was recrystallized using mixture of chloroform and ethyl acetate (1:1.5). The percentage yield of **PB1** was 11%.

FT-IR (ν_{\max} , cm^{-1}): 1509 and 1577 (C=C aromatic ring), 1602 (C=N), 1745 (C=O), 2849 and 2916 (C-H stretching). ^1H NMR (400 MHz, CDCl_3): δ/ppm 0.87 (3H, t, 7.2 Hz, - CH_3), 1.26-1.42 (16H, m, $J = 7.0$ Hz, - CH_2 -), 1.74-1.76 (2H, m, $J = 7.7$ Hz, 7.4 Hz, - CH_2 -), 2.59 (2H, t, $J = 7.4$ Hz, - CH_2 -), 7.08 (2H, d, $J = 8.1$ Hz, 1.6 Hz, 0.6 Hz, Ar-H), 7.26 (2H, d, $J = 8.1$ Hz, 1.5 Hz, 0.6 Hz, Ar-H), 7.34 (2H, d, $J = 8.0$ Hz, 1.2 Hz, 0.5 Hz, Ar-H), 7.51 (2H, d, $J = 8.5$ Hz, 1.4 Hz, 0.5 Hz, Ar-H), 7.97 (2H, d, $J = 8.0$ Hz, 1.8 Hz, 0.5 Hz, Ar-H), 8.23 (2H, d, $J = 8.5$ Hz, 1.7 Hz, 0.5 Hz, Ar-H), 8.43 (1H, s, - $\text{CH}=\text{N}$ -). ^{13}C NMR (400 MHz, CDCl_3): δ/ppm 14.24 (- CH_3), 22.79, 24.92, 29.44, 32.01, 34.51 (- CH_2 -), 110.28 (aromatic C ortho to Br), 116.80 and 119.45 (aromatic C ortho to - $\text{OC}=\text{O}$ -), 122.30 (aromatic C-Br), 122.70 (aromatic C ortho to - $\text{N}=\text{CH}$ -), 130.04 (aromatic C-COO-), 131.06 (aromatic C ortho to - $\text{CH}=\text{N}$ -), 131.47 (aromatic C ortho to - COO -), 134.12 (aromatic C- $\text{CH}=\text{N}$ -), 150.87 (aromatic C- $\text{N}=\text{CH}$ -), 153.47 and 155.37 (aromatic C- $\text{OC}=\text{O}$ -), 159.58 (- $\text{CH}=\text{N}$ -), 163.90 (- COO -), 171.80 (- COO -). Anal. Calcd. (%): C, 66.44; H, 6.23; N, 2.42. Found (%): C, 70.90; H, 6.46; N, 1.8.

Synthesis of *N*-4-[4-(4-hexadecanoyloxybenzoyloxy)benzylidene]bromoaniline (**PB2**)

A 0.0075 mol of oxalyl chloride was added to 0.005 mol of palmitic-based spacer with 4 drops of DMF and 3 mL of triethylamine. The resulted solution was stirred for 3 hours at room temperature. The subsequent steps were similar to the synthesis of **PB1** except the recrystallization of **PB2** used a mixture of chloroform to ethyl acetate at 1:1 ratio. The percentage yield of **PB2** was 34%.

FT-IR (ν_{\max} , cm^{-1}): 1509 and 1577 (C=C aromatic ring), 1602 (C=N), 1745 (C=O), 2849 and 2916 (C-H stretching). ^1H NMR (400 MHz, CDCl_3): δ/ppm 0.87 (3H, t, $J = 7.2$ Hz, - CH_3), 1.26-1.42 (24H, m, $J = 7.0$ Hz, - CH_2 -), 1.72-1.76 (2H, m, $J = 7.7$ Hz, 7.4 Hz, - CH_2 -), 2.59 (2H, t, $J = 7.4$ Hz, - CH_2 -), 7.07 (2H, d, $J = 8.1$ Hz, 1.6 Hz, 0.6 Hz, Ar-H), 7.26 (2H, d, $J = 8.1$ Hz, 1.5 Hz, 0.6 Hz, Ar-H), 7.33 (2H, d, $J = 8.0$ Hz, 1.2 Hz, 0.5 Hz, Ar-H), 7.50 (2H, d, $J = 8.5$ Hz, 1.4 Hz, 0.5 Hz, Ar-H), 7.98 (2H, d, $J = 8.0$ Hz, 1.8 Hz, 0.5 Hz, Ar-H), 8.22 (2H, d, $J = 8.5$ Hz, 1.7 Hz, 0.5 Hz, Ar-H), 8.44 (1H, s, - $\text{CH}=\text{N}$ -). ^{13}C NMR (400 MHz, CDCl_3): δ/ppm 14.24 (- CH_3), 22.79, 24.92, 29.44, 32.01, 34.51 (- CH_2 -), 110.28 (aromatic C ortho to Br), 116.80 and 119.45 (aromatic C ortho to - $\text{OC}=\text{O}$ -), 122.30 (aromatic C-Br), 122.70 (aromatic C ortho to - $\text{N}=\text{CH}$ -), 130.04 (aromatic C-COO-), 131.06 (aromatic C ortho to - $\text{CH}=\text{N}$ -), 131.47 (aromatic C ortho to - COO -), 134.12 (aromatic C- $\text{CH}=\text{N}$ -), 150.87 (aromatic C- $\text{N}=\text{CH}$ -), 153.47 and 155.37 (aromatic C- $\text{OC}=\text{O}$ -), 159.58 (- $\text{CH}=\text{N}$ -), 163.90 (- COO -), 171.80 (- COO -). Anal. Calcd. (%): C, 68.15; H, 6.96; N, 2.21. Found (%): C, 64.00; H, 6.31; N, 1.11.

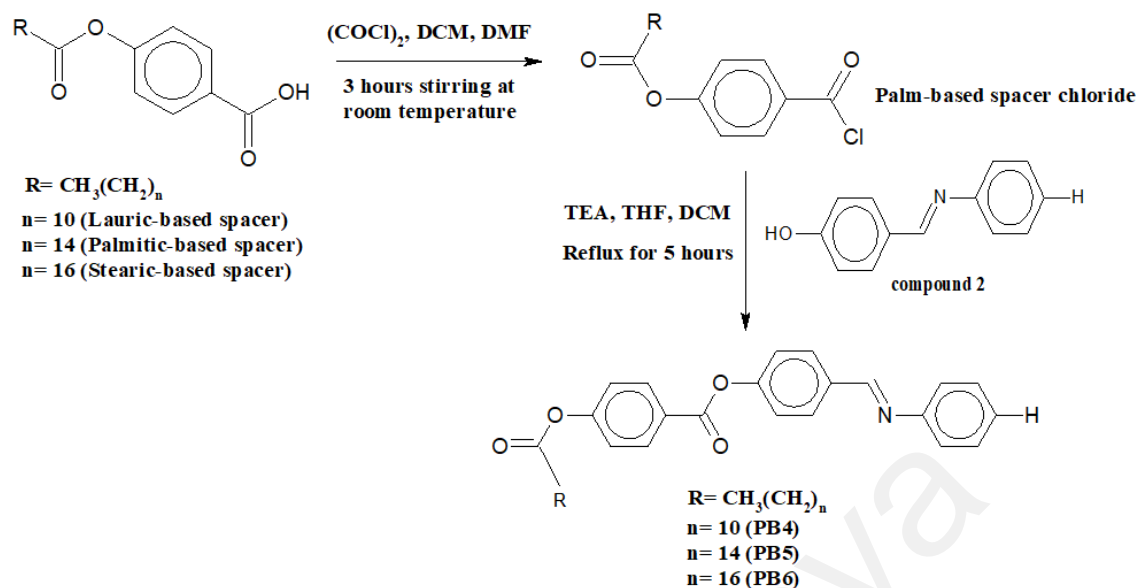
Synthesis of *N*-4-[4-(4-octadecanoyloxybenzoyloxy)benzylidene]bromoaniline (**PB3**)

A 0.0075 mol of oxalyl chloride was added to 0.005 mol of stearic-based spacer with 4 drops of DMF and 3 mL of triethylamine. The resulted solution was stirred for 3 hours at room temperature. The subsequent steps were similar to that described in the synthesis of **PB2**. The percentage yield of **PB3** was 35%.

FT-IR (ν_{\max} , cm^{-1}): 1509 and 1577 (C=C aromatic ring), 1602 (C=N), 1745 (C=O), 2849 and 2916 (C-H stretching). ^1H NMR (400 MHz, CDCl_3): δ/ppm 0.87 (3H, t, $J = 7.2$ Hz - CH_3), 1.26-1.42 (28H, m, $J = 7.0$ Hz - CH_2 -), 1.74-1.76 (2H, m, $J = 7.7$ Hz, 7.4 Hz, - CH_2 -), 2.59 (2H, t, $J = 7.4$ Hz, - CH_2 -), 7.08 (2H, d, $J = 8.1$ Hz, 1.6 Hz, 0.6 Hz, Ar-H), 7.27 (2H, d, $J = 8.1$ Hz, 1.5 Hz, 0.6 Hz, Ar-H), 7.32 (2H, d, $J = 8.0$ Hz, 1.2 Hz, 0.5 Hz, Ar-H), 7.51 (2H, d, $J = 8.5$ Hz, 1.4 Hz, 0.5 Hz, Ar-H), 7.97 (2H, d, $J = 8.0$ Hz, 1.8 Hz, 0.5 Hz, Ar-H), 8.23 (2H, d, $J = 8.5$ Hz, 1.7 Hz, 0.5 Hz, Ar-H), 8.43 (1H, s, - $\text{CH}=\text{N}$ -). ^{13}C NMR (400 MHz, CDCl_3): δ/ppm 14.24 (- CH_3), 22.79, 24.92, 29.44, 32.01, 34.51 (- CH_2 -), 110.28 (aromatic C ortho to Br), 116.80 and 119.45 (aromatic C ortho to - $\text{OC}=\text{O}$ -), 122.30 (aromatic C-Br), 122.70 (aromatic C ortho to - $\text{N}=\text{CH}$ -), 130.04 (aromatic C-COO-), 131.06 (aromatic C ortho to - $\text{CH}=\text{N}$ -), 131.47 (aromatic C ortho to - COO -), 134.12 (aromatic C- $\text{CH}=\text{N}$ -), 150.87 (aromatic C- $\text{N}=\text{CH}$ -), 153.47 and 155.37 (aromatic C- $\text{OC}=\text{O}$ -), 159.58 (- $\text{CH}=\text{N}$ -), 163.90 (- COO -), 171.80 (- COO -). Anal. Calcd. (%): C, 68.89; H, 7.26; N, 2.21. Found (%): C, 65.90; H, 7.10; N, 0.84.

3.2.4 Synthesis of 3-ring Schiff base ester-based LCs without terminal -Br group (PB4 – PB6).

Scheme 3.4 shows the synthetic route for the second series of compounds. Briefly, each palm-based spacer was activated before reacted with compound **2** synthesized previously to form **PB4 – PB6**.



Scheme 3.4: Synthetic route for PB4 – PB6

Synthesis of N-4-[4-(4-dodecanoyloxybenzoyloxy)benzylidene]aniline (PB4)

A 0.0075 mol of oxalyl chloride was added to 0.005 mol of lauric-based spacer with 4 drops of DMF and 3 mL of triethylamine. The resulted solution was stirred for 3 hours at room temperature. Then, the solution was evaporated to dryness under reduced pressure and the solid obtained was dissolved in 40 mL of dichloromethane followed by the addition of 8 mL of triethylamine. To this solution, 0.0065 mol of compound **2** that dissolved in minimum amount of THF was added. The resulting mixture was heated under reflux for 5 hours followed by a filtration. The solvent was removed by evaporation and the remaining solid was recrystallized using suitable ratio of chloroform to ethyl acetate (1:1.5). The percentage yield of **PB4** was 14%.

FT-IR (ν_{max} , cm^{-1}): 1509 and 1578 (C=C aromatic ring), 1600 (C=N), 1730 (C=O), 2851 and 2920 (C-H stretching). ¹H NMR (400 MHz, CDCl₃): δ /ppm 0.86 (3H, t, $J = 7.2$ Hz, -CH₃), 1.23-1.41 (16H, m, $J = 8.0$ Hz, -CH₂-), 1.75 (2H, m, $J = 7.7$ Hz, 7.4 Hz, -CH₂-), 2.58 (2H, t, $J = 7.4$ Hz, -CH₂-), 7.07 (1H, m, $J = 7.8$ Hz, 1.4 Hz, Ar-H), 7.23 (8H, m, $J = 8.5$ Hz, 1.4 Hz, 0.5 Hz, Ar-H), 7.39 (2H, d, $J = 8.0$ Hz, 1.8 Hz, 0.5 Hz, Ar-H), 7.96 (2H, d, $J = 8.5$ Hz, 1.7 Hz, 0.5 Hz, Ar-H), 8.28 (1H, s, -CH=N-). ¹³C NMR (400 MHz,

CDCl₃): 14.21 (-CH₃), 22.77, 24.91, 29.42, 31.98, 34.49 (-CH₂-), 118.64 (aromatic C ortho to -OC=O-), 121.90 (aromatic C ortho to -N=CH-), 129.64 (aromatic C-COO-), 131.27 (aromatic C ortho to -CH=N-), 131.67 (aromatic C ortho to -COO-), 134.12 (aromatic C-CH=N-), 154.89 (aromatic C-N=CH-), 155.30 and 155.01 (aromatic C-OC=O-), 163.78 (-CH=N-), 163.80 and 171.70 (-COO-).

Synthesis of N-4-[4-(4-hexadecanoyloxybenzoyloxy)benzylidene]aniline (PB5)

A 0.0075 mol of oxalyl chloride was added to 0.005 mol of palmitic-based spacer with 4 drops of DMF and 3 mL of triethylamine. The resulted solution was stirred for 3 hours at room temperature. The subsequent steps were similar to the one described in the synthesis of **PB4** except that the ratio of chloroform to ethyl acetate used for recrystallization of **PB5** was 1:1. The percentage yield of **PB5** was 43%.

FT-IR (ν_{\max} , cm⁻¹): 1509 and 1578 (C=C aromatic ring), 1600 (C=N), 1730 (C=O), 2851 and 2920 (C-H stretching). ¹H NMR (400 MHz, CDCl₃): δ /ppm 0.86 (3H, t, $J = 7.2$ Hz, -CH₃), 1.23-1.41 (24H, m, 7.0 Hz, -CH₂-), 1.75 (2H, m, $J = 7.7$ Hz, 7.4 Hz, -CH₂-), 2.58 (2H, t, $J = 7.4$ Hz, -CH₂-), 7.07 (1H, m, $J = 7.8$ Hz, 1.4 Hz, Ar-H), 7.23 (8H, m, $J = 8.5$ Hz, 1.4 Hz, 0.5 Hz, Ar-H), 7.39 (2H, d, $J = 8.0$ Hz, 1.8 Hz, 0.5 Hz, Ar-H), 7.96 (2H, d, $J = 8.5$ Hz, 1.7 Hz, 0.5 Hz, Ar-H), 8.28 (1H, s, -CH=N-). ¹³C NMR (400 MHz, CDCl₃): 14.21 (-CH₃), 22.77, 24.91, 29.42, 31.98, 34.49 (-CH₂-), 118.64 (aromatic C ortho to -OC=O-), 121.90 (aromatic C ortho to -N=CH-), 129.64 (aromatic C-COO-), 131.27 (aromatic C ortho to -CH=N-), 131.67 (aromatic C ortho to -COO-), 134.12 (aromatic C-CH=N-), 154.89 (aromatic C-N=CH-), 155.30 and 155.01 (aromatic C-OC=O-), 163.78 (-CH=N-), 163.80 and 171.70 (-COO-).

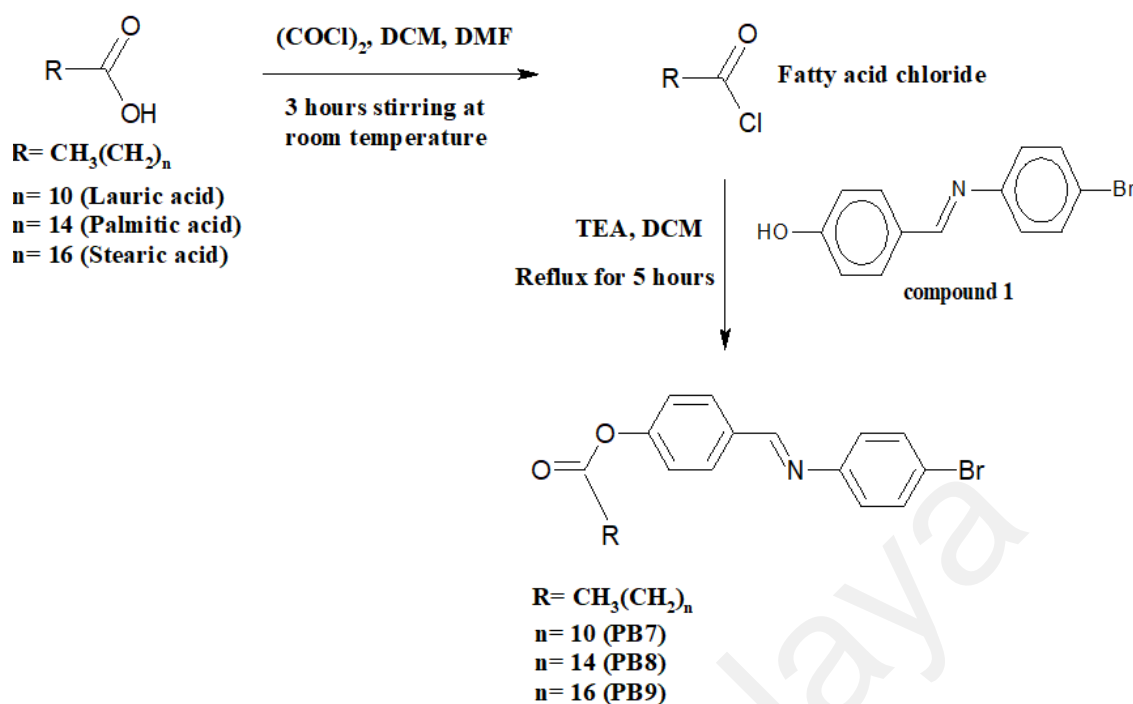
Synthesis of N-4-[4-(4-octadecanoyloxybenzoyloxy)benzylidene]aniline (PB6)

A 0.0075 mol of oxalyl chloride was added to 0.005 mol of stearic-based spacer with 4 drops of DMF and 3 mL of triethylamine. The resulted solution was stirred for 3 hours at room temperature. The subsequent steps were similar to that described in the synthesis of **PB5**. The percentage yield of **PB6** was 35%.

FT-IR (ν_{\max} , cm^{-1}): 1509 and 1578 (C=C aromatic ring), 1600 (C=N), 1730 (C=O), 2851 and 2920 (C-H stretching). ^1H NMR (400 MHz, CDCl_3): δ /ppm 0.86 (3H, t, $J = 7.2$ Hz, $-\text{CH}_3$), 1.23-1.41 (28H, m, $J = 7.0$ Hz, $-\text{CH}_2-$), 1.75 (2H, m, $J = 7.7$ Hz, 7.4 Hz, $-\text{CH}_2-$), 2.58 (2H, t, $J = 7.4$ Hz, $-\text{CH}_2-$), 7.07 (1H, m, $J = 7.8$ Hz, 1.4 Hz, Ar-H), 7.23 (8H, m, $J = 8.5$ Hz, 1.4 Hz, 0.5 Hz, Ar-H), 7.39 (2H, d, $J = 8.0$ Hz, 1.8 Hz, 0.5 Hz, Ar-H), 7.97 (2H, d, $J = 8.5$ Hz, 1.7 Hz, 0.5 Hz, Ar-H), 8.46 (1H, s, $-\text{CH}=\text{N}-$). ^{13}C NMR (400 MHz, CDCl_3): 14.21 ($-\text{CH}_3$), 22.77, 24.91, 29.42, 31.98, 34.49 ($-\text{CH}_2-$), 118.64 (aromatic C ortho to $-\text{OC}=\text{O}-$), 121.90 (aromatic C ortho to $-\text{N}=\text{CH}-$), 129.64 (aromatic C-COO-), 131.27 (aromatic C ortho to $-\text{CH}=\text{N}-$), 131.67 (aromatic C ortho to $-\text{COO}-$), 134.12 (aromatic C- $\text{CH}=\text{N}-$), 154.89 (aromatic C- $\text{N}=\text{CH}-$), 155.30 and 155.01 (aromatic C- $\text{OC}=\text{O}-$), 163.78 ($-\text{CH}=\text{N}-$), 163.80 and 171.70 ($-\text{COO}-$). Anal. Calcd. (%): C, 78.22; H, 8.41; N, 2.40. Found (%): C, 79.41; H, 7.85; N, 2.19.

3.2.5 Synthesis of 2-ring Schiff base ester-based LCs with terminal -Br group (PB7 – PB9).

The third series of compounds (**PB7 – PB9**) were synthesized in accordance to Scheme 3.5 in which activated palm-fatty acid was esterified with compound **1** synthesized previously.



Scheme 3.5: Synthetic route for PB7 – PB9

Synthesis of *N*-4-(4-dodecanoyloxy)benzylidene)-4-bromoaniline (PB7)

A 0.0075 mol of oxalyl chloride was added to 0.005 mol of lauric acid with four drops of DMF and the mixture was then stirred for 3 hours at room temperature to produce fatty acid chloride. Next, the solution was allowed to dry under reduced pressure and the resulting solid was dissolved in 10 mL of dichloromethane. To this solution, 0.0065 mol of compound **1** that dissolved in minimum amount of THF was added followed by the addition of 4 ml of triethylamine. The mixture was then heated under reflux for 5 hours. Finally, the reaction mixture was filtered, and the solvent was removed under reduced pressure. The solid obtained was further purified by recrystallization in a suitable ratio of chloroform to ethyl acetate (1:1.5). The percentage yield obtained for **PB7** was 11%.

FT-IR (ν_{max} , cm^{-1}): 1602 (C=N), 1748 (C=O), 2850 and 2918 (C-H stretching). ¹H NMR (400 MHz, CDCl₃): δ /ppm 0.87 (3H, t, $J = 7.2$ Hz -CH₃), 1.26-1.41 (16H, m, $J = 7.0$ Hz, -CH₂-), 1.74-1.77 (2H, m, $J = 7.7$ Hz, 7.4 Hz, -CH₂-), 2.57 (2H, t, $J = 7.4$ Hz, -CH₂-), 7.08 (2H, d, $J = 8.1$ Hz, 1.6 Hz, 0.6 Hz, Ar-H), 7.48 (2H, d, $J = 8.1$ Hz, 1.5 Hz, 0.6 Hz, Ar-H), 7.91 (4H, m, $J = 8.0$ Hz, 1.5 Hz, 0.5 Hz, Ar-H), 8.39 (1H, s, -CH=N-).

^{13}C NMR (400 MHz, CDCl_3): 14.22 (- CH_3), 22.79, 24.97, 29.44, 31.99, 34.52 (- CH_2 -), 116.80 (aromatic C ortho to - $\text{OC}=\text{O}$ -), 122.30 (aromatic C-Br), 122.71 (aromatic C ortho to - $\text{N}=\text{CH}$ -), 130.25 (aromatic C ortho to - $\text{CH}=\text{N}$ -), 131.70 (aromatic C- $\text{CH}=\text{N}$ -), 132.08 (aromatic C ortho to Br), 150.80 (aromatic C- $\text{N}=\text{CH}$ -), 153.40 (aromatic C- $\text{OC}=\text{O}$ -), 159.60 (- $\text{CH}=\text{N}$ -), 171.70 (- COO -). Anal. Calcd. (%): C, 65.52; H, 6.99; N, 3.10. Found (%): C, 67.35; H, 6.79; N, 3.20.

Synthesis of N-4-(4-hexadecanoyloxy)benzylidene)-4-bromoaniline (PB8)

A 0.0075 mol of oxalyl chloride was added to 0.005 mol of palmitic acid with four drops of DMF and the mixture was then stirred for 3 hours at room temperature to produce fatty acid chloride. The subsequent steps were similar to that described in the synthesis of **PB7** except the ratio of chloroform to ethyl acetate used for recrystallization of **PB8** was 1:1. The percentage yield of **PB8** was 51%.

FT-IR (ν_{max} , cm^{-1}): 1602 (C=N), 1748 (C=O), 2850 and 2918 (C-H stretching). ^1H NMR (400 MHz, CDCl_3): δ /ppm 0.87 (3H, t, $J = 6.8$ Hz, - CH_3), 1.26-1.41 (24H, m, $J = 7.0$ Hz, - CH_2 -), 1.73-1.77 (2H, m, $J = 7.6$ Hz, 7.4 Hz, - CH_2 -), 2.55 (2H, t, $J = 7.4$ Hz, - CH_2 -), 7.08 (2H, d, $J = 8.1$ Hz, 1.6 Hz, 0.6 Hz, Ar-H), 7.48 (2H, d, $J = 8.1$ Hz, 1.5 Hz, 0.6 Hz, Ar-H), 7.91 (4H, m, $J = 8.0$ Hz, 1.5 Hz, 0.5 Hz, Ar-H), 8.39 (1H, s, - $\text{CH}=\text{N}$ -). ^{13}C NMR (400 MHz, CDCl_3): 14.22 (- CH_3), 22.79, 24.97, 29.44, 31.99, 34.52 (- CH_2 -), 116.80 (aromatic C ortho to - $\text{OC}=\text{O}$ -), 122.30 (aromatic C-Br), 122.71 (aromatic C ortho to - $\text{N}=\text{CH}$ -), 130.25 (aromatic C ortho to - $\text{CH}=\text{N}$ -), 131.70 (aromatic C- $\text{CH}=\text{N}$ -), 132.08 (aromatic C ortho to Br), 150.80 (aromatic C- $\text{N}=\text{CH}$ -), 153.40 (aromatic C- $\text{OC}=\text{O}$ -), 159.60 (- $\text{CH}=\text{N}$ -), 171.70 (- COO -). Anal. Calcd. (%): C, 67.72; H, 7.78; N, 2.72. Found (%): C, 69.64; H, 7.52; N, 2.84.

Synthesis of N-4-(4-octadecanoyloxy)benzylidene)-4-bromoaniline (PB9)

A 0.0075 mol of oxalyl chlorides were added to 0.005 mol of stearic acid with four drops of DMF and the mixture was then stirred for 3 hours at room temperature to produce fatty acid chloride. The subsequent steps were similar to that described in the synthesis of **PB8**. The percentage yield of **PB9** was 48%.

FT-IR (ν_{\max} , cm^{-1}): 1602 (C=N), 1748 (C=O), 2850 and 2918 (C-H stretching). ^1H NMR (400 MHz, CDCl_3): δ /ppm 0.87 (3H, t, $J = 6.4$ Hz, $-\text{CH}_3$), 1.26-1.41 (28H, m, $J = 7.0$ Hz, $-\text{CH}_2-$), 1.73-1.77 (2H, m, $J = 7.6$ Hz, 7.4 Hz, $-\text{CH}_2-$), 2.55 (2H, t, $J = 7.4$ Hz, $-\text{CH}_2-$), 7.08 (2H, d, $J = 8.1$ Hz, 1.6 Hz, 0.6 Hz, Ar-H), 7.48 (2H, d, $J = 8.1$ Hz, 1.5 Hz, 0.6 Hz, Ar-H), 7.91 (4H, m, $J = 8.0$ Hz, 1.5 Hz, 0.5 Hz, Ar-H), 8.39 (1H, s, $-\text{CH}=\text{N}-$). ^{13}C NMR (400 MHz, CDCl_3): 14.22 ($-\text{CH}_3$), 22.79, 24.97, 29.44, 31.99, 34.52 ($-\text{CH}_2-$), 116.80 (aromatic C ortho to $-\text{OC}=\text{O}-$), 122.30 (aromatic C-Br), 122.71 (aromatic C ortho to $-\text{N}=\text{CH}-$), 130.25 (aromatic C ortho to $-\text{CH}=\text{N}-$), 131.70 (aromatic C- $\text{CH}=\text{N}-$), 132.08 (aromatic C ortho to Br), 150.80 (aromatic C- $\text{N}=\text{CH}-$), 153.40 (aromatic C- $\text{OC}=\text{O}-$), 159.60 ($-\text{CH}=\text{N}-$), 171.70 ($-\text{COO}-$). Anal. Calcd. (%): C, 68.64; H, 8.12; N, 2.58. Found (%): C, 70.70; H, 7.82; N, 2.65.

3.3 Characterization and instrumentation

3.3.1 Fourier Transform Infrared Spectroscopy (FT-IR)

All FT-IR spectra were obtained using Spotlight 400 PerkinElmer spectrometer with 16 scans using attenuated total reflectance (ATR) method. The wavenumber used was ranging from 650 to 4000 cm^{-1} . All data was processed using built in Spectrum v6.3.1.0132 software.

3.3.2 Nuclear magnetic Resonance Spectroscopy (NMR)

NMR spectroscopy, a non-destructive method, was used to determine the molecular structure of synthesized compounds. ^1H and ^{13}C NMR measurements were performed with JOEL JNM-LA 400 MHz spectrometer. All synthesized compounds were dissolved in appropriate amount of solvent (deuterated chloroform (CDCl_3) and deuterated dimethyl sulfoxide (DMSO-d_6)) at room temperature to give a viscous solution in an NMR tube with at least 4 cm height, for a better resolution. The signals at 7.26 ppm (^1H NMR) and 77.00 ppm (^{13}C NMR) were assigned as chloroform peak, whereas 2.40 ppm and 3.34 ppm (^1H NMR) and 40.60 ppm (^{13}C NMR) for dimethyl sulfoxide (DMSO-d_6) peaks.

3.3.3 CHN Elemental Analysis

PB1 – PB9 were subjected to CHN elemental analysis (Perkin Elmer CHNS 2400 Series II) using the classical Pregl-Dumas method in which small quantity of samples were combusted in a pure oxygen environment and the resulting gases were measured automatically. The calibration standard was acetanilide.

3.3.4 Differential Scanning Calorimetry (DSC)

Phase transition temperatures and the associated enthalpy changes of the synthesized **PB1 – PB9** were measured using Differential Scanning Calorimeter (DSC), TA instrument (DSC25). A 5 mg of the sample was spread evenly on the sample pan and measurement was carried out as follows: sample was first heated from 30 to 250°C, then cooled to 30°C followed by second heating to 250°C under nitrogen atmosphere at the rate of 10°C per minute and held for 3 minutes before cooled and heated again to remove any previous thermal history. The data recorded was analysed using TA software.

3.3.5 Polarized Optical Microscopy (POM)

The mesophase behaviour of **PB1 – PB9** was investigated using Mettler Toledo FP82HT hot stage with a temperature controller (FP90 Central Processor) and viewed through an Olympus BX51 microscope fitted with crossed polarizing filters. The sample was placed in between two thin glass slips and was heated until it reached its isotropic phase. The image was taken upon slow cooling at the rate of 1°C per minute for better observation of texture.

3.3.6 Small Angle X-ray Scattering (SAXS)

Small Angle X-ray Scattering (SAXS) analysis was performed for **PB1 – PB9** with SAXSpace (Anton Paar, Austria) equipped with an X-ray tube (DX-Cu 12 x 0.45, SERFERT). The analysis was done by using the Cu-K α radiation beam ($\lambda = 1.542 \text{ \AA}$). The diameter of the X-ray beam was controlled by a 3-slit optical system set to 250 μm . The sample was wrapped with silver behenate, which acted as calibrant for all measurements. Temperature was controlled by a hot stage (Mettler Toledo Inc. Switzerland) with a accuracy of $\pm 0.1^\circ\text{C}$. Each sample was equilibrated for 10 minutes at a selected temperature followed by 10 minutes exposure time for measurement. The mesophase and its corresponding lattice parameter were determined by SGI software (Space Group Indexing, v.03.2012).

3.3.7 Thermogravimetric Analysis (TGA)

The thermal stability and decomposition patterns of **PB1 – PB9** were studied with Thermogravimetric Analyser, Mettler Toledo. A 5 mg of the sample was measured and placed at the centre of the sample pan on the sample platform. The sample was analyzed under nitrogen atmosphere at a heating rate of 20°C per minute from 30 to 900°C. All data obtained was processed using the equipped software (Pyris v9.1.0.0203).

CHAPTER 4: RESULTS AND DISCUSSION

4.1 Design of palm-based liquid crystals

A calamitic LC molecule is typically composed of multiple moieties, which technically means, its synthesis route could be rather complex and usually encompasses multi-step reactions. As discussed in Section 2.3, the fundamental design of a LC molecule involves numerous linking groups, bridging the rigid mesogenic core structure with various terminal substituents. With the intention of striking a balance between the rigid and the flexible portions of LC molecule, embracing a terminal flexible unit is inevitable.

As in any organic synthesis, amongst the first consideration is the source of starting material. It is evident from literature so far that either alkyl or alkoxy chains from petrochemicals derived non-renewable fossil fuel are commonly used as flexible unit in LCs synthesis. In line with one of the pillars of palm oil industry to diversify the use of palm oil in non-food applications, renewable palm fatty acids possess the potential in acting as flexible unit in LC molecule owing to its long and flexible alkyl chain.

Palm oil consists of lauric acid (0.1%), myristic acid (1.0%), palmitic acid (42.8%), stearic acid (4.5%), oleic acid (40.5%), linoleic acid (10.1%) and linolenic acid (0.2%) (Montoya *et al.*, 2014). At the downstream industry, palm oil is further being processed into five building blocks of the oleochemical industry, namely, fatty acid, fatty alcohol, fatty acid methyl ester, fatty amine and glycerol. Of these, fatty acid is selected for the present study due to its good reactivity for chemical modification as well as ease of handling.

The term 'fatty' in palm fatty acid denotes its origin from plants and contains longer carbon chain length longer than four (4). Therefore, fatty acid is basically carboxylic acid with a longer acyl chain. It has an even number of carbons due to its biosynthetic pathway

that allows the addition of 2C each time. Being a natural fatty acid, the acyl chain is unbranched with full saturation or mono-, di- or polyunsaturation.

The inherent property of palm fatty acids possesses only an even number of carbon atoms making them a superior choice as building blocks in the synthesis of LCs. Coincidentally, it fits in the interest of odd-even effect where even number of carbons tends to promote longer mesophase range due to stronger intermolecular force of attractions (Chong *et al.*, 2016). Besides, utilization of non-toxic palm fatty acids in LCs synthesis could be a good initiative in realizing the concept of green chemistry. As a results, these serve as the basis of the idea of synthesizing palm-based liquid crystals (PBLCs) in this research. Three saturated palm fatty acids were chosen to be investigated in this study, namely, lauric acid (C12), palmitic acid (C16) and stearic acid (C18). All are solid at room temperature, which ease handling and storage.

Though from the literature, the incorporation of heterocyclic rings as part of mesogenic core is of current interest as it could induce unique mesomorphic behaviour and higher birefringence for specific device applications (Matharu & Chambers-Asman, 2007; Seed & Sampson, 2017; Subrao *et al.*, 2015). However, due to its low linearity, the resulted mesophase is known to be unstable (Ali & Tomi, 2018; Kovářová *et al.*, 2014). As a consequence, with the aim of synthesizing LC molecules with stable mesophase, 1,4-disubstituted benzene rings were chosen to be the main constituent of mesogenic core (to preserve linearity) along with Schiff base and ester groups as linking unit in the PBLCs designed in this study. Both Schiff base and ester are known to be an eminent linking unit in the synthesis of LC molecules that promote mesophase stability (Ahmed *et al.*, 2020b; Devadiga & Ahipa, 2019). To further enhance molecular polarizability, the incorporation of a compact terminal substituent, such as halogens was planned. Halogens are polar in nature with strong inductive effect on the mesogenic core and this is especially true for halogen with a bigger atomic radius due to the ease of distortion of electron cloud.

Therefore, the presence of -Br group in PBLCs as terminal substituent is expected to improve the anticipated mesophase range. The molecular structure of all synthesized PBLCs and their respective percentage yield is presented in Table 4.1. It is apparent that the percentage yield of all PBLCs was found to be relatively low. This could be attributed the inherent waxy properties of palm fatty acids. These waxes may affect crystallization process which in turn lowering the yield of the product. The effect may be more significant due to repeated recrystallization process.

Table 4.1: Molecular structure and percentage yield of PBLCs

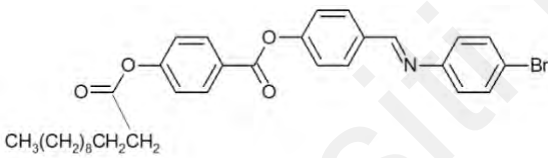

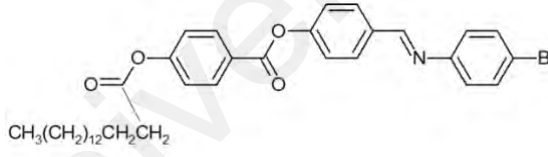
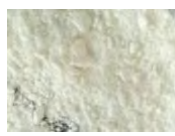
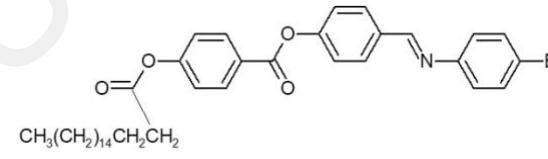

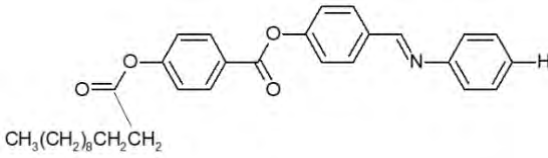

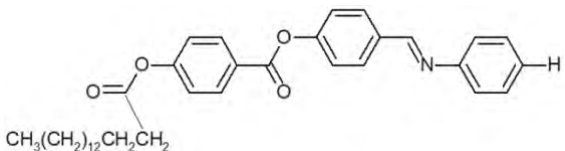
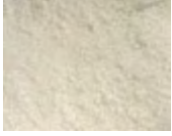
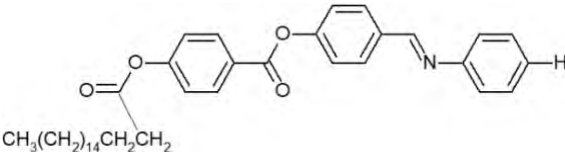
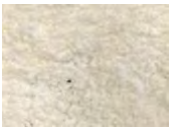
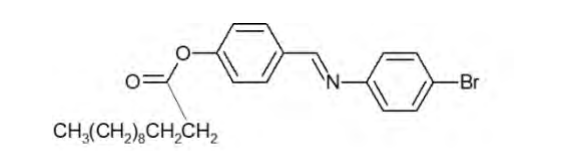

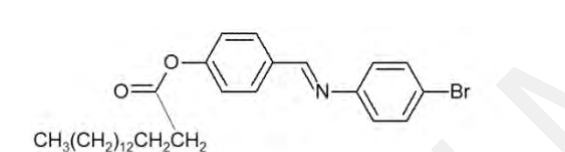
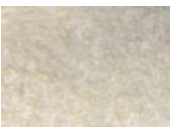
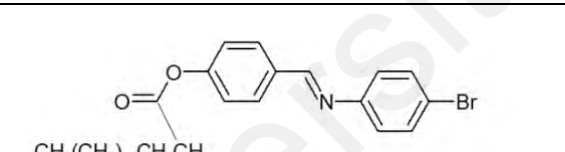
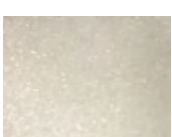
Molecular structure of PBLC	Palm fatty acid	Physical appearance	Percentage yield (%)
 <p>PB1</p>	Lauric acid (C12)		11
 <p>PB2</p>	Palmitic acid (C16)		34
 <p>PB3</p>	Stearic acid (C18)		35
 <p>PB4</p>	Lauric acid (C12)		14

Table 4.1, continued

 <p>PB5</p>	<p>Palmitic acid (C16)</p>		<p>43</p>
 <p>PB6</p>	<p>Stearic acid (C18)</p>		<p>35</p>
 <p>PB7</p>	<p>Lauric acid (C12)</p>		<p>27</p>
 <p>PB8</p>	<p>Palmitic acid (C16)</p>		<p>51</p>
 <p>PB9</p>	<p>Stearic acid (C18)</p>		<p>48</p>

4.2 Synthesis of palm-based liquid crystals

As illustrated in Table 4.1, three series of structurally different PBLCs were synthesized. **PB1 – PB3** series composed of a 3-ring Schiff base ester mesogenic core with a flexible palm fatty acid chain that varied in length (C12, C16 or C18) at one terminal and a polar -Br group at the other. **PB4 – PB6** are the unsubstituted analogues to the series of **PB1 – PB3**. In comparison with the other two series, the only structural difference for **PB7 – PB9** series is that the mesogenic core consists of only 2 phenyl rings

with one less ester group. Two typical reaction mechanisms were employed to synthesize PBLCs, specifically condensation and esterification.

Schiff base linkage that provides a stepped core structure within the mesogenic unit of PBLCs was synthesized by reacting an aromatic amine with aldehydes derivatives. In the case of **PB1 – PB3** and **PB7 – PB9**, a 4-hydroxybenzaldehyde was used to react with 4-bromoanilines forming compound **1**. While on the contrary, aniline to react with 4-hydroxybenzaldehyde in **PB4 – PB6** series forming compound **2**. Taking compound **2** as an example, the detailed mechanism is shown in Figure 4.1. During the reaction, nitrogen atom from aniline acts as a nucleophile (presence of lone pair of electrons) to attack an electron-deficient carbonyl atom of 4-hydroxybenzaldehyde forming an unstable intermediate carbinolamine. This is followed by an acid-catalysed dehydration leading to the formation of a stable Schiff base linked mesogen. While compound **1** and compound **2** are insoluble in water, it is critical to remove water formed from the reaction to minimize any possibility of side reaction that may occur such as hydrolysis.

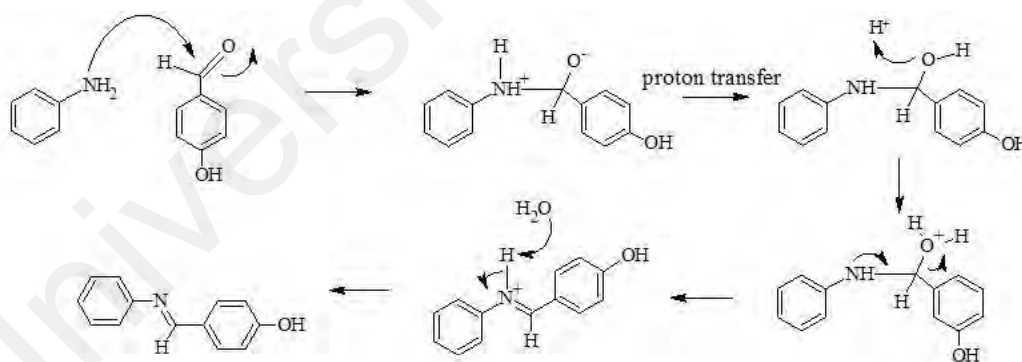


Figure 4.1: The mechanism of condensation reaction between 4-hydroxybenzaldehydes and aniline forming Schiff base linked mesogenic core

Following condensation reaction, esterification is another reaction that plays a pivotal role in bridging either a palm-based spacer (PBS) or a flexible palm fatty acid chain to the Schiff base linked mesogenic core. Steglich esterification was on top of the consideration list, especially for the formation of palm-based spacer, a reaction between palm fatty acid and 4-hydroxybenzoic acid. This is due to the fact that it is a mild reaction

that involves dicyclohexylcarbodiimide (DCC) as a coupling agent and dimethylaminopyridine (DMAP) as a catalyst. However, due to lack of chemoselectivity, the formation of O-acylisourea intermediate between palm fatty acid and DCC made difficult with the interference of 4-hydroxybenzoic acid. Moreover, the dicyclohexylurea (DCU) formed as a by-product complicated the synthesis further. Therefore, Steglich esterification was not successful experimentally for the synthesis of PBS.

Hence, an alternative route was then engaged in which palm fatty acid was first activated into a highly reactive acyl chloride (with a better leaving group than -OH) prior to the esterification reaction. Activation of carboxylic acids is not new and thionyl chloride has already been used and reported to ease the esterification reaction (Jia *et al.*, 2018). However, in the present study, oxalyl chloride was selected over thionyl chloride, as the former appears to be more appealing as it produces non-toxic CO₂ gas instead. Activation of acids using thionyl chloride on other hand, produces toxic SO₂ gas as one of the by-products. As a consequence, oxalyl chloride was chosen, coupled with *N,N*-dimethylformamide (DMF) as catalyst, to activate palm fatty acid and the corresponding PBS. The activation process undergoes a 2-step reaction, step 1 involves the formation of Vilsmeier-Haack reagent between DMF and oxalyl chloride followed by nucleophilic acyl substitution of palm fatty acid or palm-based spacer in step 2. Figures 4.2 and 4.3 demonstrate the reaction mechanism for the activation of lauric acid and lauric-based spacer, respectively.

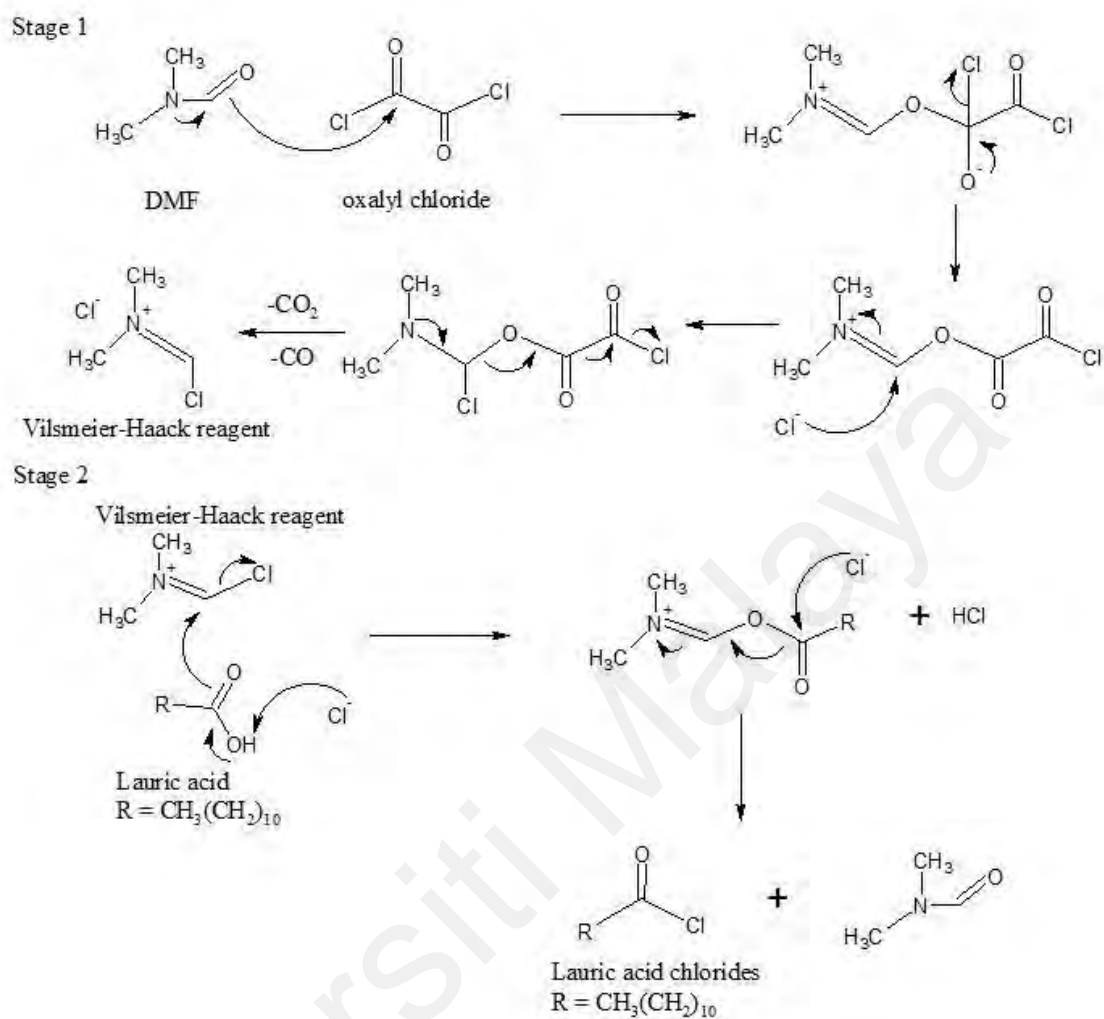


Figure 4.2: The mechanism for the activation of lauric acid using oxalyl chloride

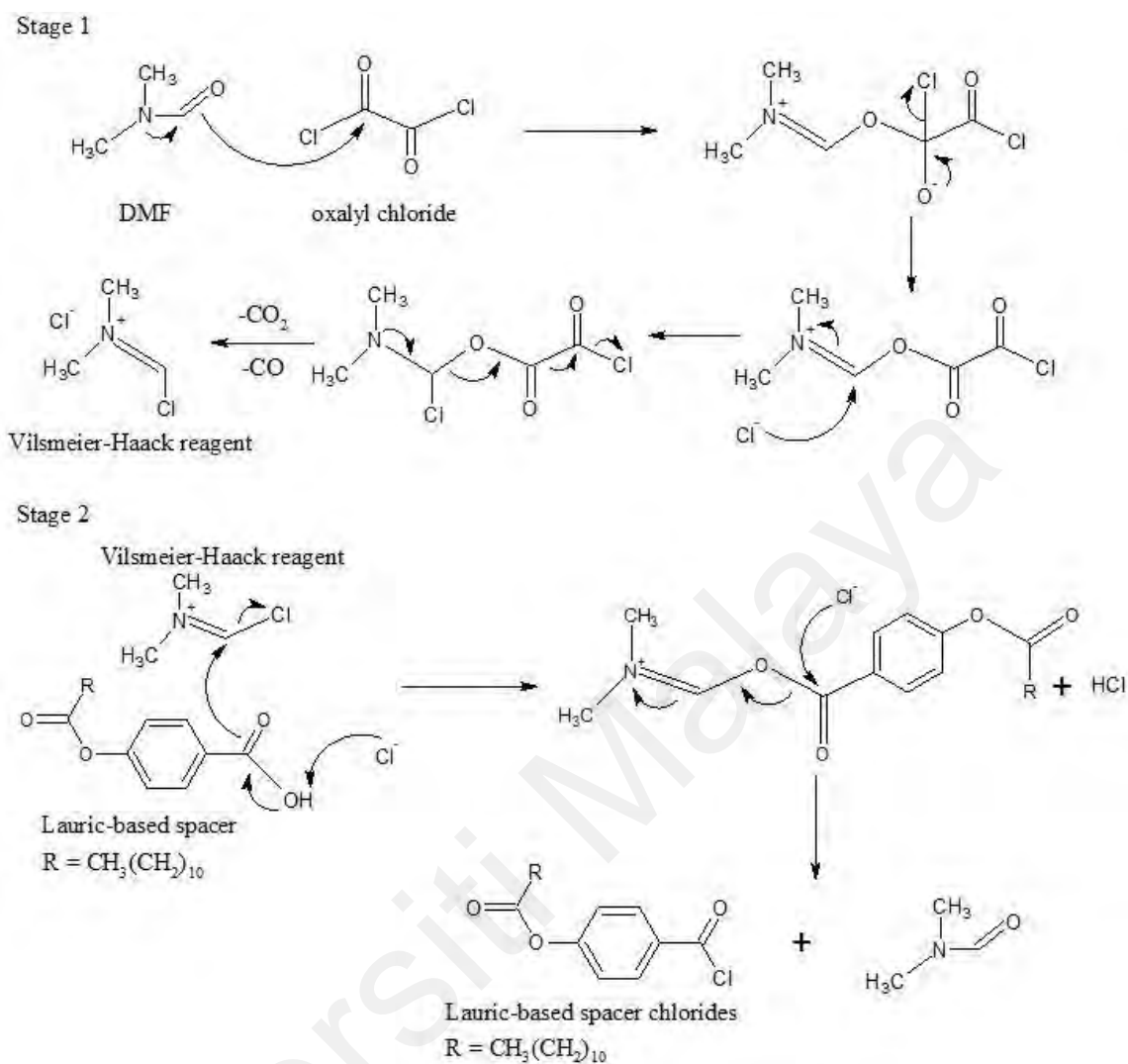


Figure 4.3: The mechanism for the activation of lauric-based spacer using oxalyl chloride

The activated palm fatty acid was either esterified with compound **1** which resulted in **PB7-PB9** series or with 4-hydroxybenzoic acid resulting in the corresponding PBS. Figure 4.4 and Figure 4.5 present the reaction mechanism for the formation of **PB7** and lauric-based spacer.

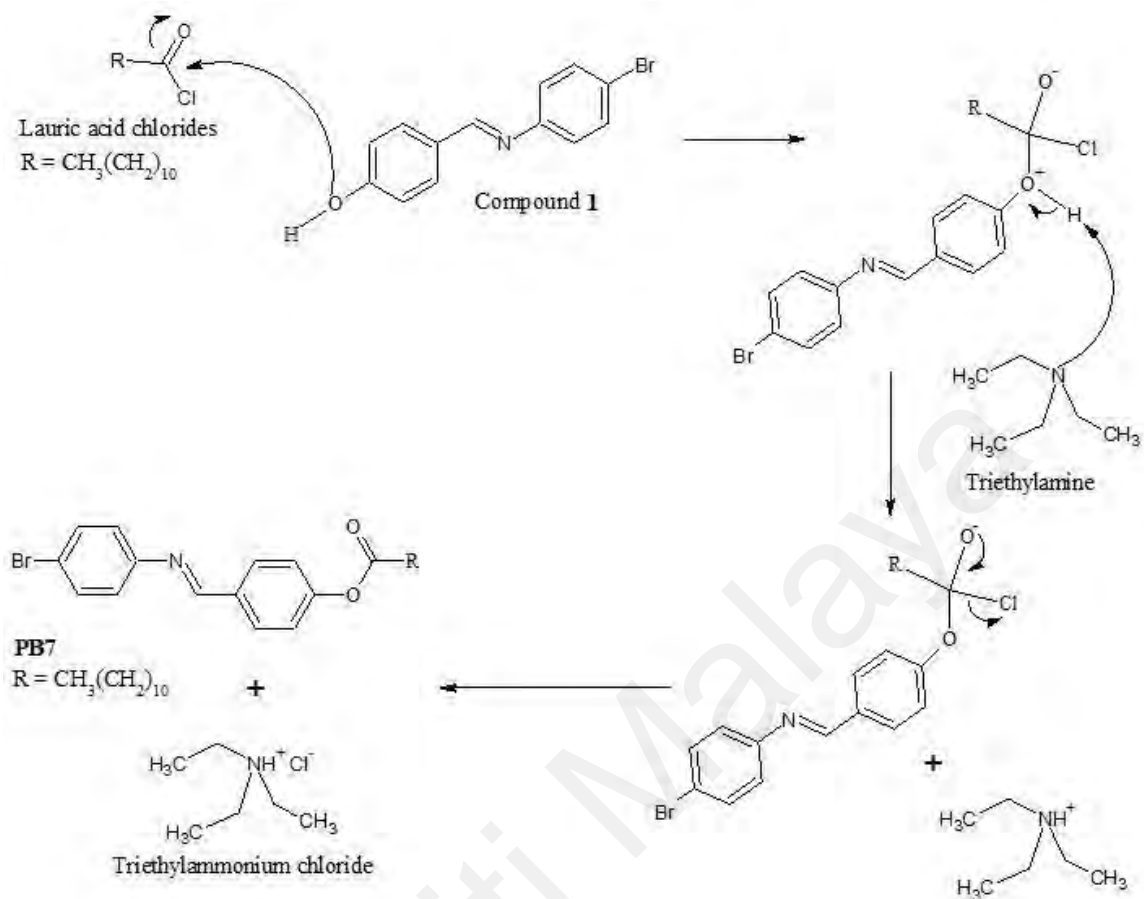


Figure 4.4: The mechanism for the esterification between activated lauric acid and compound 1

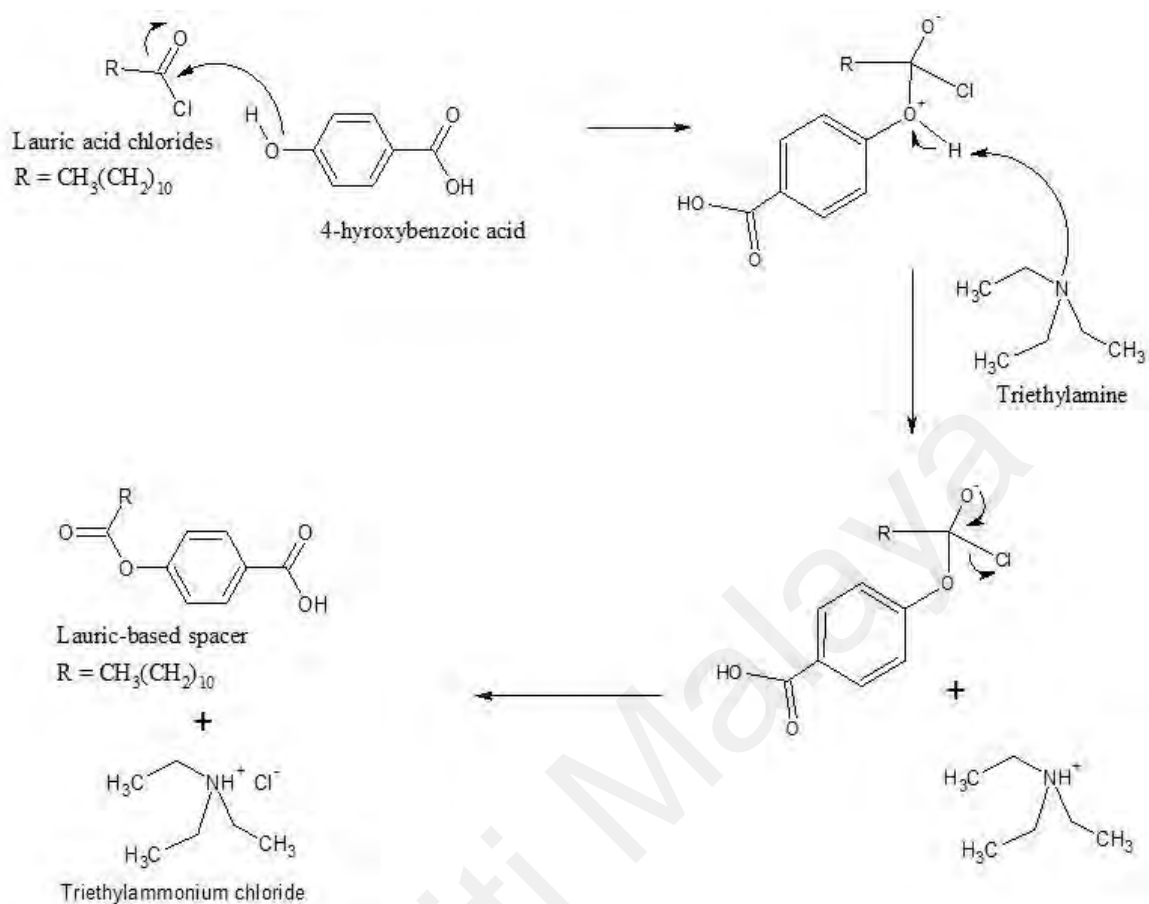


Figure 4.5: The mechanism for the esterification between activated lauric acid and 4-hydroxybenzoic acid

As for the synthesis of **PB1-PB3** and **PB4-PB6** series, activated PBS was subjected to an esterification reaction with compound **1** and compound **2**, respectively. A representative reaction mechanism for the esterification between activated lauric-based spacer and compound **1** forming **PB1** is shown in Figure 4.6.

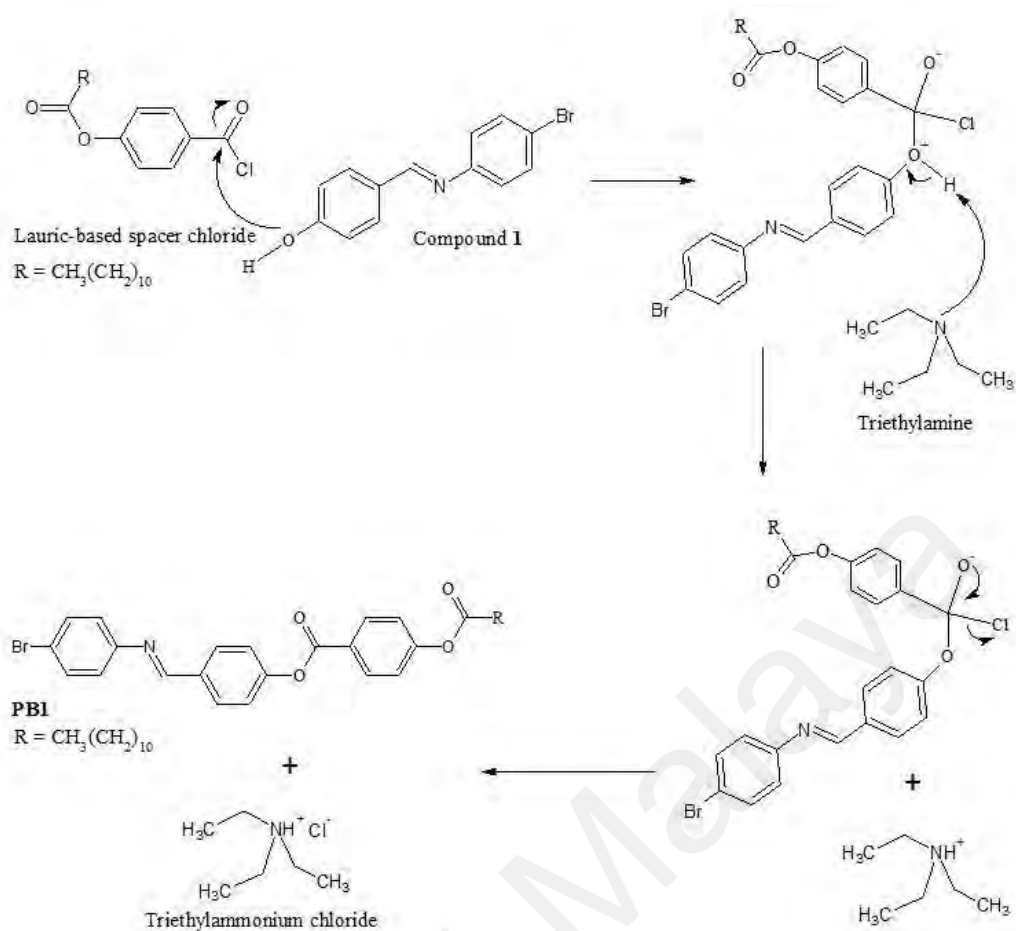


Figure 4.6: The mechanism for the esterification between activated lauric-based spacer and compound 1

4.3 Structural determination

The molecular structure of all synthesized palm-based liquid crystals (PBLCs) including their intermediates was characterized by Fourier Transform Infrared Spectroscopy (FT-IR), ^1H and ^{13}C Nuclear Magnetic Resonance (NMR). Results obtained were found to be consistent with the designed structures.

4.3.1 Fourier Transform Infrared Spectroscopy (FT-IR)

FT-IR is a technique used to detect different functional groups of an unknown organic compound based on infrared absorption of various bond stretching and bending. In the present study, it is also employed as a tool to confirm chemical conversion has proceeded to yield the targeted products. In general, compound 1 and 2 exhibited similar FT-IR

spectrum with slight deviations in wavenumber for the characteristic peak of various functional groups. Figure 4.7(a) shows the FT-IR spectrum of compound **1**. The presence of OH group is affirmed with the appearance of a broad OH peak at 3436 cm^{-1} . Peaks that appeared at 1571 cm^{-1} and 1612 cm^{-1} can be associated with the presence of C=N stretching of the Schiff base group and the aromatic C=C stretching of the phenyl group, respectively. Owing to the structural similarities among all palm-based spacers, lauric-based spacer was used a representative for discussion and its FT-IR spectrum is shown in Figure 4.7(b). The symmetrical and asymmetrical stretching of methylene group can be located at 2850 cm^{-1} and 2919 cm^{-1} . The emergence of a vibrational peak at 1754 cm^{-1} confirmed the presence of ester carbonyl group within lauric-based spacer. Another two characteristic peaks at 1605 cm^{-1} and 1681 cm^{-1} can be attributed to the existence of aromatic C=C stretching. As for the spectrum shown in Figure 4.7(c), **PB1** was chosen to be discussed as it shared similar functional groups with other PBLCs. A vibrational signal of C=N stretching at 1602 cm^{-1} confirmed the presence of Schiff base group. As for the ester carbonyl group, it is reflected as a strong absorption band at 1745 cm^{-1} . The two absorption bands at 2849 cm^{-1} and 2916 cm^{-1} can be identified as the symmetrical and asymmetrical of C-H stretching of the flexible lauric acid chain. Not least of all, the aromatic C=C stretching can be found at 1509 and 1577 cm^{-1} .

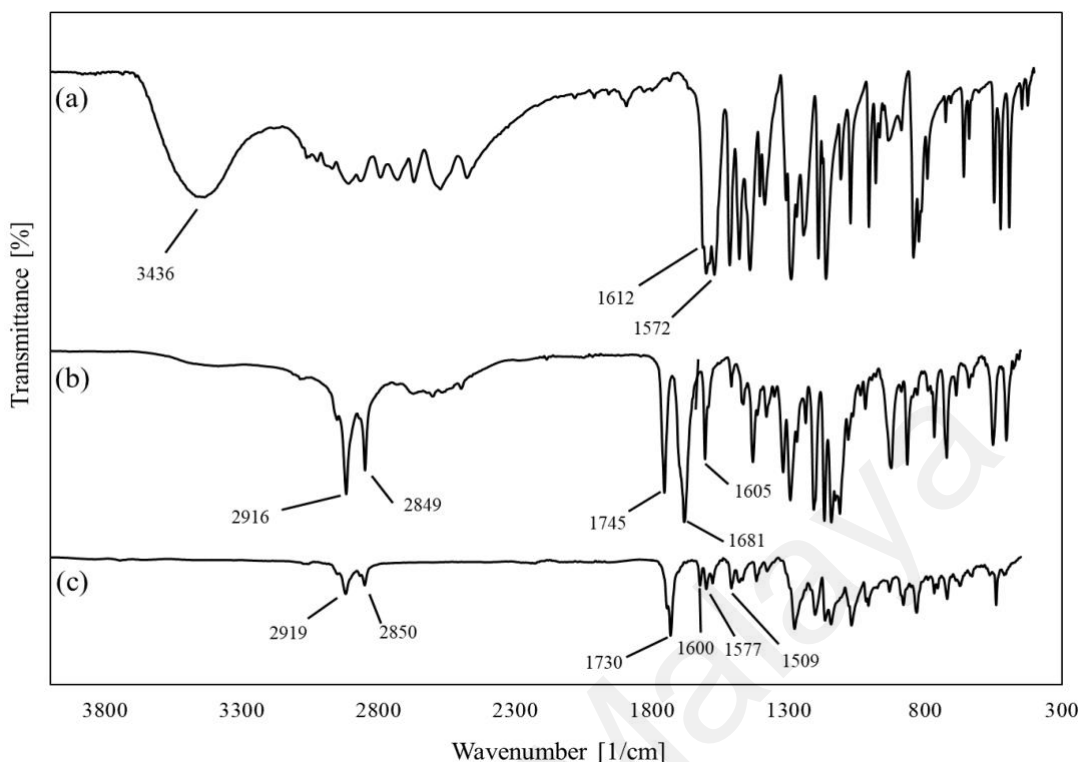


Figure 4.7: FT-IR spectra of (a) compound 1, (b) lauric-based spacer, (c) PB1

4.3.2 ^1H NMR spectra

Nuclear Magnetic Resonance (NMR) is one of the common spectroscopic techniques used to measure the magnetic properties of nuclei. In this section, the magnetic behaviour of hydrogen nuclei (or protons) within a PBLC molecule and its intermediates when exposed to external magnetic field will be discussed.

Figure 4.8 shows the ^1H NMR spectrum of compound **1**. The doublets that resonate in the range of 6.88 to 7.77 ppm (2, 3, 5 and 6) can be attributed to the aromatic protons. By virtue of the delocalized π system of the disubstituted phenyl rings, these peaks appeared to be de-shielded. There are two singlets observed at a higher chemical shift, 8.45 ppm (4) and 10.16 ppm (1), which can be ascribed to the Schiff base proton ($\text{CH}=\text{N}$) and the OH group, respectively. Signal that developed as singlet is associated with the fact that there are no adjacent protons. These signals are highly de-shielded due to the

electronegativity of oxygen and nitrogen atoms as well as the diamagnetic anisotropic effect of π electrons from the double bond. The ^1H NMR spectrum of compound **2** (as shown in Figure 4.9) is rather similar to compound **1** as they bear structural similarities except that compound **2** exhibits signals at 7.16 (5) and 7.34 ppm (4) as multiplet due to the unsubstituted terminal.

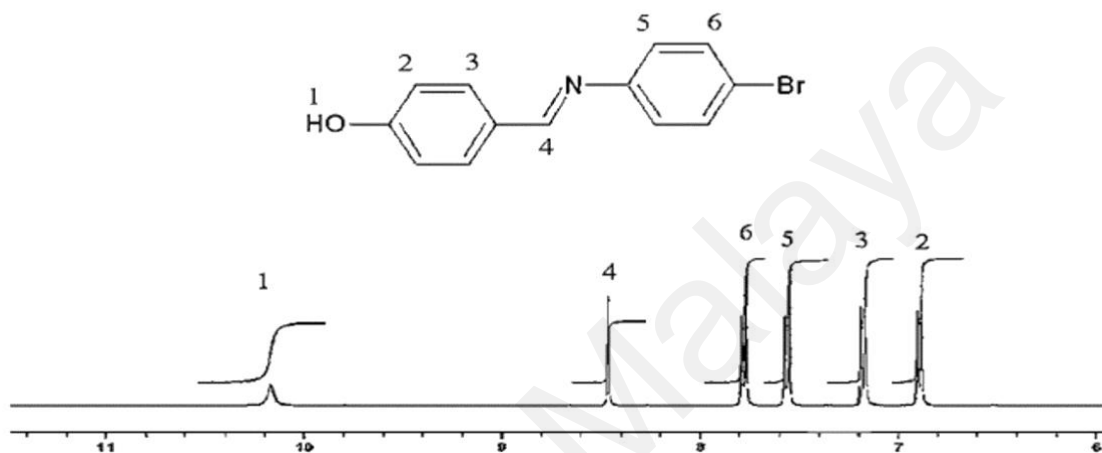


Figure 4.8: ^1H NMR spectrum of compound **1**

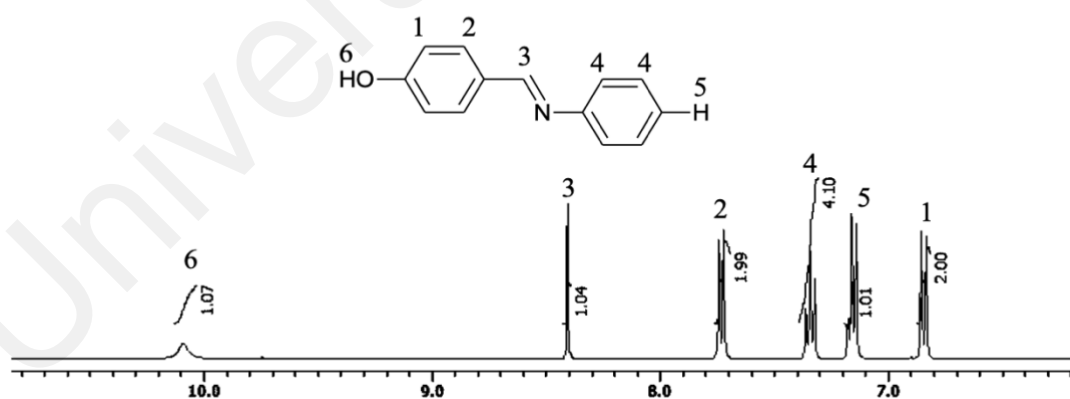


Figure 4.9: ^1H NMR spectrum of compound **2**

Considering structural similarities among palm-based spacers, only ^1H NMR spectrum for lauric-based spacer will be discussed. As depicted in Figure 4.10, a triplet signal at 0.86 ppm (1) is assigned to the protons of terminal methyl group with two neighbouring

protons from the adjacent carbon. Whereas, for signals that resonate at the region of 1.25 to 2.58 ppm (2 – 4) are owing to the methylene protons of the flexible lauric acid chain. As for the aromatic protons, located at 7.18 (5) and 8.16 ppm (6), these peaks are highly de-shielded due to the anisotropic field of circulating π electrons from the phenyl ring.

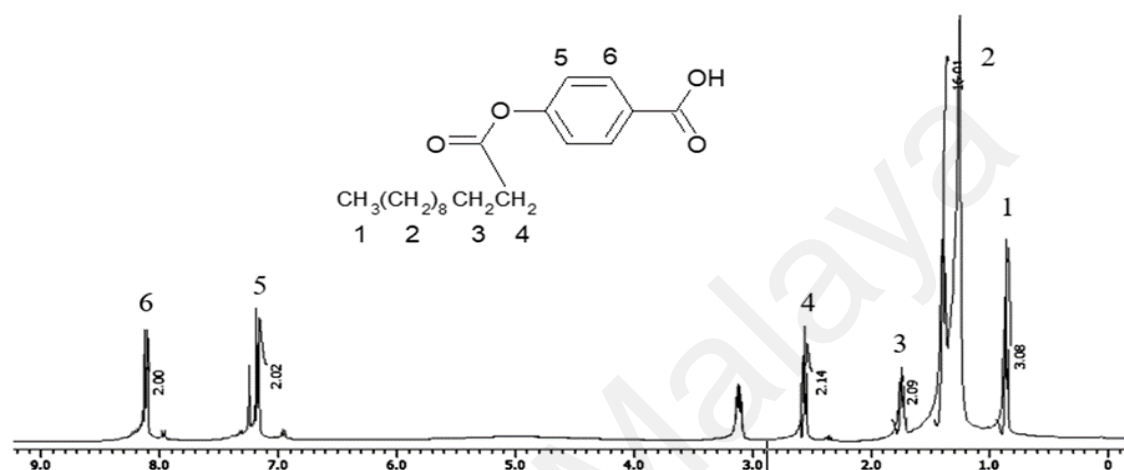


Figure 4.10: ^1H NMR spectrum of lauric-based spacer

Figure 4.11 illustrates the ^1H NMR spectrum of **PB1** with its molecular structure. The peak observed at 0.87 ppm (1) is assigned to the protons of the methyl group. While peaks that appeared between 1.27 to 2.59 ppm (2 – 4) are due to the protons of the methylene units from the flexible C16 acyl chain. Aromatic protons that resonate at the de-shielded region from 7.08 to 8.23 ppm (5 – 8 and 10 – 11) are attributed to the diamagnetic anisotropic field generated by the delocalized π electrons from the three disubstituted phenyl rings. A singlet that emerged at the most downfield region, 8.43 ppm (9), is due to the Schiff base proton. This proton experiences a strong de-shielding effect from the highly electronegative nitrogen atom as well as the π electrons from the double bond. The appearance of singlet is clearly due to the absence of adjacent protons. Taking into

account structural similarity, **PB2** and **PB3** exhibited similar ^1H NMR spectra as outlined for **PB1**.

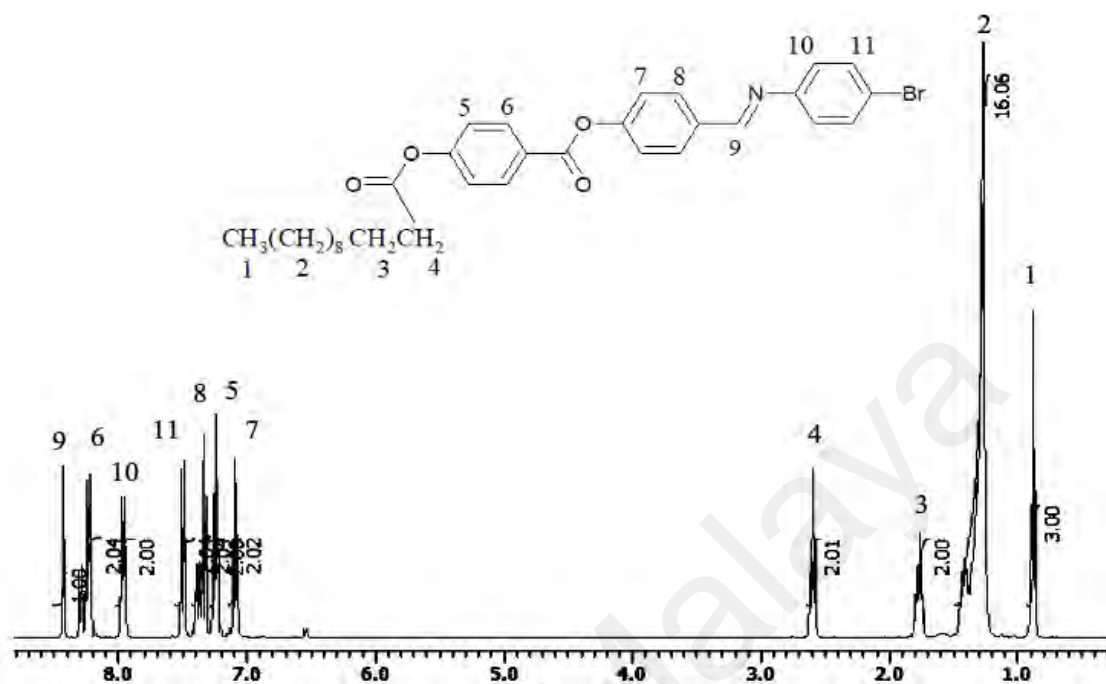


Figure 4.11: ^1H NMR spectrum for **PB1**

As **PB4** – **PB6** bear similar molecular structures except for the flexible palm fatty acid chain length, **PB4** was chosen as a representative for ^1H NMR spectral discussion (Figure 4.12). Owing to the electron-withdrawing effect of nitrogen atom, Schiff base proton appeared as a singlet at the most downfield region with chemical shift at 8.28 ppm (9). This is followed by aromatic protons which resonate at 7.07 to 7.96 ppm (5 – 8 and 10 – 12) region due to the circulating π electrons from the Schiff base and ester linked phenyl rings. In comparison with **PB1** – **PB3** series, the only structural difference of **PB4** – **PB6** series is the absence of terminal Br group, which results in a multiplet signal that can be seen at 7.07 ppm (12) for **PB4**. The protons of the methyl group and the methylene units can be observed at 0.86 ppm (1) and 1.23 – 2.58 ppm (2 – 4), respectively.

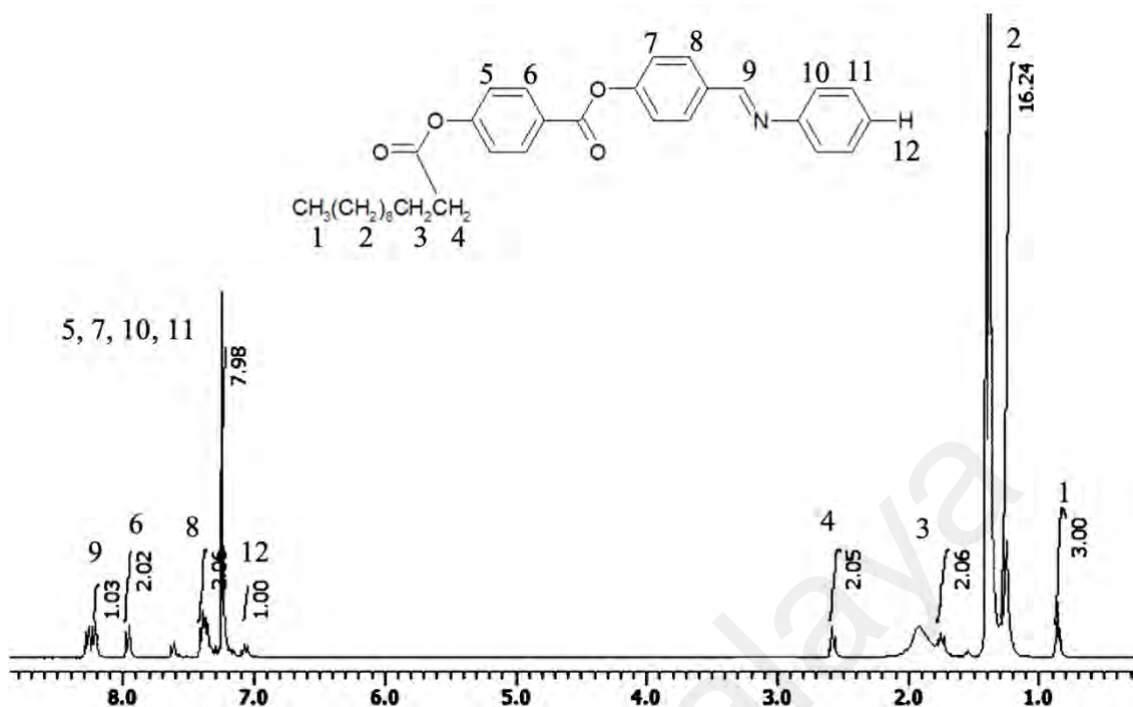


Figure 4.12: ¹H NMR spectrum for PB4

Figure 4.13 depicts the ¹H NMR spectrum of **PB7** together with its molecular structure. Signal that emerged as triplet (0.87 ppm) can be ascribed to the terminal methyl group (1), whereas methylene protons from the flexible lauric acid chain are resonating in the range of 1.26 – 2.56 ppm (2 – 4) with different multiplicity. While on the downfield region, under the influence of the electronegative nitrogen atom as well as the delocalized π system, Schiff base proton appeared at 8.39 ppm (7) following the aromatic protons at the region of 7.08 – 7.91 ppm (5, 6, 8 and 9). As **PB8** and **PB9** are structurally similar to **PB7**, their ¹H NMR spectral are parallel to **PB7**.

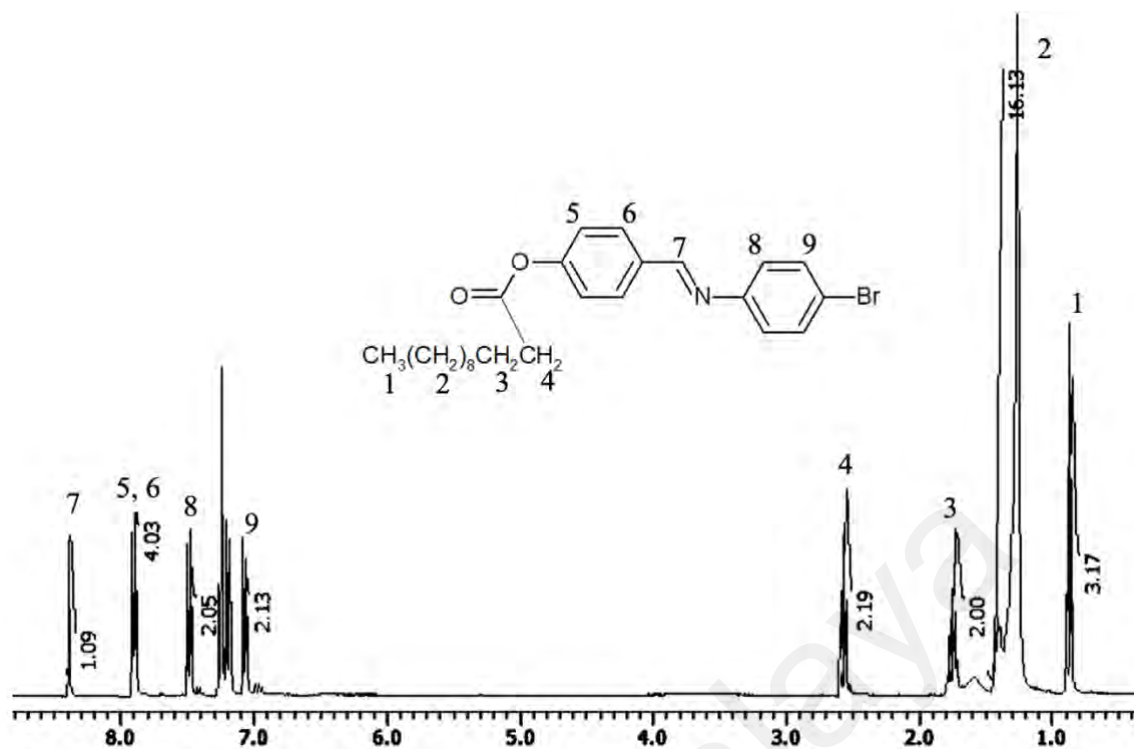


Figure 4.13: ¹H NMR spectrum for PB7

4.3.3 ¹³C NMR spectra

Carbon and hydrogen are the backbones of organic molecules. Therefore, it is crucial to study the magnetic behaviour of carbon nuclei under different chemical environments which subsequently helps to determine the molecular conformation of PBLCs.

Figure 4.14 presents the ¹³C NMR spectrum of **PB1** along with its molecular structure. Signals that emerged at the most downfield region, namely, at 171.80, 163.90 and 159.58 ppm are assigned to C7, C12 and C17, respectively. This is owing to the fact that these carbons are either attached to highly electronegative nitrogen and oxygen atoms and/or phenyl rings with delocalized π system. The anisotropic effect of sp² hybridization has resulted in aromatic carbons (C9, C10, C11, C14, C15, C16, C19, C20 and C21) appeared at a moderately high field region (116 – 134 ppm). Aromatic carbons that assigned as C8 (153.47 ppm), C13 (155.37 ppm) and C18 (150.87 ppm) were found to resonate at a higher chemical shift, and this can be attributed to the electron-withdrawing effect of oxygen and nitrogen atoms coupled with local diamagnetic current of π electrons from the phenyl rings. It is manifest that C8, C13, C16 and C18 possessed lower intensity than

comparison to **PB1-PB3** series, the unsubstituted analogues (**PB4-PB6** series) demonstrated almost identical ^{13}C NMR spectra except for the peaks that assigned as C19, C20 and C21 as shown in Figure 4.15 (^{13}C NMR spectrum of **PB4** as a representative). Both C19 and C20 were found to resonate at a lower chemical shift (more shielded) in lacking electron-withdrawing bromo group. Whereas, without the relativistic heavy-atom effect, the delocalized π system of the phenyl ring has contributed a significant deshielding effect around C21. As compared to **PB1-PB3** series, it is apparent that **PB7-PB9** series is lacking one phenyl ring with an ester group, therefore, the ^{13}C NMR spectra showed less signal counting as shown in Figure 4.16 (^{13}C NMR spectrum of **PB7** as a representative).

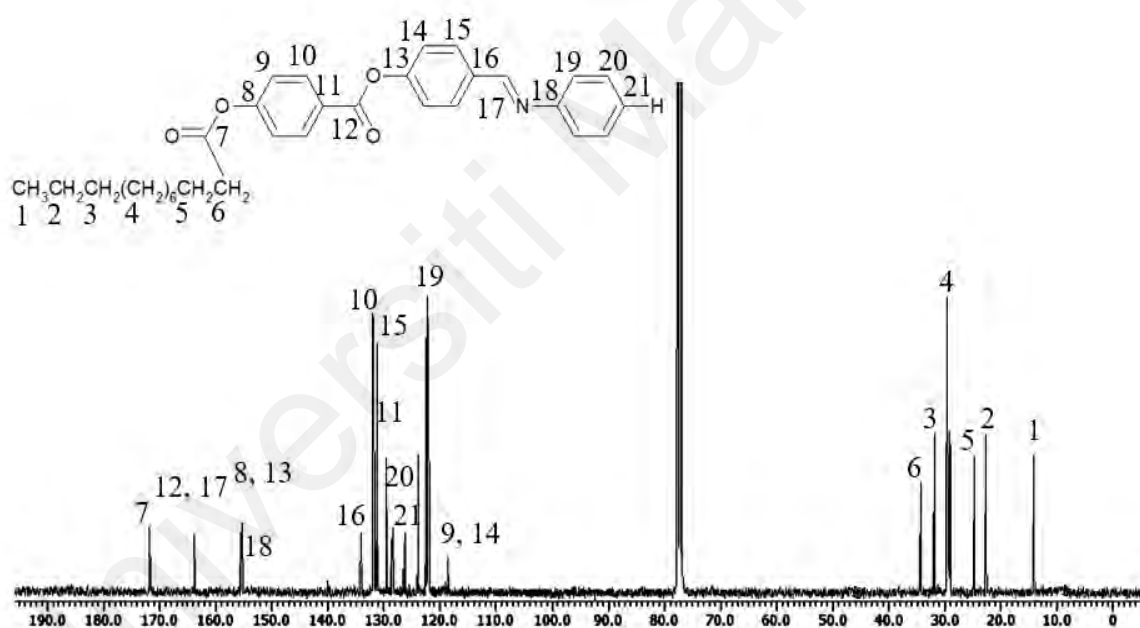


Figure 4.15: ^{13}C NMR spectrum for **PB4**

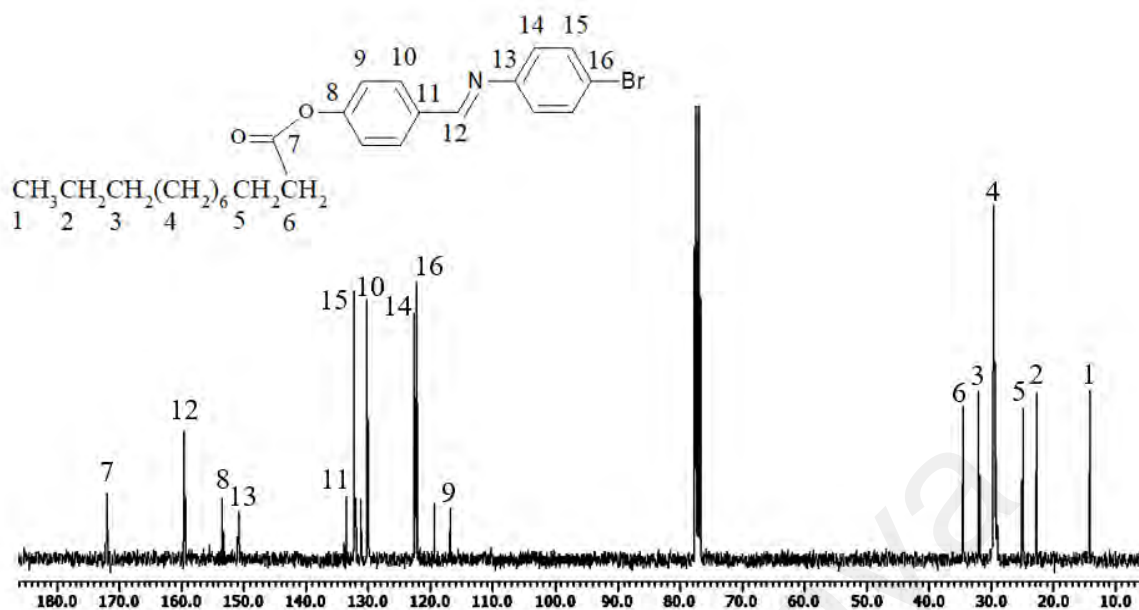


Figure 4.16: ^{13}C NMR spectrum for PB7

4.4 Thermal degradation of palm-based liquid crystals.

Thermogravimetric analyser (TGA) was employed to study the thermal degradation of all synthesized PBLCs. The measurement was done within the temperature range of 30 – 900°C with heating rate 20°C/min under nitrogen atmosphere. Figure 4.17 and Figure 4.18 present the TGA scans and their corresponding derivative thermogravimetric (DTG) curves, respectively.

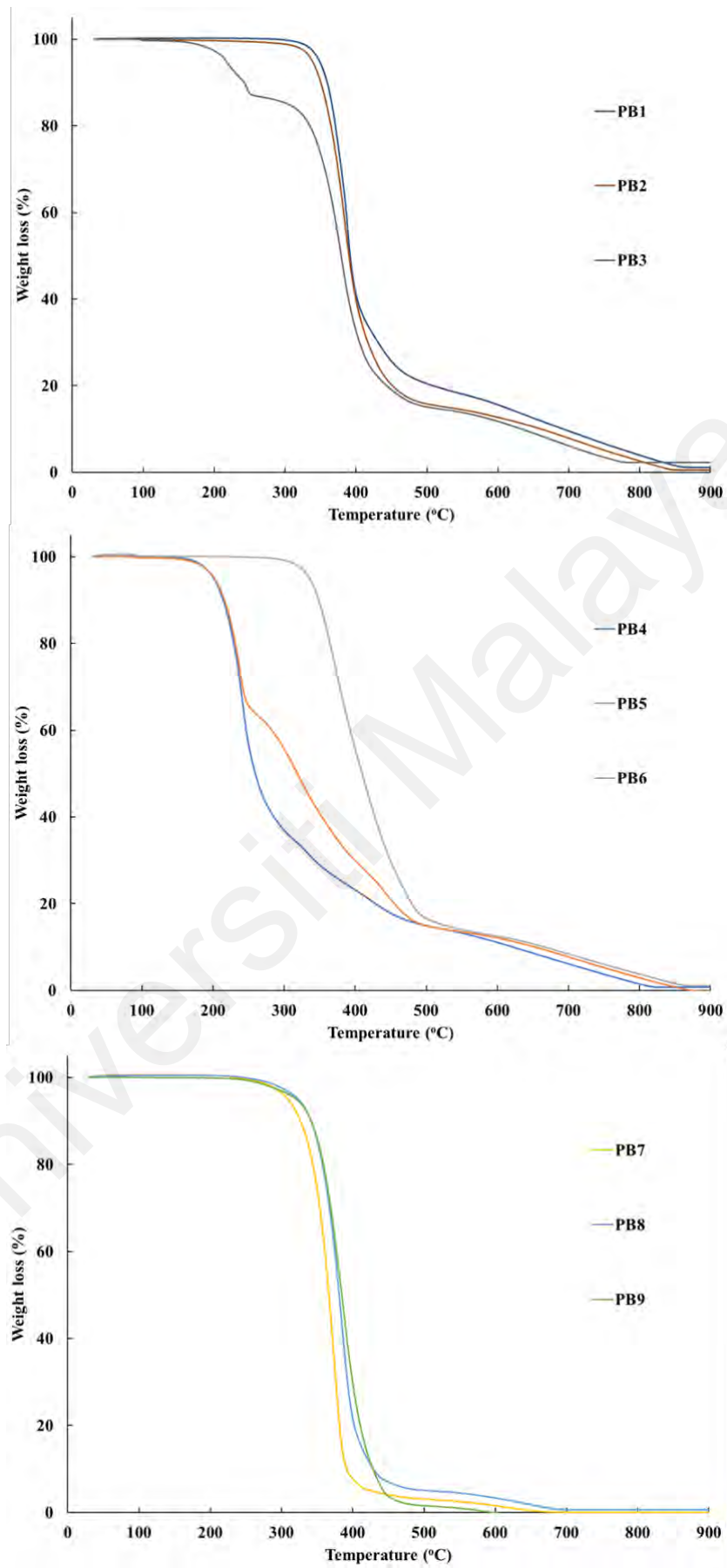


Figure 4.17: TGA scans for PBLCs

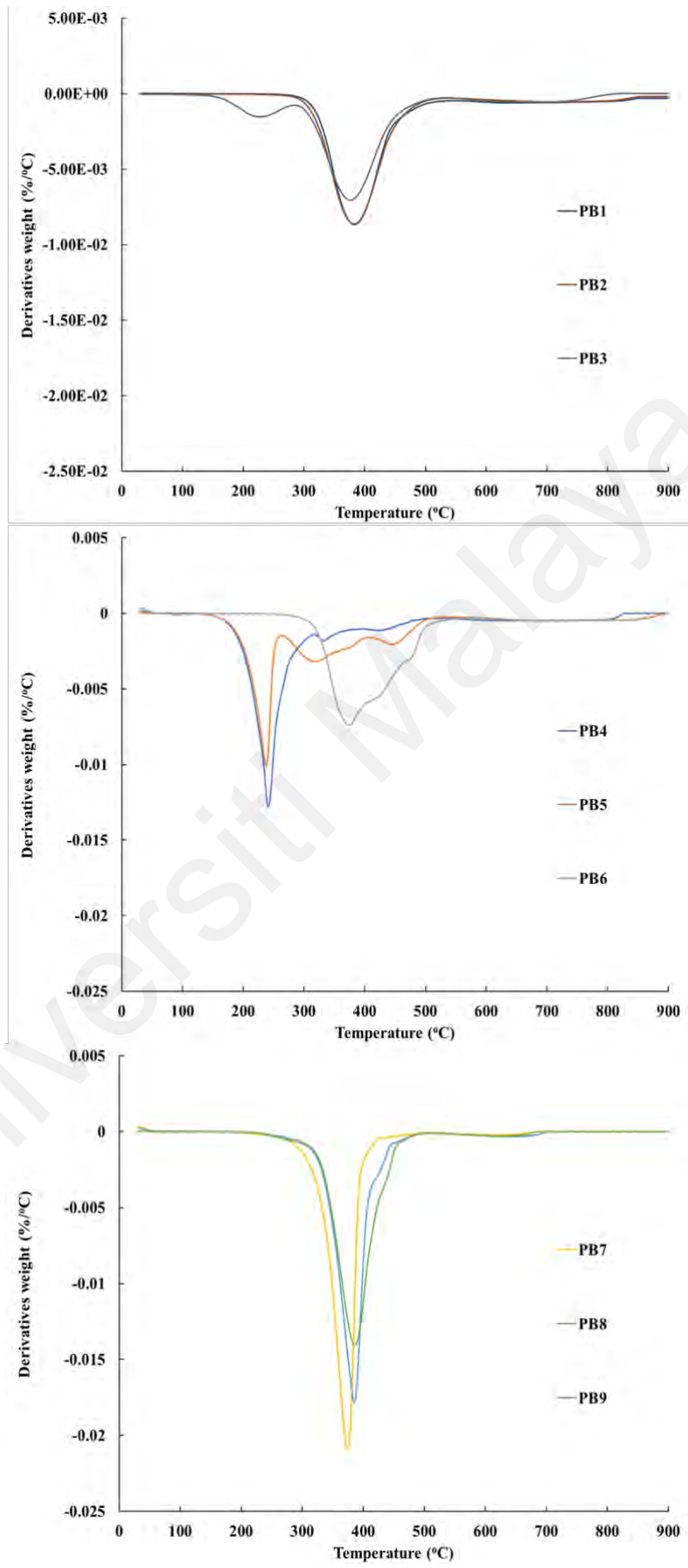


Figure 4.18: DTG curves for PBLCs

It is noted that **PB1**, **PB2** and **PB6 – PB9** exhibited a single-stage degradation within the temperature range of 267 – 530°C. On the contrary, **PB3** showed a 2-stage degradation whereas **PB4** and **PB5** were found to decompose in 3 different stages.

In the case of **PB4** and **PB5**, stage 1 decomposition involves the cleavage of the flexible palm fatty acid chain (lauric acid for **PB4**; palmitic acid for **PB5**) at a temperature range of 178 – 314°C. This is followed by second-stage degradation that occurred from 270 – 408°C which includes the thermal breakdown of Schiff base group, C-O bond and carbonyl group of ester linkage. Higher heat resistant of ester and Schiff base linkages is not only because of strong bond energy but also due to the appearance of charge-separated resonance structure of ester group. Owing to the overlapping of π and σ bonds, much energy required for the decomposition of aromatic moiety which resulted in a higher temperature range, 405 – 517°C. This can be identified as the final stage of degradation.

PB3 consists of chemical moieties similar to that of **PB4** and **PB5**, it underwent a 2-stage degradation instead of 3 stages. This phenomenon may be due to the presence of a terminal bromo group that tends to elevate overall molecular polarizability which subsequently induced stronger intermolecular attraction. As a result, the amount of energy needed would have been sufficient to decompose the flexible stearic acid chain, both ester and Schiff base linkages as well as the aromatic rings in one stage (310 – 530°C). The earlier stage of degradation that took place at a range of 200 – 280°C can be ascribed to the breakdown of the heavy terminal bromo group.

As for **PB1** and **PB2**, both decomposed in a single-stage degradation which covers a temperature range of 330 – 530°C. This can be attributed to fact that both structures are highly rigid (shorter flexible chain length as compared to **PB3**) with high molecular polarizability (due to the presence of bromo group). Similar explanation can be applied to **PB7 – PB9** in which the decomposition occurred in one stage (267 – 500°C). Given

the fact that **PB7 – PB9** series is having one less phenyl ring together with an ester group, the overall decomposition temperature range appeared to be lower than **PB1** and **PB2**. Although **PB6** has no bromo group attached, the long flexible palm fatty acid chain length causes it to decompose in one stage as the energy needed to breakdown the additional methylene groups would have been enough to decompose the rest of the structure.

Table 4.2 shows the quantitative values of temperature at 5% ($T_{d\ 5\%}$) and 50% ($T_{d\ 50\%}$) weight loss for all PBLCs. Taking $T_{d\ 5\%}$ as a benchmark for thermal stability, **PB1**, **PB2**, **PB6 – PB9** were found to have high thermal resistance as their corresponding $T_{d\ 5\%}$ is more than 300°C. For **PB3 – PB5**, nevertheless, they showed to exhibit a lower $T_{d\ 5\%}$ as shown in Table 4.2. In order to study the effect of compact terminal substituent, a comparison between **PB1 – PB3** (with terminal bromo group) and **PB4 – PB6** (without terminal bromo group) has been made. It was found that PBLCs with terminal bromo group are thermally more stable (see Table 4.2). This is due to the presence of bromo group in which the overall molecular polarizability can be enhanced and eventually leads to stronger intermolecular attraction. In comparison to **PB1 – PB3** (3-ring mesogenic core), it is evidenced that **PB7 – PB9** (2-ring mesogenic core with one less ester group) tend to exhibit lower $T_{d\ 5\%}$, 308.79 – 320.19°C. Clearly, with an additional phenyl ring (higher rigidity) and an ester group (higher polarizability), **PB1 – PB3** showed greater thermal resistance. Besides, thermal stability of PBLCs was found to be flexible chain length dependent. In general, thermal stability improves with longer fatty acid chain length. This is because longer chain length (higher number of methylene units) would require more energy to achieve 5% weight loss. This trend can be seen in **PB4 – PB6** series ($T_{d\ 5\%}$, 201.04 – 335.58°C) and **PB7 – PB9** series ($T_{d\ 5\%}$, 308.79 – 320.19°C). However, the opposite trend was observed for the series of **PB1 – PB3** in which the $T_{d\ 5\%}$ covers the range of 347.66 – 281.66°C. This could be due the antagonistic effect between the longer fatty acid chain length and the presence of heavy terminal bromo group. Longer

fatty acid chain length tends to reduce molecular rigidity and hence less energy needed to accomplish 5% weight loss with the removal of the heavy bromo group. The same elucidation can be used for the case of **PB9** which experienced a slight decline in T_d 5%, 320.19°C from 323.04°C for **PB8**.

Table 4.2: TGA data for PBLCs

PBLCs	Palm fatty acid	Mesogenic core unit	Linking group	Terminal group	Temperature (°C)	
					5% weight loss	50% weight loss
PB1	Lauric acid (C12)	3 phenyl rings	Schiff base ester	-Br	347.66	394.25
PB2	Palmitic acid (C16)				338.56	392.55
PB3	Stearic acid (C18)				281.66	381.75
PB4	Lauric acid (C12)	3 phenyl rings	Schiff base ester	-H	201.04	259.19
PB5	Palmitic acid (C16)				201.61	318.48
PB6	Stearic acid (C18)				335.58	409.13
PB7	Lauric acid (C12)	2 phenyl rings	Schiff base ester	-Br	308.79	366.37
PB8	Palmitic acid (C16)				323.04	380.62
PB9	Stearic acid (C18)				320.19	384.04

4.5 Mesomorphic behaviour of palm-based liquid crystals

This study has successfully synthesized and demonstrated the technical feasibility of producing palm-based liquid crystals (PBLCs). The liquid crystallinity of all synthesized PBLCs was evidenced by polarizing optical microscopy (POM), differential scanning calorimetry (DSC) and small-angle X-ray scattering (SAXS). Table 4.3 shows the phase transition temperatures, the associated enthalpy changes and mesophase range of all PBLCs obtained from DSC. Meanwhile, Figure 4.19 depicts the DSC thermograms of **PB1 – PB9**. First heating curve from DSC is usually omitted from the data as it was intended to remove thermal history as well as residual solvent. Therefore, only first cooling and second heating curves were illustrated in Figure 4.19 except for **PB3 – PB5** in which only first heating curve is available. This is by virtue of the phase transition temperature range of **PB3 – PB5** exceeded its thermal stability window (see Section 4.3) and hence, partial decomposition occurred upon first heating. Similar anomaly was observed in an article reported by Ha *et al.* (2010).

Table 4.3: Phase transition temperatures and associated enthalpy changes of PBLCs on heating and cooling runs at a scan of 10°C min⁻¹ by DSC. The phase identity was determined from POM

PBLCs	Palm fatty acid	Mesogenic core unit	Terminal group	Scan	Phase transition temperature, (°C) [enthalpy changes, J g ⁻¹]	Mesophase range (°C)
PB1	Lauric acid (C12)	3-ring Schiff base ester	-Br	Heating	Cr ₁ 99.74 [24.76] Cr ₂ 124.50 [6.47] SmA 254.36 [3.39] I	129.86
				Cooling	I 260.96 [2.95] SmA 103.16 [0.78] Cr ₂ 82.10 [13.65] Cr ₁	157.80
PB2	Palmitic acid (C16)			Heating	Cr 103.83 [64.33] SmA 218.13 [12.60] I I 222.82 [12.88] SmA 103.25 [3.99] Cr ₂ 88.96 [58.86] Cr ₁	114.30
				Cooling		119.57
PB3	Stearic acid (C18)			Heating	Cr 101.84 [87.65] SmA 199.90 [12.02] I	98.06
				Cooling	No cooling data provided due to partial decomposition	-
PB4	Lauric acid (C12)	Heating	Cr 142.66 [11.49] SmA 243.46 [54.62] I	100.80		
		Cooling	No cooling data provided due to partial decomposition.	-		
PB5	Palmitic acid (C16)	Heating	Cr ₁ 87.49 [4.79] Cr ₂ 102.75 [42.38] SmA 193.79 [9.19] I	91.04		
		Cooling	No cooling data provided due to partial decomposition.	-		
PB6	Stearic acid (C18)	Heating	Cr 104.36 [74.31] SmA 154.63 [7.03] I	50.27		
		Cooling	I 152.45 [7.41] SmA 83.31 [67.14] Cr	69.14		

Table 4.3, continued

PB7	Lauric acid (C12)	2-ring Schiff base ester	-Br	Heating	Cr ₁ 91.47 [68.24] SmA 110.11 [14.89] I	18.64
				Cooling	I 108.31 [15.15] SmA 89.24 [5.69] Cr ₂ 34.10 [26.85] Cr ₁	19.07
PB8	Palmitic acid (C16)			Heating	Cr 97.76 [96.48] SmA 109.39 [15.53] I	8.36
				Cooling	I 103.72 [17.29] SmA 84.02 [6.18] Cr ₂ 62.20 [88.05] Cr ₁	19.70
PB9	Stearic acid (C18)			Heating	Cr 106.31 [141.80] I	-
				Cooling	I 107.49 [19.06] SmA 79.75 [118.64] Cr	27.74

Abbreviation: Cr = crystal; I = isotropic liquid; SmA = smectic A; - = no mesophase range was measured.

Universiti Malaysia

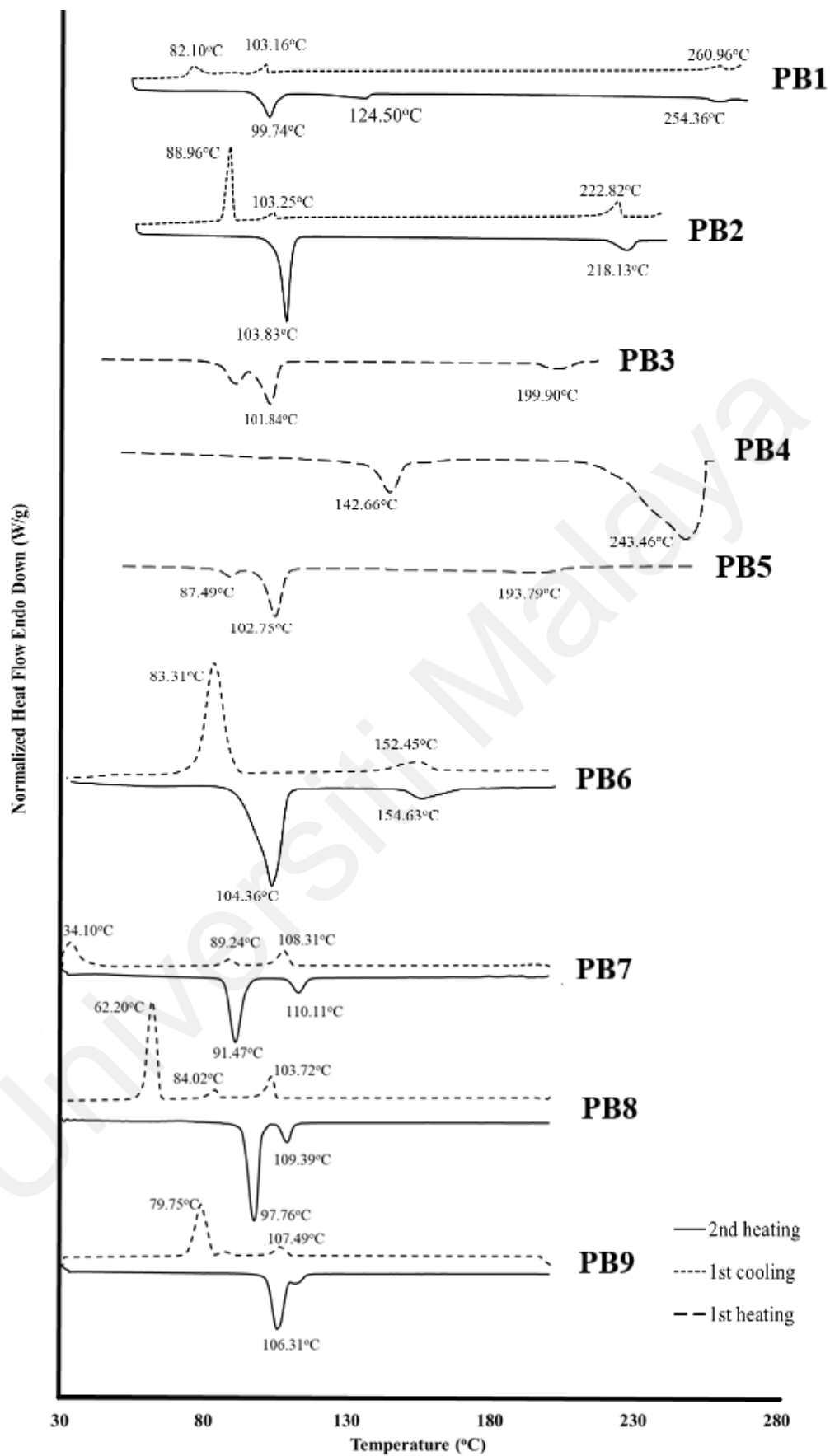


Figure 4.19: DSC thermograms for PBLCs

As shown in Figure 4.19, **PB2** showed to exhibit two endothermic peaks upon heating. The first peak that appeared at the lower temperature end (103.83°C) indicates crystal to mesophase transition with an associated enthalpy change of 64.33 J g^{-1} . The value of enthalpy change implies that a considerable amount of energy has been absorbed to overcome majority of intermolecular attractions within the rigid crystalline structure which consequently resulted in a smaller enthalpy change (12.60 J g^{-1}) for the transition of mesophase into isotropic liquid. This is because only small amount energy needed to disrupt the short-range orientational order of molecules (mesophase) into random molecular ordering (isotropic liquid). Likewise, upon cooling, transition from isotropic liquid to mesophase was noted at 222.82°C with an enthalpy change of only 12.88 J g^{-1} . This is followed by a crystallization peak that emerged at 103.25°C . An additional exothermic peak was observed at 88.96°C with a larger enthalpy change (58.86 J g^{-1}). This could probably be due to a crystal-to-crystal transition rather than a possibility of having another mesophase and it can be verified through the images observed under POM. Figure 4.20 shows the mesophase texture of **PB2** upon cooling. A typical focal conic fan-shaped of SmA phase together with homeotropic texture (dark area) was identified when temperature cooled from 224 to 201°C and to 196°C (see Figure 4.20(a) and Figure 4.20(b), respectively). The dark area observed can be attributed to the homeotropic alignment of liquid crystal molecules under polarized light. As shown in Figure 4.20(c), a hybrid texture of SmA phase and crystalline solid was clearly observed at 90°C whereas a pure crystalline structure appeared at 85°C (see Figure 4.20(d)).

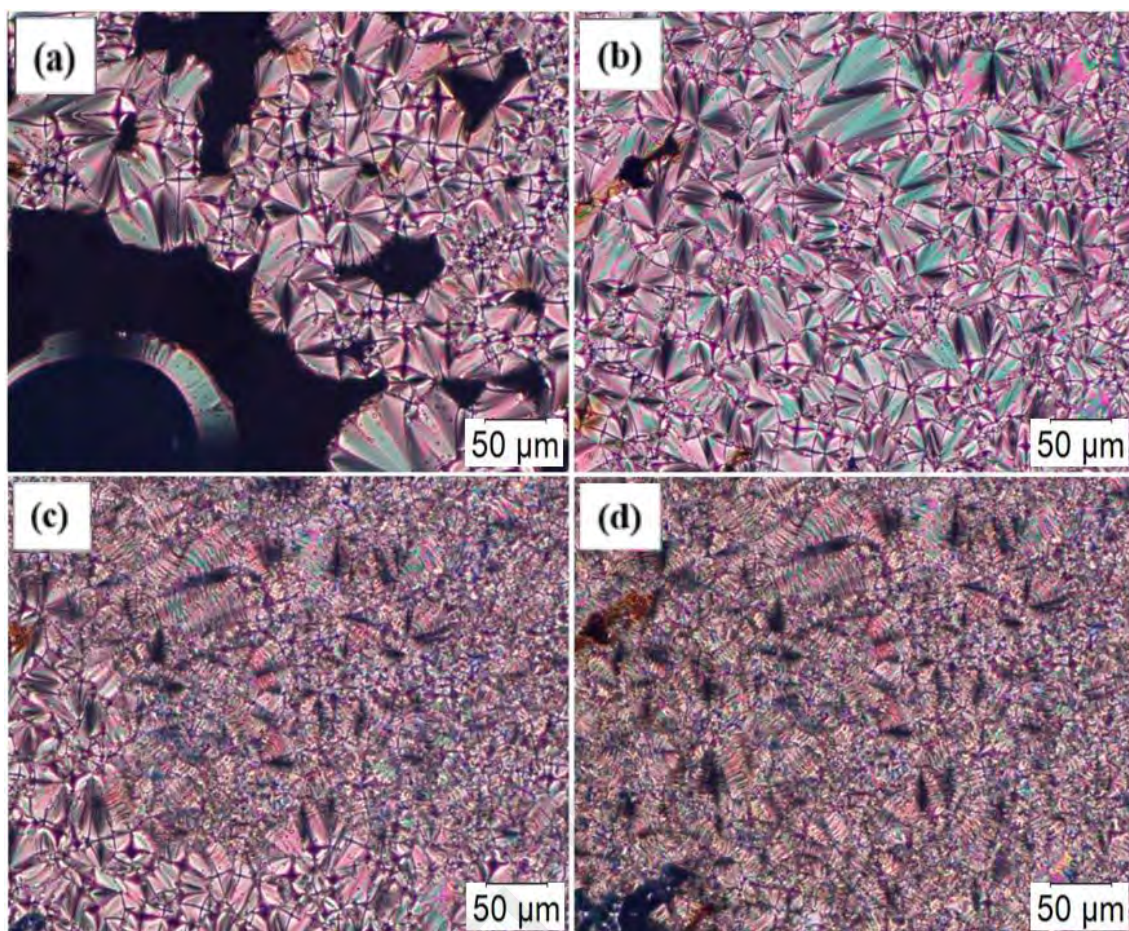


Figure 4.20: POM textures of PB2 upon cooling: (a) SmA phase with focal conic fan-shaped and homeotropic textures at 201°C, (b) SmA with focal conic fan-shaped texture at 196°C, (c) transition from SmA phase to crystalline structure at 90°C, (d) crystalline structure at 85°C

Within the same series, **PB1** consists of a rather similar DSC thermogram in which three exothermic peaks were observed upon first cooling. Nonetheless, upon second heating, a direct transition from crystal to mesophase was noted without going through a crystal-to-crystal transition as seen in **PB2**. **PB1** showed to display a wider mesophase range (157.80°C upon cooling) than **PB2** (119.57°C) and this may be due to the difference in palm fatty acid chain length which will be discussed further in Section 4.6. As for **PB3**, due to partial decomposition, only first heating was recorded. Similar to **PB1**, a direct transition from crystal to mesophase was observed at 101.84°C and followed by isotropization at 199.90°C. Owing to its longest flexible palm fatty acid chain length (C18) within the series of **PB1** – **PB3**, the mesophase range of **PB3** was found to be the

least stable (see Section 4.6 for further discussion). Under POM analysis, both **PB1** and **PB3** showed similar mesophase texture as **PB2** which is the typical focal conic fan-shaped of SmA phase (see Figure 4.21 and Figure 4.22, respectively).

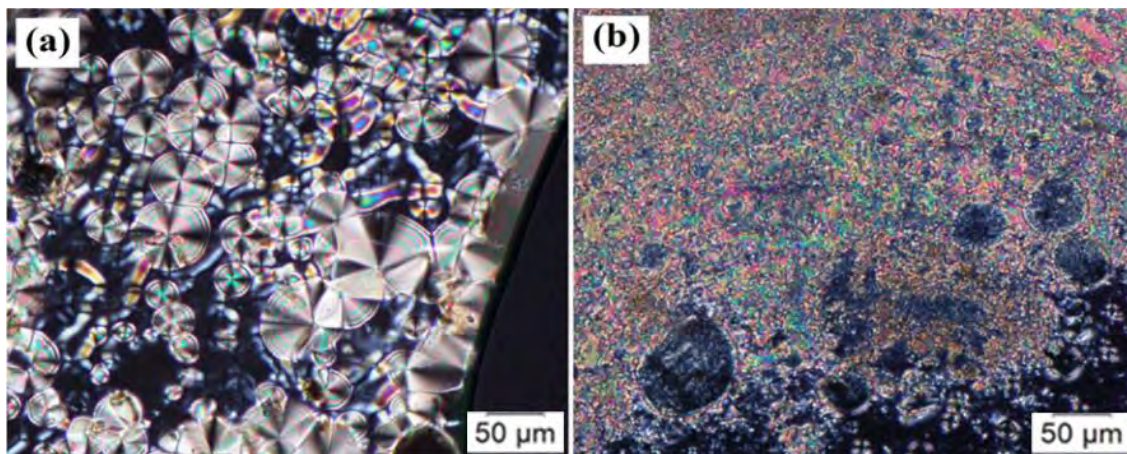


Figure 4.21: POM textures of PB1 upon heating: focal conic fan-shaped of SmA phase at (a) 254°C, (b) 224°C

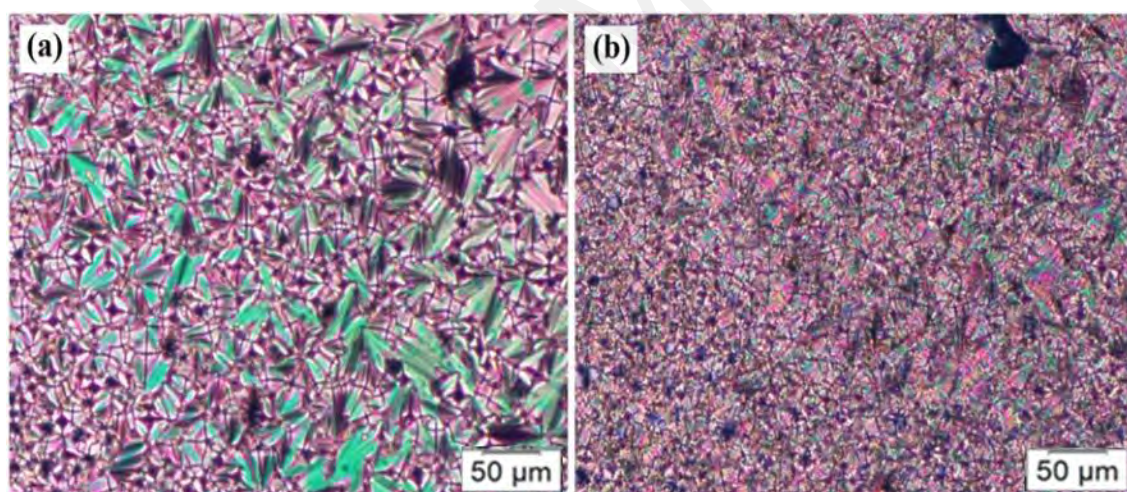


Figure 4.22: POM textures of PB3 upon cooling: (a) focal conic fan-shaped of SmA phase at 203°C, (b) crystalline structure at 50°C

It is convinced that **PB5** has undergone partial degradation at isotropization (193.79°C) during the first heating in DSC thermal analysis since it decomposes with 5% weight loss at 201.61°C. Hence, only first heating data will be discussed. As shown in Figure 4.19, the thermogram of **PB5** showed three endotherms which reflects crystal-to-crystal transition at 87.49°C, the appearance of mesophase at 102.75°C (melting) and clearing to isotropic liquid at 193.79°C. It is manifest that melting of **PB5** involved greater enthalpy

change (42.38 J g^{-1}) than that of clearing (9.19 J g^{-1}). This is because less energy is needed to disrupt mesophase that has less rigid molecular arrangement than its corresponding crystal structure. The phase transition temperatures were found to be in good agreement with POM analysis. Figure 4.23(a) illustrates the batonnets texture of smectic phase upon cooling at 147°C which then coalesce into focal conic fan-shaped of SmA phase at 138°C as shown in Figure 4.23(b). The crystal structure of **PB5** at 97°C and 86°C are presented in Figure 4.23(c) and Figure 4.23(d), respectively. Within the same series as **PB5**, **PB4** and **PB6** showed similar POM textures as presented in Figure 4.24 and Figure 4.25, respectively. As shown in Figure 4.25(b), crystalline structure of SmA phase was observed at 75°C and this is accordant with the phase transition temperature reported by DSC at which crystallization occurred at 83.13°C upon cooling.

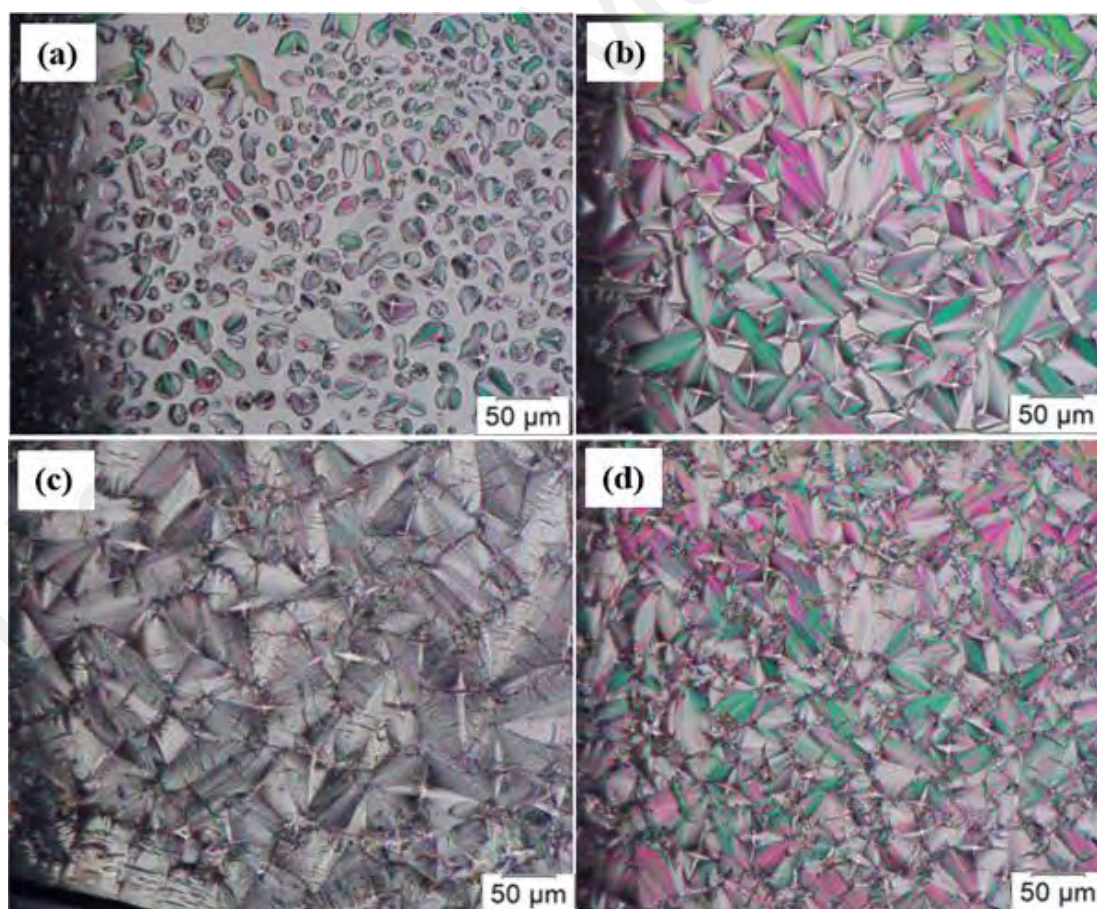


Figure 4.23: POM textures of PB5 upon cooling: (a) batonnets structure at 147°C , (b) SmA with focal conic fan-shaped at 138°C , (c) crystalline structure at 97°C , (d) crystalline structure at 86°C

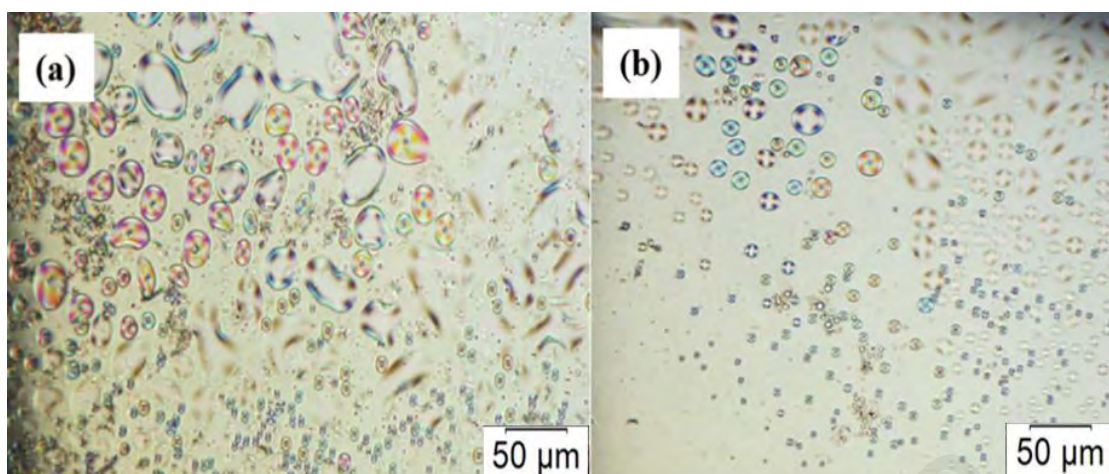


Figure 4.24: POM textures of PB4 upon cooling: smectic droplets at (a) 162°C, (b) 224°C

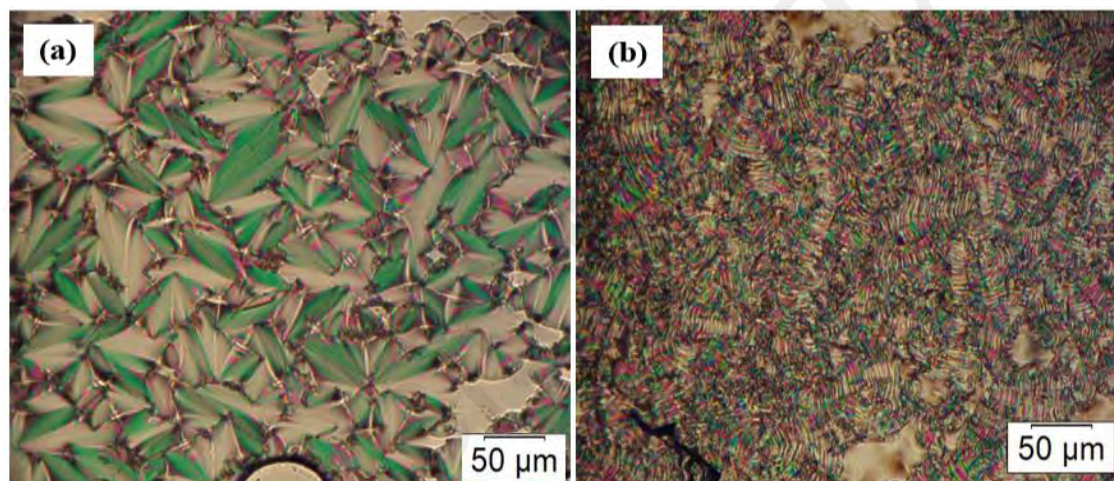


Figure 4.25: POM textures of PB6 upon cooling: (a) focal conic fan-shaped of SmA phase at 144°C, (b) crystalline structure at 75°C

From DSC analysis, the phase transition temperatures of **PB4** upon first heating (see Figure 4.19) was found to have one less endothermic peak as compared to **PB5**. This is because, without an additional crystal phase, **PB4** experienced a direct transition from crystal to mesophase at 142.66°C with an enthalpy change of 11.49 J g⁻¹. Theoretically, clearing of mesophase should involve smaller enthalpy change as less energy needed to disrupt short-range molecular ordering (mesophase) into random molecular arrangement (isotropic liquid). However, much higher enthalpy change was observed (54.62 J g⁻¹) at clearing point of **PB4**. This could be attributed to the partial decomposition process that occurred at isotropization. Although **PB4** – **PB6** shared similar molecular structure, with

a longer flexible palm fatty acid chain, **PB6** was found to be thermally more stable (as discussed in Section 4.4) in which transition temperature range is within its thermal stability window. Therefore, both first cooling and second heating thermograms can be retrieved from DSC analysis. Upon cooling, the phase transition temperatures, from isotropic to mesophase (152.45°C) and to crystallization (83.31°C) were conforming to its second heating cycle as shown in Figure 4.19. Nevertheless, the crystallization temperature (83.31°C) was found to be lower than its corresponding melting temperature (104.36°C) and this could be due to the supercooling effect (Rathgeber *et al.*, 2015). Similar to **PB1 – PB3** series, the mesophase range of **PB4 – PB6** appeared to be inversely proportional to palm fatty chain length. This will be further discussed in Section 4.6.

Since the molecular structures of **PB7 – PB9** are comparable with each other, it is anticipated that their mesomorphic behaviour will be rather similar. Nonetheless, as depicted in Figure 4.19, **PB9** exhibited a direct melting from crystal to isotropic liquid at 106.31°C whereas both **PB7** and **PB8** demonstrated liquid crystal phase upon heating. This phenomenon can be ascribed to fact that **PB9** possessed the longest flexible palm fatty acid chain (stronger cohesion between LC molecules) which require large amount of energy to disrupt its rigid crystalline structure and this in turn causes the short-range orientational order of mesophase to be disrupted entirely. It is for this reason that a huge enthalpy change (141.80 J g⁻¹) was recorded for the direct transition. As for **PB8**, instead of direct melting to isotropic liquid, a short mesophase range was observed upon heating (8.36°C) as it possessed a slightly shorter palm fatty chain than **PB9**. Upon cooling, however, the presence of an extra crystal phase has resulted in an additional exothermic peak at 84.02°C before clearing point at 103.72°C. In the case of **PB7**, the heating cycle composed of two endothermic peaks which appeared at 91.47°C (crystal to mesophase) and 110.11°C (clearing temperature) which resulted in a mesophase range of 18.64°C. While on the cooling cycle, similar transition peaks were observed with the exception of

an extra peak at 83.31°C wherein a crystal-to-crystal transition occurred. Interestingly, the mesophase range of **PB7 – PB9** showed to exhibit ascending trend upon cooling (see Table 4.3) which is in contrast with the other two series (**PB1 – PB3** and **PB4 – PB6**). This can be attributed to the structure-mesomorphic property relationship of PBLCs which will be discussed in Section 4.6. All DSC data presented are accordant with the transition temperatures observed under POM. SmA phase with focal conic fan-shaped was noted under polarized light for **PB7 – PB9** as shown in Figure 4.26. Taking **PB7** as an example, upon cooling down to 90°C which is below its crystallization point (91.47°C) reported by DSC, the SmA phase was in a transition to its corresponding crystal structure as shown in Figure 4.26(b). Conclusively, all PBLCs were found to be enantiotropic in nature as mesophase was observed during both heating and cooling cycles except for **PB9** in which mesophase can only be seen in the cooling cycle under POM.

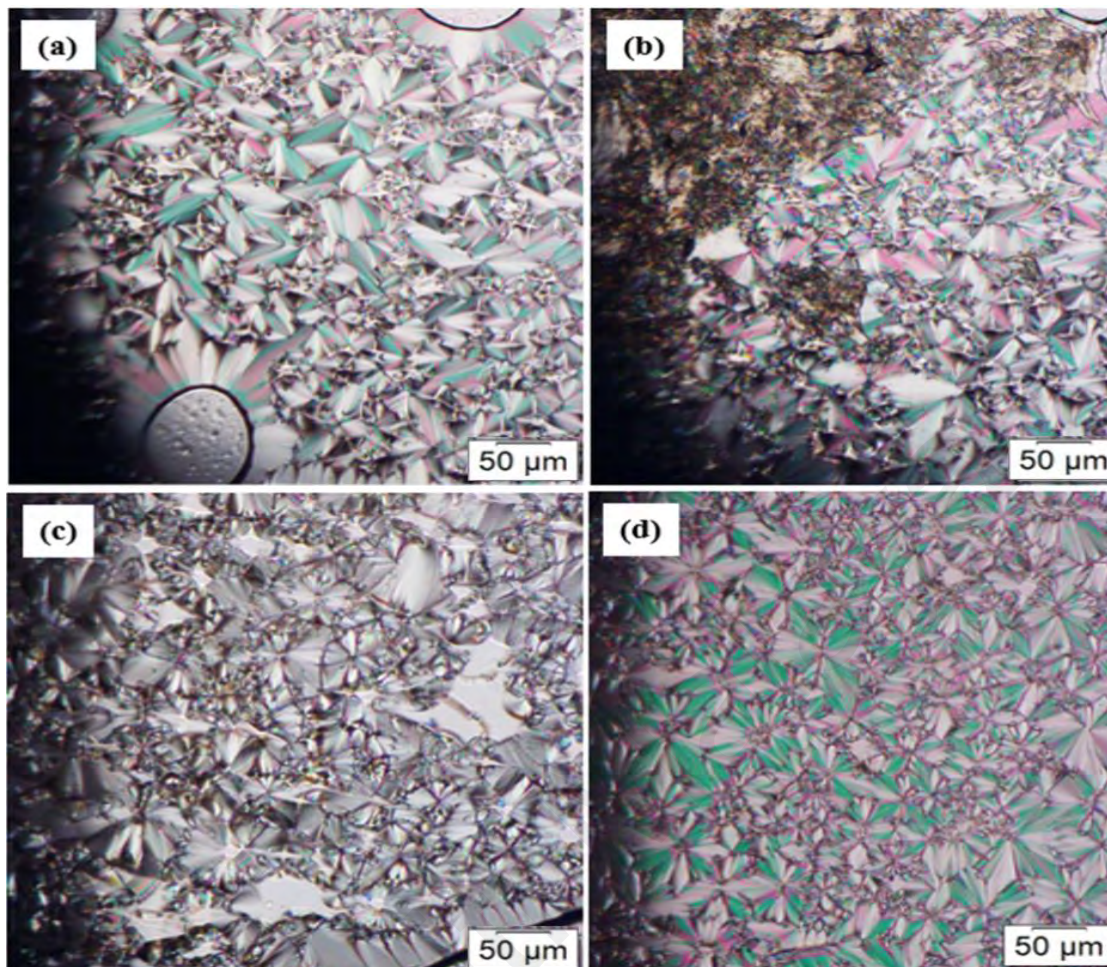


Figure 4.26: POM textures upon cooling: (a) focal conic fan-shaped of PB7 at 101°C, (b) transition of SmA phase to crystalline structure of PB7 at 90°C, (c) focal conic fan-shaped of PB8 at 90°C, (d) focal conic fan-shaped of PB9 at 104°C

Though both DSC and POM provide invaluable insight about the mesomorphic behaviour of PBLCs, SAXS analysis was used as a tool to further verify the type of mesophase present. The scattering pattern of each PBLC was recorded upon heating except for **PB9**. Owing to its monotropic nature, SAXS analysis for **PB9** was done upon cooling. All measurements were taken at a temperature within the mesophase range of each sample. Figure 4.27 shows the scattering profiles of **PB1** – **PB3** as representative. Sharp peaks that emerged at low q region ($1.3 - 2.0 \text{ nm}^{-1}$) implies that molecular ordering was in a typical smectic phase orientation (lamellar arrangement) (Mandle, 2016). In the lamellar arrangement of smectic phase, molecules can be organized in singular molecular layers or semi-bilayer and/or bilayer structures depending on the longitudinal force of

attractions between adjacent molecules. Typically, singular molecular layers arrangement exhibits layer spacing that is either smaller or equals to the molecular length of a LC molecule. However, due to the overlapping of molecules in a semi-bilayer or bilayer structure, the layer spacing is therefore greater than the molecule length of a single LC molecule (Foo *et al.*, 2014; Goodby *et al.*, 2008).

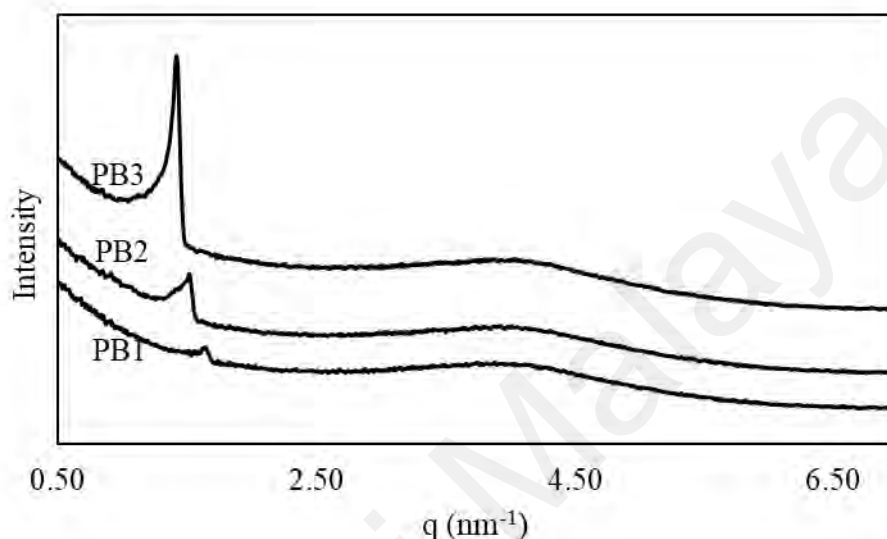
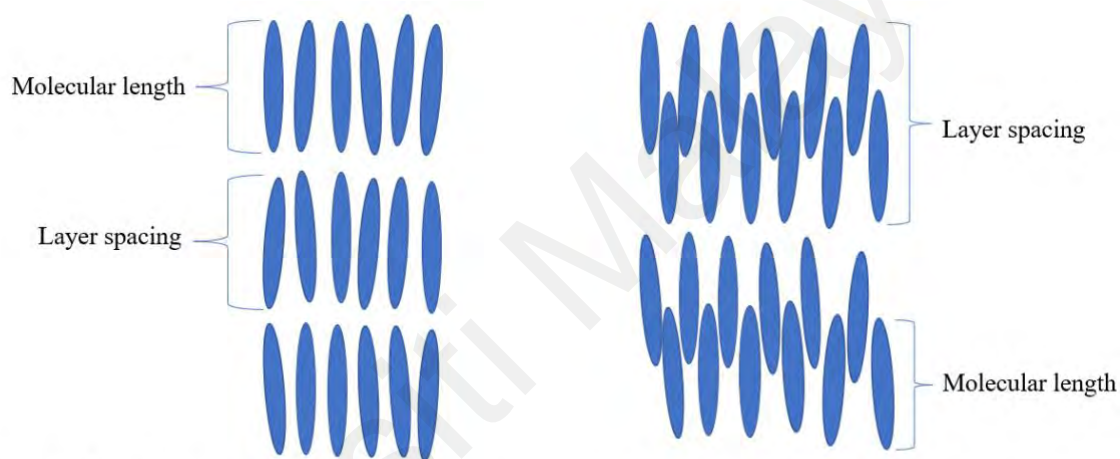


Figure 4.27: SAXS pattern of PB1 – PB3 at 180°C confirming SmA phase

Figure 4.28 shows the schematic representation of singular molecular layers and bilayer arrangement. A well-defined layer spacing for all PBLCs was obtained from SAXS analysis as shown in Table 4.4. Furthermore, the estimated molecular length of PBLCs from its most extended conformation was derived from ACD/Chemsketch software and is illustrated in Table 4.4 for comparison purposes. In general, it is manifest that the layer spacing of PBLCs is larger than its corresponding molecular length and this can be ascribed to the ether oxygen of ester linkages is in conjugation with the Schiff base unit, aromatic rings of the mesogenic core and the polar terminal bromo group (except for **PB4 – PB6**) and hence strengthening the longitudinal dipole which resulted in out-of-layer fluctuations (Sales *et al.*, 2020). Out-of-layer fluctuations give rise to an interdigitated bilayer structure which composed of an antiparallel arrangement of PBLC molecules with the overlap of mesogenic cores (Dąbrowski, 2015; Hagar *et al.*, 2019b;

Kumar, 2001). With such molecular orientation, the repulsion force between PBLC molecules can be minimized (stronger lateral force of attraction between mesogenic cores) and subsequently allows the flexible palm fatty acid chains to fill up more spaces while reducing void volume in molecular packing. As a result, mesophase stability could be enhanced (Goodby *et al.*, 2015). A diffused broad peak that was observed at a higher q region ($3.5 - 4.5 \text{ nm}^{-1}$) (see Figure 4.27) indicates the existence of only short-range order of molecular packing which is also a typical characteristic of SmA phase (Goodby *et al.*, 2008).



Smectic A phase in singular molecular layers

Smectic A phase in bilayer structure

Figure 4.28: Schematic representation of singular molecular layers and bilayer structure

Table 4.4: Layer spacing and estimated molecular length of PBLCs

PBLCs	Mesogenic core unit	Linking group	Terminal group	Estimated molecular length (nm)	Layer spacing (nm)
PB1	3 phenyl rings	Schiff base ester	-Br	3.310	3.815
PB2				3.761	4.136
PB3				4.091	4.404
PB4	3 phenyl rings	Schiff base ester	-H	3.364	4.184
PB5				3.859	4.091
PB6				4.042	4.389
PB7	2 phenyl rings	Schiff base ester	-Br	2.702	2.994
PB8				3.167	3.435
PB9				3.440	3.803

4.6 Structure-mesomorphic property of palm-based liquid crystals

There is no fast way to accurately determine the presence of mesophase or its type by merely examining the chemical structure. Mesophase can only be determined and confirmed experimentally as discussed previously, by using DSC, POM and SAXS. Although some extent of insights on the structure-mesomorphic property relationship has been reported, there is still some gaps to be filled because there are too many combinations of chemical moieties that can make up a LC molecule. This section presents some findings on the structure-mesomorphic property relationship based on the designed and characterized in the present study.

It is well documented that the mesomorphic behaviour of a calamitic LC molecule is heavily reliant on its molecular architecture. As discussed in Section 4.1, PBLCs synthesized in the present study can be classified into three different series, namely, **PB1 – PB3** series (3-ring Schiff base ester-based LCs with terminal bromo group), **PB4 – PB6** series (unsubstituted analogues of **PB1 - PB3**) and **PB7 – PB9** series (2-ring Schiff base ester-based LCs with terminal bromo group) (see Figure 4.29). All three series of PBLCs were incorporated with different chain length of palm fatty acids (lauric acid (C12), palmitic acid (C16) and stearic acid (C18)).

PBLCs

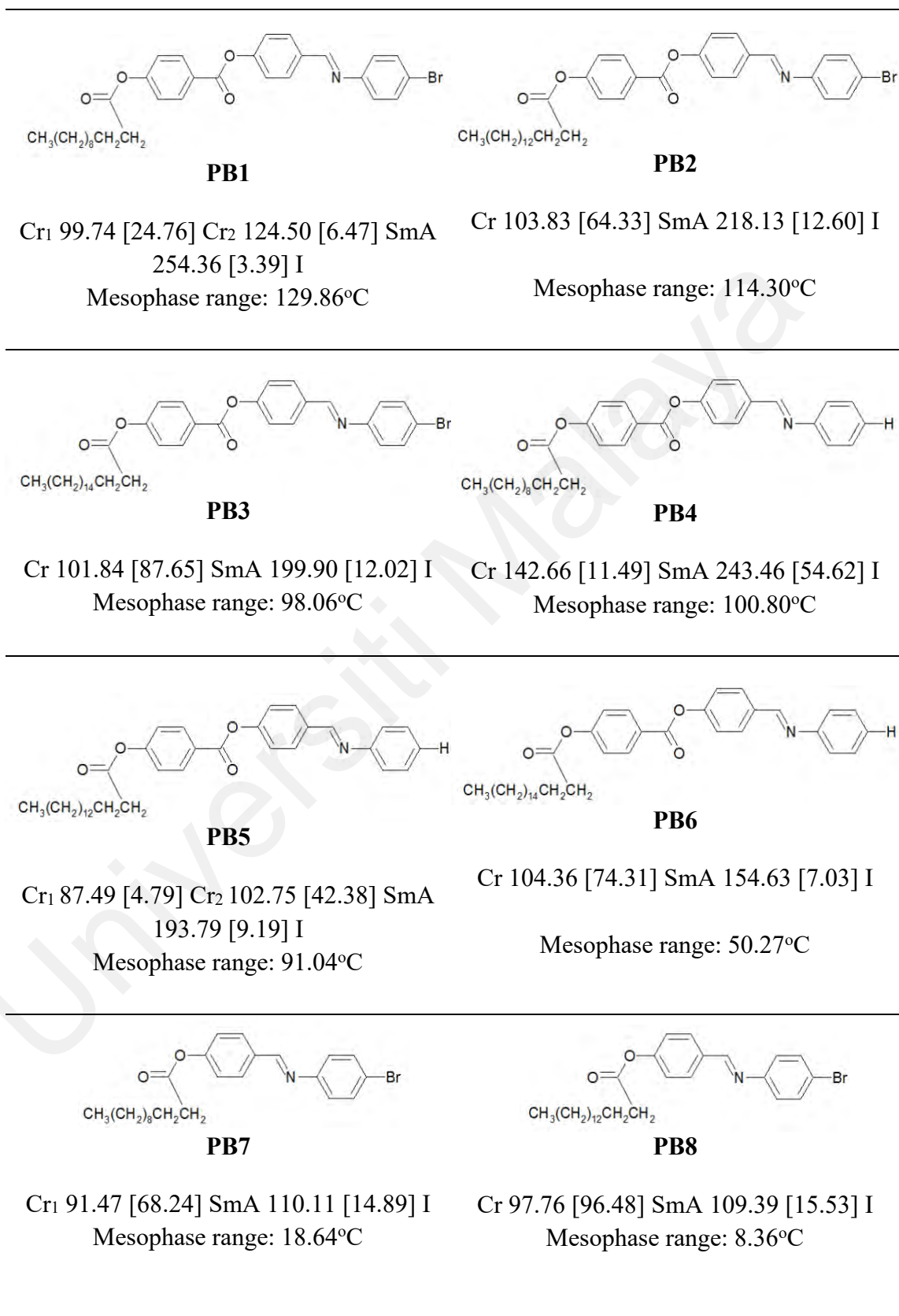
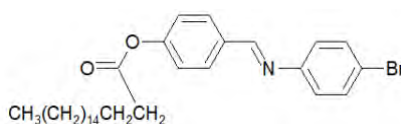


Figure 4.29: Chemical structures, phase transition temperatures and mesophase range of PBLCs



PB9

I 107.49 [19.06] SmA 79.75 [118.64] Cr
 Mesophase range: 27.74°C

Figure 4.29, continued

4.6.1 Effect of flexible palm fatty acid chain

The observed mesomorphic behaviour in Section 4.4 demonstrates that all PBLCs are smectogenic in nature wherein they exhibited only SmA phase. This could probably be due to the presence of long flexible palm fatty acid chain which reduces the rigidity of mesogenic core and thus preventing it from parallel molecular arrangement within the nematic phase but rather it favours lamellar packing of molecules in smectic phase (Foo *et al.*, 2014; Lim *et al.*, 2017). In addition, a direct transition from isotropic to smectic or smectic to isotropic without forming nematic mesophase can also be attributed to the long flexible palm fatty acid chain length (more than 8 carbons) (Hamad & Salih, 2017; Jamain *et al.*, 2020) which allows more attractions and intertwining between palm fatty acid chains. This in turn suppress nematic packing while promoting smectic phase (Yeap *et al.*, 2006b).

Figure 4.30 depicts a plot of phase transition temperatures upon heating against number of carbons in flexible palm fatty acid chain. It is evident that both melting and clearing temperatures were greatly altered by flexible palm fatty chain length. The melting points of **PB1 – PB3** series were found to decline with increasing fatty acid chain length and this may be attributed to the enhanced molecular flexibility (Ha & Lee, 2014). Similar trend was observed for clearing temperature in which **PB1** exhibited the highest clearing temperature, 254.36°C, followed by 218.13°C for **PB2** and **PB3** showed the lowest which is 199.90°C. This can be ascribed to the dilution of mesogenic core induced

by longer palm fatty acid chain length which subsequently weaken the mesophase stability. With both melting and clearing temperatures in a descending order, the mesophase range should be rather constant. However, the overall decrease in melting temperature (by 18.86°C) is far less than that of clearing temperature (by 54.46°C), this attribute to the phenomenon where mesophase range of **PB1 – PB3** decreased from 129.86°C to 98.06°C (see Table 4.3). SmA phase that exists over a broad temperature range could also be ascribed to the odd-even effect. This is because even number of carbons in the flexible palm fatty acid chain tends to instigate stronger intermolecular attractions due to higher molecular linearity which eventually stabilize lamellar packing of SmA phase (Bhat *et al.*, 2018; Chong *et al.*, 2016).

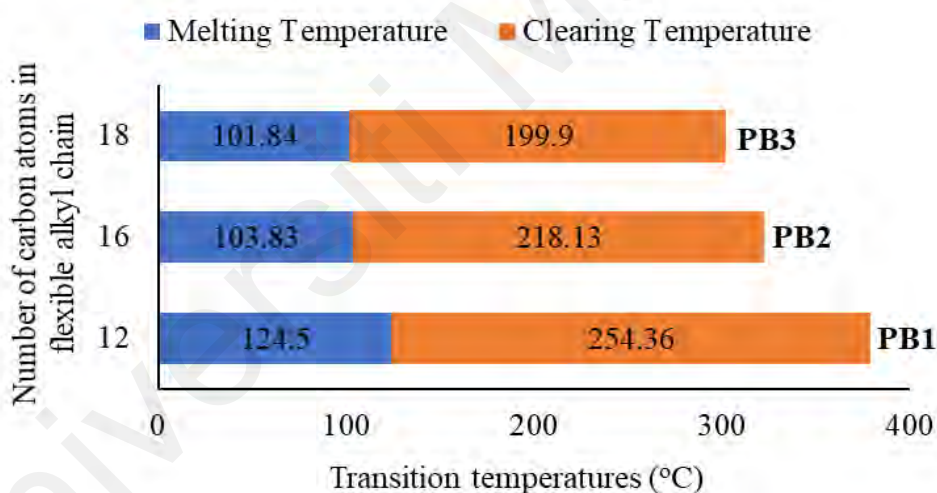


Figure 4.30: Plot of transition temperatures of PB1 – PB3 against the number of carbon atoms in flexible alkyl chain during the heating cycle

PB4 – PB6 series projected a similar trend as described for **PB1 – PB3** series as the only structural difference is the absence of terminal bromo group. With the absence of terminal bromo group, however, the mesophase range of **PB4 – PB6** (100.80°C, 91.04°C and 50.27°C, respectively) appeared to be shorter than that of **PB1 – PB3** (129.86°C, 114.30°C and 98.06°C, respectively). This could be due to the difference in molecular polarizability which will be discussed in Section 4.6.2.

Interestingly, a contradictory trend was observed for **PB7 – PB9**. With longer fatty acid chain length, mesophase range tends to be wider (19.07 – 27.74°C). This may be attributed to the synergistic effect between a shorter mesogenic core (2-ring Schiff base ester-based mesogen) and a longer flexible fatty acid chain length. Longer palm fatty acid chain length tends to induce stronger intermolecular cohesion forces while expecting smaller repulsive forces between shorter mesogenic core and consequently led to the enhancement of mesophase stability (Kapernaum *et al.*, 2009). The effect of mesogenic core structure on mesomorphic properties will be discussed further in Section 4.6.3.

4.6.2 Effect of compact terminal substituent

The overall inductive effect from a compact terminal substituent such as halogens can be regarded as an important determinant in mesophase stability. This is by virtue of the electron-withdrawing or electron-donating effect from the terminal substituent towards the mesogenic core system which ultimately promotes higher molecular polarizability (Begum *et al.*, 2013). With enhanced molecular polarizability, the molecular arrangement within mesophase can be sustained over a broader range of temperature (Hagar *et al.*, 2019c). In order to investigate the effect of compact terminal substituent, a comparison in terms of mesophase range has been made between **PB1 – PB3** (with terminal bromo group) and **PB4 – PB6** (the unsubstituted analogues). The presence of terminal bromo group has weakened the π electron density of the attached phenyl ring (due to electron-withdrawing effect) which subsequently enhance π - π stacking interactions between conjugated mesogenic cores (stronger intermolecular attractions). This phenomenon explains the wider mesophase range observed for **PB1 – PB3** (129.86 – 98.06°C) as compared to **PB4 – PB6** (100.80 – 50.27°C) (Mohammady *et al.*, 2021; Wheeler, 2013). Furthermore, owing to its larger atomic radius, the terminal bromo group can be polarized at ease (electrons are not strongly held by nuclear charge) (Yeap *et al.*, 2006a) and has

the tendency to promote asymmetrical characteristic of the LC molecules (Mieczkowski *et al.*, 2003). For that reason, the molecular orientation within the mesophase can be retained. The overall molecular polarizability between the two series (**PB1 – PB3** and **PB4 – PB6**) can be verified by referring to the calculated polarizability using the ACD/Chemsketch software as shown in Table 4.5. Indeed, the calculated polarizability of **PB1 – PB3** ($62.35 \pm 0.5 \times 10^{-24} - 73.31 \pm 0.5 \times 10^{-24} \text{ cm}^3$) is reasonably higher than **PB4 – PB6** ($59.35 \pm 0.5 \times 10^{-24} - 70.32 \pm 0.5 \times 10^{-24} \text{ cm}^3$). Similar findings were reported by Nafee *et al.* (2020) in which LC molecule with electron-withdrawing group as terminal substituent tends to exhibit wider mesophase range as a result of an increase in polar anisotropy.

Table 4.5: Polarizability value for PBLCs calculated from ACD/Chemsketch software

PBLC	Mesogenic core unit	Linking group	Terminal group	Polarizability value ($\pm 0.5 \times 10^{-24} \text{ cm}^3$)
PB1	3 phenyl rings	Schiff base ester	-Br	62.35
PB2				69.66
PB3				73.31
PB4	3 phenyl rings	Schiff base ester	-H	59.35
PB5				66.66
PB6				70.32
PB7	2 phenyl rings	Schiff base ester	-Br	49.68
PB8				56.99
PB9				60.65

4.6.3 Effect of mesogenic core structure

One can be considered as a versatile mesogenic core unit if the rigidity, linearity as well as the polarizability can be optimized. As discussed in Section 4.1, the intention of incorporating 3 and 2 disubstituted phenyl rings as mesogenic core unit for **PB1 – PB3** and **PB7 – PB9**, respectively, was to enhance the rigidity and linearity of PBLCs. On top of that, the inclusion of Schiff base group as linking unit is capable of providing a stepped core structure for higher linearity (Patel *et al.*, 2010). In addition, the presence of ester

linkage would help in promoting molecular polarizability due to the highly polarizable nature of carbonyl group (Collings, 1997). Taking mesophase range as a benchmark for mesophase stability, **PB7 – PB9** showed to exhibit less stable SmA phase (mesophase range: 19.07 – 27.74°C) than **PB1 – PB3** (mesophase range: 129.86 – 98.06°C). This could be due to the fact that **PB1 – PB3** has an additional phenyl ring which consequently promote higher linearity (increase in length-to-breadth ratio) and polarizability (due to the enhanced conjugated π system among aromatic rings). The same trend was observed in an investigation conducted by He *et al.* (2017) wherein mesophase range was suppressed with a decrease in length-to-breadth ratio. Besides, the presence of an extra ester linking unit in **PB1 – PB3** series has resulted in greater molecular polarizability and thus elevated cohesive forces between mesogenic core units. This is in favour of the interdigitated bilayer structure of SmA phase as previously discussed in Section 4.5. Clearly, as shown in Table 4.5, the calculated polarizability of **PB1 – PB3** ($62.35 \pm 0.5 \times 10^{-24} - 73.31 \pm 0.5 \times 10^{-24} \text{ cm}^3$) with an additional ester linkage was found to be much higher than **PB7 – PB9** ($49.68 \pm 0.5 \times 10^{-24} - 60.65 \pm 0.5 \times 10^{-24} \text{ cm}^3$). Therefore, the enhanced molecular rigidity, linearity and polarizability has led to a highly stable SmA phase.

In summation, the synthesis of application-driven LC materials with anticipated mesophases by introducing various chemical moieties is no doubt a complex topic to discuss in a single section. However, taking the literatures and the structure-mesomorphic property correlation of PBLCs that has been developed in this study, some idealized molecular architectures have been identified for the ease of accessing mesophase and to attain certain types of mesophase over a practical range of temperature (mesophase stability).

The foundational approach in assembling a molecule that shows liquid crystallinity is to gain a balance between rigidity and flexibility. Thus, a rigid mesogenic core that is

usually composed of multiple aromatic rings (connected through various linking groups) and a flexible terminal unit is inevitable. **PB4** that comprised of 3-ring Schiff base ester linked mesogen with a 12 carbons flexible palm fatty acid chain can be a basic template structure in accessing mesophase over a range of 100.80°C upon heating. The broad mesophase range observed can be attributed to the high linearity and rigidity of the mesogenic core (three well-conjugated aromatic rings interconnected by Schiff base and ester linkages). Schiff base linking group is well-known for its stepped core structure which preserve linearity (Patel *et al.*, 2010) and the presence of ester linkage is capable of promoting high molecular polarizability which can substantially improve mesophase stability (Ahmed *et al.*, 2020b; Mohiuddin *et al.*, 2017). As far as thermal stability of mesophase is concerned, the mesophase range can be further escalated with the introduction of terminal polar group. **PB1**, the bromo substituted analogues, was found to exhibit a wider mesophase range (129.86°C) than **PB4**. With the presence of bromine as terminal substituent, which is known to be highly polarizable in nature due to its larger atomic size and coupled with its electron withdrawing effect, the overall molecular polarizability as well as the π - π stacking interactions between mesogenic cores of LC molecules can be enhanced. As a result, the molecular orientation of mesophase can be retained over a wider range of temperatures.

LC materials have brought about a technological revolution in the field of information display, and little did one realize that the application of LC has also been extended to the biomedical field. As such, low melting point (low transition temperature to mesophase) LC molecules are apparently more practical. LC molecule with lower phase transition temperature can be synthesized by incorporating a longer terminal flexible unit or by introducing a less rigid mesogenic core (Aljamali *et al.*, 2021). Generally, in the present study, the melting point of PBLCs was found to be flexible chain length dependent. Taking **PB1 – PB3** series as an example, **PB3** with the longest palm fatty acid chain

length (18 carbons) showed the lowest melting temperature (101.84°C) whereas **PB1**, with 12 carbons palm fatty acid chain, transit into mesophase at 124.50°C. This can be attributed to the enhanced molecular flexibility and therefore favour the molecular arrangement of mesophase rather than its corresponding rigid crystal structure (Ha & Lee, 2014). Besides, melting point of LC molecule can also be reduced by incorporating a less rigid or a shorter mesogenic core while maintaining the same length of flexible unit. For instance, the melting point of **PB7** (2-ring Schiff base ester mesogen with 12 carbons palm fatty acid chain) is 33.03°C lower than that of **PB1** (3-ring Schiff base ester mesogen with 12 carbons palm fatty acid chain). Nonetheless, it is worthy of mention that though **PB7** exhibits lower melting temperature but the overall mesophase range has significantly reduced due to the decrease in linearity of the mesogen (mesophase range of **PB7** upon cooling: 19.07°C; mesophase range of **PB1** upon cooling: 157.80°C). Hence, it is recommended to embrace longer flexible unit while preserving high linearity and rigidity of the mesogenic core.

In anticipating the type of mesophase, an impression of having only smectic phase if a longer flexible unit is used in a LC molecule was given by the fact that all synthesized PBLCs were found to be monomorphic, only SmA phase was observed, with a minimum length of 12 carbons in the flexible palm fatty acid chain. Moreover, there are numerous studies indicating the same where a flexible chain length of more than 8 carbons in a calamitic LC molecule, smectic phase is favoured rather than nematic. (Alnoman *et al.*, 2019; Hamad & Salih, 2017; Jamain *et al.*, 2020). This is owing to the conformation of a LC molecule with long flexible alkyl chain that favour lamellar arrangement between molecules. Moreover, some studies also suggest that coupled with the effect of long flexible alkyl chain length, the presence of electron-withdrawing terminal group and Schiff linkage facilitate the formation of the smectic phase (Hagar *et al.*, 2018; Saad *et al.*, 2019).

Table 4.6 summarizes molecular structures and phase transition temperatures of **PB2**, **PB5**, **PB8** and along with structurally related compounds reported in the literature. It is no surprise that both **PB2** and compound **12** (Yeap *et al.*, 2006) shared similar mesomorphic behaviour as both molecules are identical. From the perspective of green chemistry, however, they are in fact beyond comparison. It is apparent that the use of renewable and non-toxic palm fatty acid as flexible moiety in **PB2** is capable of achieving similar mesomorphic properties as compound **12** in which its flexible moiety was made up of alkyl chain derived from non-renewable fossil fuel. Additionally, a greener activating agent, oxalyl chloride, was used in the synthesis of **PB2** rather than thionyl chloride that was proposed in the synthesis of compound **12**. The use of thionyl chloride could lead to the formation of toxic sulphur dioxide gas as by-product whereas a non-toxic CO₂ gas is expected from the utilization of oxalyl chloride.

In spite of structural similarity, **PB5** showed to exhibit different mesomorphic behaviour than compound **9** (Tiong Ha *et al.*, 2009). **PB5** showed a wider mesophase range than compound **9** by 42.5°C and instead of smectic A phase, compound **9** exhibited nematic phase. The differences in mesophase behaviour could, perhaps, owing to the use of palm fatty acid rather than petrochemical derived alkyl chain as flexible moiety and this has affirmed the fact that there is no way to identify the type of mesophase as well as its stability by just assessing the molecular structure. The mesomorphic properties can solely be determined experimentally using DSC, POM and SAXS.

Similarly, **PB8** showed a slightly wider smectic A phase than that of **16ABBA** (Ha *et al.*, 2012) and this could probably be due to the synthesis approach used. A milder Steglich esterification was proposed in the synthesis of **16ABBA** which uses dicyclohexylcarbodiimide (DCC) as a coupling agent. This would have led to the formation of dicyclohexylurea (DCU) as impurity which could have probably narrowed the mesophase range.

Table 4.6: Mesomorphic data of structurally related compounds

Compounds	Structure	Transition Temperature (°C)
PB2		Cr 103.83 SmA 218.13 I
Compound 12		Cr 104.60 SmA 232.3 I
PB5		Cr 103.83 SmA 218.13 I
Compound 9		Cr 99.70 N 171.50 I
PB8		Cr 84.02 SmA 103.72 I
16ABBA		Cr 94.35 SmA 107.13 I

4.7 Potential applications of palm-based liquid crystals

Palm-based liquid crystals (PBLCs) were synthesized with the utilization of non-toxic palm fatty acids as building block (in substitution of petrochemicals-derived flexible alkyl chain). This is in accordance with one of the research and development strategies of the palm oil industry whereby the value chain of palm-based products could be appreciated in various uses. Results reveal that all PBLCs are monomorphic, exhibiting only smectic A phase in both heating and cooling cycles (except for **PB9** which was found to be monotropic). In light of the stable SmA phase formed, PBLCs could offer exciting potential as a material in solving technological complications. The layers of bulk molecules in smectic phase have led to the appearance of unique curvatures and defects. These interesting morphologies can be applied in a vast range of applications such as toric focal conic domain (TFCD) arrays. The TFCD defects can be utilized as basic constituents for micro lens arrays, functional surfaces and soft lithography (Kim & Yoon, 2018). Curvatures in the biomedical field is just as important. For instance, the red blood cell is one of the examples of biological molecules with curvatures which allow gaseous exchange to take place. Besides, smectic liquid crystals have always been an ideal candidate in fabricating electronic devices owing to its layered packing of molecules which give rise to π - π stacking interactions. As a result, hopping of electrons can be facilitated which consequently enhanced charge mobility (Lim *et al.*, 2017). Given the fact that smectic LCs possess a certain degree of positional order, it makes them a promising material in sensing technology. The disruption of molecular orientation upon the arrival of targeted species within the smectic phase could lead to a change in optical properties and thus generating signals in the form of colour changes under polarized light (Luan *et al.*, 2020). Among all synthesized PBLCs, **PB7** – **PB9** series possess high potentiality in the aforementioned applications as they exhibit lower melting temperature

(low transition temperature to mesophase). This is because most of the technological applications are operating at its optimum level at low or ambient temperature.

Universiti Malaya

CHAPTER 5: CONCLUSION AND FUTURE STUDIES

5.1 Conclusion

In the present study, with the exploitation of palm fatty acids, namely, lauric acid, palmitic acid and stearic acid as flexible moiety in a Schiff base ester-based LC molecule, has led to the formation of nine PBLCs through condensation and esterification reactions. It is a new application established for palm fatty acids and the first report of PBLCs. These nine PBLCs can be further classified into three (3) different series based on their molecular architecture (Figure 4.29). **PB1 – PB3** series composed of a 3-ring Schiff base ester-based mesogenic core with bromo group at one terminal while at the other is terminally bonded to palm fatty acid varying in length from 12 carbons (lauric acid) to 16 carbons (palmitic acid) and to 18 carbons (stearic acid), whereas, **PB4 – PB5** series is the unsubstituted analogues (without terminal bromo group) to **PB1 – PB3** series. As for the third series, **PB7 – PB9**, it shared the similar structure as **PB1 – PB3** except the fact that it has one less phenyl ring and ester group. The molecular structure of all synthesized PBLCs was characterized and confirmed by FT-IR, ¹H and ¹³C NMR.

As far as thermal stability is concerned, TGA was employed to study the thermal behaviour of PBLCs in a temperature range of 30 to 900°C. All PBLCs were found to be thermally stable with temperature at 5% weight loss, T_{d 5%} of more than 200°C. From the DTG curves, it was found that **PB1**, **PB2** and **PB6 – PB9** exhibited a single-stage degradation within the temperature range of 267 – 530°C. While on the contrary, **PB3** showed a 2-stage degradation whereas **PB4** and **PB5** were found to decompose in 3 stages. The presence of terminal bromo group in **PB1 – PB3** series has led to higher thermal stability as compared to its unsubstituted analogues, **PB4 – PB5**. This can be ascribed to the stronger intermolecular attraction as a result of the enhanced molecular

polarizability. As compared to **PB7 – PB9** series, **PB1 – PB3** showed greater thermal resistance due to the additional phenyl ring (higher rigidity) and an ester group (higher polarizability). Thermal stability of PBLCs was found to be chain length dependent in which $T_{d 5\%}$ increases with increasing number of carbons in palm fatty acid chain. This trend is clearly shown by the series of **PB4 – PB6** and **PB7 – PB9**. However, the reversal of this trend was observed for **PB1 – PB3** series. This is due to the antagonistic effect between the longer fatty acid chain length and the presence of heavy terminal bromo group. Longer fatty acid chain length tends to reduce molecular rigidity and hence less energy needed to accomplish 5% weight loss with the removal of the heavy bromo group.

The mesomorphic behaviour of PBLCs was characterized by DSC and the data obtained are accordant with the transition temperatures observed under POM. All PBLCs were found to be enantiotropic in nature as mesophase was observed during both heating and cooling cycles under POM except for **PB9** in which mesophase can only be seen upon cooling. The mesophase texture of PBLCs that visualized under POM was the typical focal conic fan-shaped of smectic A phase and this was further verified by SAXS. From the scattering pattern observed, sharp peaks that emerged at low q region ($1.3 - 2.0 \text{ nm}^{-1}$) coupled with diffused broad peaks at higher q region ($3.5 - 4.5 \text{ nm}^{-1}$) confirmed that the molecular orientation was in lamellar arrangement of smectic A phase with only short-range order. Owing to the fact that the layer spacing of PBLCs (derived from SAXS) is greater than its corresponding molecular length, therefore it can be concluded that the molecular orientation of PBLCs was in an interdigitated bilayer structure. This is an antiparallel arrangement of PBLC molecules with the overlap of mesogenic cores and subsequently allows the flexible palm fatty chains to fill up more spaces while reducing void volume in molecular packing. As a consequence, mesophase stability can be enhanced. Making mention to mesophase stability, **PB1 – PB3** series showed the broadest mesophase range followed by **PB4 – PB6** while **PB7 – PB9** series showed to exhibit the

least stable mesophase range. In terms of structure-mesomorphic property relationship, the presence of a 3-ring Schiff base ester based mesogenic core with a terminal bromo group within the series of **PB1 – PB3** has led to higher molecular linearity and polarizability which in turn stabilizes molecular orientation of smectic A phase. On the other hand, with the absence of terminal bromo group, **PB4 – PB6** series appeared to exhibit lower molecular polarizability and hence shorter mesophase range was observed. The narrowest mesophase range was shown by **PB7 – PB9** series. The lack of one phenyl ring together with an ester group in the series of **PB7 – PB9** attribute to a marked decrease in overall molecular polarizability and a lower length-to-breadth ratio, thus diminish cohesion forces between PBLC molecules. Last but not least, with increasing length of palm fatty acid chain (from 12 carbons to 16 carbons and to 18 carbons), **PB1 – PB3** and **PB4 – PB6** series showed a descending trend in both melting and clearing temperatures. This can be attributed to the increased molecular flexibility and dilution of mesogenic core, respectively. Given the fact that clearing temperature decreases more than melting, the overall mesophase range was found to be narrower with longer palm fatty acid chain length. Nevertheless, the opposite trend was noted for **PB7 – PB9** series. This may be attributed to the synergistic effect between a shorter mesogenic core and a longer flexible palm fatty acid chain length. In a nutshell, all synthesized PBLCs are pure smectogen with stable mesophase range and could offer exiting potential as a material for technological advancement.

Following the studies of structure-mesomorphic property of PBLCs, some idealized molecular architectures have been identified for the ease of accessing mesophase and to attain certain types of mesophase over a practical range of temperature. As a template structure to access LC phases, a mesogenic core that promotes high linearity and polarizability is inevitable. This can be fulfilled by incorporating two or more phenyl rings (high rigidity) with a suitable linking group such as Schiff base linkage that

promotes stepped core structure (high linearity) and an ester group that could enhance overall molecular polarizability (stable mesophase range). The flexible moiety of a LC molecule is just as important not only in accessing mesophase but in lowering phase transition temperatures as well as anticipating the type of mesophases for various applications. As far as mesophase stability is concerned, a polar terminal substituent can be added to further enhance molecular polarizability to such an extent where a mesophase is stable over a broad range of temperature.

5.2 Future studies

Since the mesomorphic behaviour of the synthesized PBLCs is rather convincing, hence the potential of palm oil as building blocks in LC synthesis is worthy of further investigation. With the knowledge gained in this study, it is convinced that the conformation of palm fatty acid as flexible moiety would have an impact on mesophase stability. The acyl chain of palm fatty acids is known to exhibit different degree of unsaturation (mono, di or poly) and it is worth noting that unsaturated palm fatty acids are always in cis conformation. Due to rotational restriction upon double bond, cis isomers of unsaturated palm fatty acids tend to exhibit structural features that would be beneficial to mesophase formation, this includes but not limited to a less compact molecular arrangement which may induce lower phase transition temperatures and higher molecular polarity that may enhance cohesion forces between molecules within the mesophase. Therefore, unsaturated palm fatty acids such as oleic acid and linoleic acid could also be used as flexible moiety in the synthesis of PBLCs for a wider range of properties. Additionally, the resulting unsaturated PBLCs can serve as polymerizable monomers to produce high molar mass liquid crystalline polymers (LCPs) with better mechanical properties. While palm fatty acids have good reactivity for chemical modifications, there are other building blocks from processed palm oil, namely, fatty

alcohol, fatty amine and glycerol which could potentially be used as chemical moiety in LC molecule.

Universiti Malaya

REFERENCES

- Abberley, J. P., Killah, R., Walker, R., Storey, J. M. D., Imrie, C. T., Salamończyk, M., Zhu, C., Gorecka, E., & Pocięcha, D. (2018). Helical smectic phases formed by achiral molecules [Article]. *Nature Communications*, 9(1), Article 228.
- Abdulnabi, N. M., Abdul Razzaq Al-Obaidy, M. M., Tomi, I. H. R., & Jaffer, H. J. (2021). New calamitic mesogens derived from a furan ring: Synthesis, characterization and study of their mesomorphic behavior. *Journal of Molecular Liquids*, 325, 114562.
- Adam, N. I., Hanibah, H., Subban, R. H. Y., Kassim, M., Mobarak, N. N., Ahmad, A., Badri, K. H., & Su'ait, M. S. (2020). Palm-based cationic polyurethane membranes for solid polymer electrolytes application: A physico-chemical characteristics studies of chain-extended cationic polyurethane. *Industrial Crops and Products*, 155, 112757.
- Aguieiras, E. C. G., Papadaki, A., Mallouchos, A., Mandala, I., Sousa, H., Freire, D. M. G., & Koutinas, A. A. (2019). Enzymatic synthesis of bio-based wax esters from palm and soybean fatty acids using crude lipases produced on agricultural residues. *Industrial Crops and Products*, 139, 111499.
- Ahmed, H. A., & A. El-Atawy, M. (2021). Synthesis, mesomorphic and geometrical approaches of new non-symmetrical system based on central naphthalene moiety. *Liquid Crystals*, 1-13.
- Ahmed, H. A., Hagar, M., El-Sayed, T. H., & B. Alnoman, R. (2019a). Schiff base/ester liquid crystals with different lateral substituents: mesophase behaviour and DFT calculations. *Liquid Crystals*, 46(7), 1-11.
- Ahmed, H. A., Hagar, M., & Saad, G. R. (2019b). Impact of the proportionation of dialkoxy chain length on the mesophase behaviour of Schiff base/ester liquid crystals; experimental and theoretical study. *Liquid Crystals*, 46(11), 1611-1620.
- Ahmed, H. A., Mansour, E., & Hagar, M. (2020a). Mesomorphic study and DFT simulation of calamitic Schiff base liquid crystals with electronically different terminal groups and their binary mixtures. *Liquid Crystals*, 47(14-15), 2292-2304.
- Ahmed, N. H. S., Saad, G. R., Ahmed, H. A., & Hagar, M. (2020b). New wide-stability four-ring azo/ester/Schiff base liquid crystals: synthesis, mesomorphic, photophysical, and DFT approaches [10.1039/C9RA10499B]. *RSC Advances*, 10(16), 9643-9656.

- Ahmed, N. H. S., Saad, G. R., & Naoum, M. M. (2018). Effect of position of the lateral fluoro substituent on the mesophase behaviour of aryl 4-alkoxyphenylazo benzoates in pure and binary mixtures. *Liquid Crystals*, 45(10), 1487-1497.
- Al-Hamdani, U. J., Abbo, H. S., Al-Jaber, A. A., & Titinchi, S. J. J. (2020). New azo-benzothiazole based liquid crystals: synthesis and study of the effect of lateral substituents on their liquid crystalline behaviour. *Liquid Crystals*, 47(14-15), 2257-2267.
- Al-Hamdani, U. J., Gassim, T. E., & Radhy, H. H. (2010). Synthesis and Characterization of Azo Compounds and Study of the Effect of Substituents on Their Liquid Crystalline Behavior. *Molecules (Basel, Switzerland)*, 15(8), 5620-5628.
- Al-Obaidy, M. M. A. R., Tomi, I. H. R., & Abdulqader, A. M. (2021). Synthesis and study the liquid crystalline behaviors of double Schiff bases bearing ester linkage as a central core. *Liquid Crystals*, 1-11.
- Alaasar, M., Prehm, M., & Tschierske, C. (2013). Influence of halogen substituent on the mesomorphic properties of five-ring banana-shaped molecules with azobenzene wings. *Liquid Crystals*, 40(5), 656-668.
- Alamro, F. S., Gomha, S. M., Shaban, M., Altowyan, A. S., Abolibda, T. Z., & Ahmed, H. A. (2021). Optical investigations and photoactive solar energy applications of new synthesized Schiff base liquid crystal derivatives. *Scientific Reports*, 11(1), 15046.
- Ali, G. Q., & Tomi, I. H. R. (2018). Synthesis and characterization of new mesogenic esters derived from 1,2,4-oxadiazole and study the effect of alkoxy chain length in their liquid crystalline properties. *Liquid Crystals*, 45(3), 421-430.
- Aljamali, N., Alqraawy, W., & Almosawy, M. (2021). Review on Liquid Crystals and their Chemical Applications. 7, 8-15.
- Alnoman, R., Al-Nazawi, F. K., Ahmed, H. A., & Hagar, M. (2019). Synthesis, Optical, and Geometrical Approaches of New Natural Fatty Acids' Esters/Schiff Base Liquid Crystals. *Molecules (Basel, Switzerland)*, 24(23), 4293.
- An, J. G., Hina, S., Yang, Y., Xue, M., & Liu, Y. (2016). Characterization of liquid crystals: A literature review. 44, 398-406.
- Andrienko, D. (2018). Introduction to liquid crystals. *Journal of Molecular Liquids*, 267, 520-541.
- Arrieta, A., García, T., & Palomo, C. (1982). Reagents and Synthetic Methods 21. Thionyl Chloride /4-(N,N-Dimethylamino) Pyridine Complex. A Simple One-Pot

Method for Esterification of Carboxylic Acids. *Synthetic Communications*, 12(14), 1139-1146.

Aziz, N. A. M., Yunus, R., Rashid, U., & Syam, A. M. (2014). Application of response surface methodology (RSM) for optimizing the palm-based pentaerythritol ester synthesis. *Industrial Crops and Products*, 62, 305-312.

Bailly-Reyre, A., & Diep, H. T. (2020). Nematic and Smectic Phases: Dynamics and Phase Transition. *Symmetry*, 12(9), 1574.

Begum, N., Turlapati, S., Debnath, S., Mohiuddin, G., Sarkar, D. D., & Nandiraju, V. S. R. (2013). Achiral unsymmetrical four-ring bent-core liquid crystals with a polar fluoro or chloro end substituent: synthesis and characterisation. *Liquid Crystals*, 40(8), 1105-1115.

Benbayer, C., Saïdi-Besbes, S., Grelet, E., & Derdour, A. (2013). Structure–property study of new [1,2,3]-triazole liquid crystalline derivatives. *Liquid Crystals*, 40(11), 1520-1528.

Bhat, S. G., Sharada Ramachandra, G., Bhagavath, P., Subrao, M., Potukuchi, D. M., & Maddasani, S. (2018). Self-assembled liquid crystalline materials with fatty acids. *Journal of Thermal Analysis and Calorimetry*, 132(2), 989-1000.

Bruce, D. W., Deschenaux, R., Donnio, B., & Guillon, D. (2007). 12.05 - Metallomesogens. In D. M. P. Mingos & R. H. Crabtree (Eds.), *Comprehensive Organometallic Chemistry III* (pp. 195-293). Elsevier.

Bubnov, A., Kašpar, M., Hamplová, V., Dawin, U., & Giesselmann, F. (2013). Thermotropic and lyotropic behaviour of new liquid-crystalline materials with different hydrophilic groups: synthesis and mesomorphic properties. *Beilstein Journal of Organic Chemistry*, 9, 425-436.

Bury, P., Veveričík, M., Černobila, F., Kopčanský, P., Timko, M., & Závěšová, V. (2020). Study of Structural Changes in Nematic Liquid Crystals Doped with Magnetic Nanoparticles Using Surface Acoustic Waves. *Crystals*, 10(11), 1023.

Camley, R., Celinski, Z., Garbovskiy, Y., & Glushchenko, A. (2018). Liquid crystals for signal processing applications in the microwave and millimeter wave frequency ranges. *Liquid Crystals Reviews*, 6(1), 17-52.

Carlton, R. J., Hunter, J. T., Miller, D. S., Abbasi, R., Mushenheim, P. C., Tan, L. N., & Abbott, N. L. (2013). Chemical and biological sensing using liquid crystals. *Liquid Crystals Reviews*, 1(1), 29-51.

- Catanescu, C. O., Wu, S.-T., & Chien, L.-C. (2004). Tailoring the physical properties of some high birefringence isothiocyanato-based liquid crystals. *Liquid Crystals*, 31(4), 541-555.
- Chandrasekhar, S., Sadashiva, B. K., & Suresh, K. A. (1977). Liquid crystals of disc-like molecules. *Pramana*, 9(5), 471-480.
- Chen, X.-F., Shen, Z., Wan, X.-H., Fan, X.-H., Chen, E.-Q., Ma, Y., & Zhou, Q.-F. (2010). Mesogen-jacketed liquid crystalline polymers [10.1039/B814540G]. *Chemical Society Reviews*, 39(8), 3072-3101.
- Chong, Y.-T., Muhamad Sarih, N., Ha, S.-T., & Sheikh, M. R. K. (2016). New Homologues Series of Heterocyclic Schiff Base Ester: Synthesis and Characterization. *Advances in Physical Chemistry*, 2016, 7647695.
- Chothani, N. J., Akbari, V. K., Patel, P. S., & Patel, K. C. (2016). The influence of the thioalkyl terminal group on the mesomorphic behavior of some 6-alkoxy-2-naphthoates derived from 1,3,4-oxadiazole. *Molecular Crystals and Liquid Crystals*, 631(1), 31-46.
- Collings, P. J., & Hird, M. (1997). *Introduction to Liquid Crystals Chemistry and Physics*. CRC Press.
- Cook, A. G., Inkster, R. T., Martinez-Felipe, A., Ribes-Greus, A., Hamley, I. W., & Imrie, C. T. (2012a). Synthesis and phase behaviour of a homologous series of polymethacrylate-based side-chain liquid crystal polymers. *European Polymer Journal*, 48(4), 821-829.
- Cook, A. G., Wardell, J. L., Brooks, N. J., Seddon, J. M., Martínez-Felipe, A., & Imrie, C. T. (2012b). Non-symmetric liquid crystal dimer containing a carbohydrate-based moiety. *Carbohydrate Research*, 360, 78-83.
- Cozan, V., Iftime, M., Sava, I., & Bronnikov, S. (2015). Synthesis and thermotropic properties of polyazomethines-containing side chain azobenzene moieties. *High Performance Polymers*, 27(5), 661-668.
- d'Alessandro, A., Martini, L., Gilardi, G., Beccherelli, R., & Asquini, R. (2015). Polarization-Independent Nematic Liquid Crystal Waveguides for Optofluidic Applications. *IEEE Photonics Technology Letters*, 27(16), 1709-1712.
- Dąbrowski, R. (2015). From the discovery of the partially bilayer smectic A phase to blue phases in polar liquid crystals. *Liquid Crystals*, 42(5-6), 783-818.
- de Gennes, P.-G. (1997). Un muscle artificiel semi-rapide. *Comptes Rendus de l'Académie des Sciences - Series IIB - Mechanics-Physics-Chemistry-Astronomy*, 324(5), 343-348.

- Devadiga, D., & Ahipa, T. N. (2019). Recent synthetic advances in pyridine-based thermotropic mesogens [10.1039/C9RA04389F]. *RSC Advances*, 9(40), 23161-23228.
- Dey, K. C., Mandal, P. K., & Kula, P. (2020). Effect of fluorinated achiral chain length on structural, dielectric and electro-optic properties of two terphenyl based antiferroelectric liquid crystals. *Journal of Molecular Liquids*, 298, 112056.
- Dierking, I. (2018). Liquid crystal sensors. *Liquid Crystals Today*, 27(3), 74-75.
- Dixit, S., & Intwala, K. (2016). Study of novel thermotropic liquid crystals with lateral nitro substituent. *Molecular Crystals and Liquid Crystals*, 631(1), 1-8.
- Doshi, A. A., & Chauhan, B. C. (2015). Study of Mesomorphism Through a Novel Homologous Series and Its Relation to Molecular Structure. *Molecular Crystals and Liquid Crystals*, 606(1), 66-74.
- Dzulkharnien, N. S. F., Salleh, N. M., Yahya, R., & Karim, M. R. (2017). Synthesis of imine-ester-linked benzothiazole mesogen containing liquid crystalline monomers with different terminal substituents. *Soft Materials*, 15(4), 292-301.
- Elmali Gülbaş, H., Coskun, D. G., Gursel, Y., & Bilgin-Eran, B. (2014). Synthesis, Characterization And Mesomorphic Properties Of Side Chain Liquid Crystalline Oligomer Having Schiff Base Type Mesogenic Group. *Advanced Materials Letters*, 5, 333-338.
- Esteves, C., Ramou, E., Porteira, A. R. P., Moura Barbosa, A. J., & Roque, A. C. A. (2020). Seeing the Unseen: The Role of Liquid Crystals in Gas-Sensing Technologies. *Advanced Optical Materials*, 8(11), 1902117.
- Fakruddin, K., Jeevan Kumar, R., Datta Prasad, P. V., & Pisipati, V. G. K. M. (2009). Orientational Order Parameter – 1 A Birefringence Study. *Molecular Crystals and Liquid Crystals*, 511(1), 133/[1603]-1145/[1615].
- Fernández, G. (2013). Exotic actuators. *Nature Materials*, 12(1), 12-14.
- Fleischmann, E.-K., & Zentel, R. (2013). Liquid-Crystalline Ordering as a Concept in Materials Science: From Semiconductors to Stimuli-Responsive Devices. *Angewandte Chemie International Edition*, 52(34), 8810-8827.
- Fong, C., Le, T., & Drummond, C. J. (2012). Lyotropic liquid crystal engineering—ordered nanostructured small molecule amphiphile self-assembly materials by design [10.1039/C1CS15148G]. *Chemical Society Reviews*, 41(3), 1297-1322.

- Foo, K.-L., Ha, S.-T., & Lee, S. (2014). Synthesis and Characterization of Thermotropic Liquid Crystals Consisting Heterocyclic Benzothiazole Core System. *Asian Journal of Chemistry*, 26, 7627-7631.
- Gallardo, H., Ferreira, M., Vieira, A. A., Westphal, E., Molin, F., Eccher, J., & Bechtold, I. H. (2011). Columnar mesomorphism of bent-rod mesogens containing 1,2,4-oxadiazole rings. *Tetrahedron*, 67(49), 9491-9499.
- Ganicz, T., & Stańczyk, W. (2009). Side-chain Liquid Crystal Polymers (SCLCP): Methods and Materials. An Overview. *Materials*, 2(1), 95-128.
- Gao, L., Shen, Z., Fan, X., & Zhou, Q. (2012). Mesogen-jacketed liquid crystalline polymers: from molecular design to polymer light-emitting diode applications [10.1039/C2PY20078C]. *Polymer Chemistry*, 3(8), 1947-1957.
- Garidel, P., Kaconis, Y., Heinbockel, L., Wulf, M., Gerber, S., Munk, A., Vill, V., & Brandenburg, K. (2015). Self-Organisation, Thermotropic and Lyotropic Properties of Glycolipids Related to their Biological Implications. *The open biochemistry journal*, 9, 49-72.
- Girdziunaite, D., Tschierske, C., Novotna, E., Kresse, H., & Hetzheim, A. (1991). New mesogenic 1,3,4-oxadiazole derivatives. *Liquid Crystals*, 10(3), 397-407.
- Giroto, E., Bechtold, I. H., & Gallardo, H. (2015). New liquid crystals derived from thiophene connected to the 1,2,3-triazole heterocycle. *Liquid Crystals*, 42(12), 1798-1807.
- Goodby, J., Demus, D., Goodby, J., Gray, G., Spiess, H. W., & Vill, V. (2008). Non-Chiral Smectic Liquid Crystals: Synthesis of Non-Chiral Smectic Liquid Crystals. In (pp. 411-440).
- Goodby, J. W. (1998). Phase Structures of Calamitic Liquid Crystals. In *Handbook of Liquid Crystals* (pp. 3-21).
- Goodby, J. W. (2011). The nanoscale engineering of nematic liquid crystals for displays. *Liquid Crystals*, 38(11-12), 1363-1387.
- Goodby, J. W. (2017). Free volume, molecular grains, self-organisation, and anisotropic entropy: machining materials. *Liquid Crystals*, 44(12-13), 1755-1763.
- Goodby, J. W., Mandle, R. J., Davis, E. J., Zhong, T., & Cowling, S. J. (2015). What makes a liquid crystal? The effect of free volume on soft matter. *Liquid Crystals*, 42(5-6), 593-622.

- Gupta, R. K., Manjuladevi, V., Karthik, C., & Choudhary, K. (2016). Thin films of discotic liquid crystals and their applications. *Liquid Crystals*, 43(13-15), 2079-2091.
- Ha, S.-T., Koh, T.-M., Lee, S.-L., Yeap, G.-Y., Lin, H.-C., & Ong, S.-T. (2010). Synthesis of new schiff base ester liquid crystals with a benzothiazole core. *Liquid Crystals*, 37(5), 547-554.
- Ha, S.-T., & Lee, T.-L. (2014). Synthesis and Mesomorphic Properties of New Fluorinated Schiff Base Liquid Crystals. *ISRN Materials Science*, 2014, 904657.
- Ha, S. T., Yeap, G.-Y., & Boey, P. L. (2009). Synthesis and liquid crystalline properties of new Schiff bases N-[4-(4-n-alkanoyloxybenzoyloxy)benzylidene] -4-Cyano-, 4-Hydroxy-, 4-Thio-and 4-Nitroanilines. *Australian Journal of Basic and Applied Sciences*, 3, 3417-3422.
- Hagar, M., Ahmed, H. A., & Alhaddad, O. A. (2019a). New azobenzene-based natural fatty acid liquid crystals with low melting point: synthesis, DFT calculations and binary mixtures. *Liquid Crystals*, 46(15), 2223-2234.
- Hagar, M., Ahmed, H. A., Nafee, S. S., El-Shishtawy, R. M., & Raffah, B. M. (2019b). The Synthesis of New Thermal Stable Schiff Base/Ester Liquid Crystals: A Computational, Mesomorphic, and Optical Study. *Molecules (Basel, Switzerland)*, 24(17), 3032.
- Hagar, M., Ahmed, H. A., & Saad, G. R. (2018). Mesophase stability of new Schiff base ester liquid crystals with different polar substituents. *Liquid Crystals*, 45(9), 1324-1332.
- Hagar, M., Ahmed, H. A., & Saad, G. R. (2019c). Synthesis and mesophase behaviour of Schiff base/ester 4-(arylideneamino)phenyl-4''-alkoxy benzoates and their binary mixtures. *Journal of Molecular Liquids*, 273, 266-273.
- Hamad, W. M., & Salih, S. K. (2017). Synthesis and Liquid Crystalline Studies of 2,4-bis(4'-n-nonyloxybenzoyloxy)benzylidene-4''-n-alkoxyaniline. *ARO-THE SCIENTIFIC JOURNAL OF KOYA UNIVERSITY*, 5(1), 24-29.
- He, W.-L., Gu, H., Zhao, P., Yang, Z., Cao, H., & Wang, D. (2017). Synthesis and mesophase behaviour of branched azobenzene-based supramolecular hydrogen-bonded liquid crystals. *Liquid Crystals*, 44(3), 593-602.
- Hosangadi, B. D., & Dave, R. H. (1996). An efficient general method for esterification of aromatic carboxylic acids. *Tetrahedron Letters*, 37(35), 6375-6378.

- Hu, J.-S., Li, D., Zhang, W.-C., & Meng, Q.-B. (2012). Synthesis, structure, and properties of chiral liquid crystal monomers and polymers based on menthol. *Journal of Polymer Science A Polymer Chemistry*, 50, 5049-5059.
- Hu, J.-s., Zhang, B.-y., Sun, K., & Li, Q.-y. (2003). Side chain cholesteric liquid crystalline elastomers: synthesis and phase behaviour. *Liquid Crystals*, 30(11), 1267-1275.
- Huang, C.-C., Hsu, C.-C., Chen, L.-W., & Cheng, Y.-L. (2014). The effect of position of (S)-2-octyloxy tail on the formation of frustrated blue phase and antiferroelectric phase in Schiff base liquid crystals [10.1039/C4SM01829J]. *Soft Matter*, 10(46), 9343-9351.
- Imrie, C. T., & Taylor, L. (1989). The preparation and properties of low molar mass liquid crystals possessing lateral alkyl chains. *Liquid Crystals*, 6(1), 1-10.
- Jadeja, U. H., Sharma, V. S., Jain, B. B., & Patel, R. B. (2016). Dependence of LC state on molecular flexibility. *Molecular Crystals and Liquid Crystals*, 630(1), 144-153.
- Jadeja, U. H., Sharma, V. S., Prajapat, V., Shah, A., & Sharma, A. S. (2019). "Synthesis and Study of Azo based Liquid Crystals: Effect of the lateral bromo and terminal alkoxy side chain on Thermal, Mesomorphic and Optical properties". *Molecular Crystals and Liquid Crystals*, 680(1), 46-64.
- Jain, B. B., Sharma, V. S., Chauhan, H. N., & Patel, R. B. (2016). Mesomorphism of azo-esters and chalcone-esters. *Molecular Crystals and Liquid Crystals*, 630(1), 102-111.
- Jamain, Z., Khairuddean, M., & Guan-Seng, T. (2020). Liquid-Crystal and Fire-Retardant Properties of New Hexasubstituted Cyclotriphosphazene Compounds with Two Schiff Base Linking Units. *Molecules (Basel, Switzerland)*, 25(9), 2122.
- Jesacher, A., Maurer, C., Schwaighofer, A., Bernet, S., & Ritsch-Marte, M. (2008). Near-perfect hologram reconstruction with a spatial light modulator. *Optics Express*, 16(4), 2597-2603.
- Jia, M., Jiang, L., Niu, F., Zhang, Y., & Sun, X. (2018). A novel and highly efficient esterification process using triphenylphosphine oxide with oxalyl chloride. *Royal Society Open Science*, 5(2), 171988.
- Kalustian, P. (1985). Pharmaceutical and cosmetic uses of palm and lauric products. *Journal of the American Oil Chemists' Society*, 62(2), 431-433.
- Kamal, S. J., Salleh, N. M., Mahmud, H. N. M. E., Abdullah, I., Gopal, S. R., Velayutham, T. S., & Zahid, N. I. (2021). Mesomorphic, optical, dielectric, and electro-optic

properties of azo-ester materials: Effect of lateral methyl and terminal substituents. *Journal of Molecular Liquids*, 336, 116308.

Kapernaum, N., Hartley, S., Roberts, J., Lemieux, R., & Giesselmann, F. (2009). Molecular length distribution and the formation of smectic phases. *Beilstein Journal of Organic Chemistry*, 5, 65.

Karanlık, G., Ocak, H., & Bilgin Eran, B. (2019). Imine based chiral liquid crystals: Effect of varying the terminal substituent and orientation of ester linking unit. *Journal of Molecular Liquids*, 275, 567-577.

Karim, M. R., Sheikh, M. R. K., Islam, M. S., Salleh, N. M., & Yahya, R. (2019). Synthesis, Crystal Structure, Mesophase Behaviour and Optical Property of Azo-ester Bridged Compounds: Azo-ester Bridged Compounds. *Journal of Scientific Research*, 11(3), 383-395.

Karim, M. R., Sheikh, M. R. K., Yahya, R., Mohamad Salleh, N., Lo, K. M., & Mahmud, H. N. M. E. (2016). The effect of terminal substituents on crystal structure, mesophase behaviour and optical property of azo-ester linked materials. *Liquid Crystals*, 43(12), 1862-1874.

Karim, M. R., Yahya, R., Sheikh, M. R. K., Salleh, N. M., Hassan, A., & Ekramul Mahmud, H. N. M. (2014). Synthesis, thermal stability, optical and electrochemical properties of halogen terminated azo-benzothiazole mesogen containing smectic side chain liquid crystalline polymers. *Journal of Polymer Research*, 21(6), 487.

Karuppusamy, A., Ramkumar, V., Kannan, P., Balamurugan, S., & Said, S. M. (2017). Effect of linking groups on 2, 5-disubstituted thiophene with chalcone as the side arm containing bent-core materials. *Soft Materials*, 15(2), 132-144.

Kelker, H., & Scheurle, B. (1969). A Liquid-crystalline (Nematic) Phase with a Particularly Low Solidification Point [Article]. *Angewandte Chemie International Edition in English*, 8(11), 884-885.

Kim, D. S., & Yoon, D. K. (2018). Curvatures of smectic liquid crystals and their applications. *Journal of Information Display*, 19(1), 7-23.

Kim, H., Yi, Y., Chen, D., Korblova, E., Walba, D. M., Clark, N. A., & Yoon, D. K. (2013). Self-assembled hydrophobic surface generated from a helical nanofilament (B4) liquid crystal phase [10.1039/C3SM27221D]. *Soft Matter*, 9(10), 2793-2797.

Kleman, M., & Lavrentovich, O. D. (2009). Liquids with conics. *Liquid Crystals*, 36(10-11), 1085-1099.

- Kovářová, A., Kohout, M., Svoboda, J., & Novotná, V. (2014). New liquid crystal based on 2-phenylthiophene central core. *Liquid Crystals*, 41(12), 1703-1718.
- Kumar, S. (2001). Liquid crystals : experimental study of physical properties and phase transitions. *Molecules (Basel, Switzerland)*, 6, 1055-1056.
- Kumar, S. (2014). Chemistry of discotic liquid crystals: from monomers to polymers. *Liquid Crystals Reviews*, 2(2), 155-156.
- Li, X., Tan, N., Pivnenko, M., Sibik, J., Zeitler, J. A., & Chu, D. (2016a). High-birefringence nematic liquid crystal for broadband THz applications. *Liquid Crystals*, 43(7), 955-962.
- Li, Y., Dong, C., Cun, D., Liu, J., Xiang, R., & Fang, L. (2016b). Lamellar Liquid Crystal Improves the Skin Retention of 3-O-Ethyl-Ascorbic Acid and Potassium 4-Methoxysalicylate In Vitro and In Vivo for Topical Preparation. *AAPS PharmSciTech*, 17(3), 767-777.
- Lim, Y.-W. C., Ha, S.-T., Yeap, G.-Y., & Sastry, S. S. (2017). Synthesis and mesomorphic properties of new heterocyclic liquid crystals with Central Ester-Chalcone linkages. *Journal of Taibah University for Science*, 11(1), 133-140.
- Liu, L., Broer, D. J., & Onck, P. R. (2019). Travelling waves on photo-switchable patterned liquid crystal polymer films directed by rotating polarized light [10.1039/C9SM01594A]. *Soft Matter*, 15(40), 8040-8050.
- Luan, C., Luan, H., & Luo, D. (2020). Application and Technique of Liquid Crystal-Based Biosensors. *Micromachines*, 11(2), 176.
- Luo, C.-C., Jia, Y.-G., Song, K.-M., Meng, F.-B., & Hu, J.-S. (2017). The effect of terminal alkoxy chain on mesophase behaviour, optical property and structure of chiral liquid crystal compounds derived from (-)-menthol. *Liquid Crystals*, 44(14-15), 2366-2378.
- Majumdar, K. C., Pal, N., Nath, S., Choudhury, S., & Rao, N. V. S. (2006). Synthesis, Characterization, and Mesogenic Properties of Anisotropic Imines. *Molecular Crystals and Liquid Crystals*, 461(1), 37-51.
- Mandle, R. J. (2016). The dependency of twist-bend nematic liquid crystals on molecular structure: a progression from dimers to trimers, oligomers and polymers [10.1039/C6SM01772J]. *Soft Matter*, 12(38), 7883-7901.
- Marcelis, A. T. M., Koudijs, A., Karczmarzyk, Z., & Sudhölter, E. J. R. (2003). Cholesterol-containing liquid crystal dimers with ether linkages between the spacer and mesogenic units. *Liquid Crystals*, 30(11), 1357-1364.

- Mat Dian, N. L. (2018). Palm oil and palm kernel oil: Versatile ingredients for food applications. *Journal of Oil Palm Research*, 29, 487-511.
- Matharu, A. S., & Chambers-Asman, D. (2007). Structure–property investigation of 2- and 3-thienylacrylates bearing laterally fluorinated azobenzene moieties. *Liquid Crystals*, 34(11), 1317-1336.
- Mazur, R., Piecek, W., Raszewski, Z., Morawiak, P., Garbat, K., Chojnowska, O., Mrukiewicz, M., Olifierczuk, M., Kedzierski, J., Dabrowski, R., & Weglowska, D. (2017). Nematic liquid crystal mixtures for 3D active glasses application. *Liquid Crystals*, 44(2), 417-426.
- Meier, G. (1975). *Applications of Liquid Crystals*. Springer Berlin Heidelberg.
- Mieczkowski, J., Mieczkowska nee Gomoła, K., Koseska, J., Pocięcha, D., Szydłowska, J., & Gorecka, E. (2003). Liquid crystal phases formed by asymmetric bent-shaped molecules. *Journal of Materials Chemistry - JMATER CHEM*, 13.
- Mohammady, S. Z., Aldhayan, D. M., Alshammri, M. A., Alshammari, A. K., Alazmi, M., Katariya, K. D., Jaremko, M., & Hagar, M. (2021). Polar Alkoxy Group and Pyridyl Effects on the Mesomorphic Behavior of New Non-Symmetrical Schiff Base Liquid Crystals. *Symmetry*, 13(10), 1832.
- Mohiuddin, G., Begum, N., Rao, N. V. S., Kaur, S., Punjani, V., Khan, R. K., Ghosh, S., & Pal, S. K. (2017). Observation of disordered mesomorphism in three-ring-based highly polar bent-core molecules: design, synthesis and characterisation. *Liquid Crystals*, 44(14-15), 2247-2258.
- Montoya, C., Cochard, B., Flori, A., Cros, D., Lopes, R., Cuellar, T., Espeout, S., Syaputra, I., Villeneuve, P., Pina, M., Ritter, E., Leroy, T., & Billotte, N. (2014). Genetic architecture of palm oil fatty acid composition in cultivated oil palm (*Elaeis guineensis* Jacq.) compared to its wild relative *E. oleifera* (H.B.K) Cortés. *PloS one*, 9(5), e95412-e95412.
- Muniprasad, M., Srinivasulu, M., Venkata Chalapathi, P., & Potukuchi, D. m. (2012). Influence of Chemical Moieties and the Flexible Chain for the Tilted Smectic Phases in Linear Hydrogen Bonded Liquid Crystals with Schiff Based Pyridene Derivatives. *Journal of Molecular Structure*, 1015, 181-191.
- Nafee, S. S., Hagar, M., Ahmed, H. A., Alhaddad, O. A., El-Shishtawy, R. M., & Raffah, B. M. (2020). New two rings Schiff base liquid crystals; ball mill synthesis, mesomorphic, Hammett and DFT studies. *Journal of Molecular Liquids*, 299, 112161.

- Nagaveni, N. G., Gupta, M., Roy, A., & Prasad, V. (2010). Photosensitive phasmid-like liquid crystalline materials with unusual mesomorphic behavior [10.1039/C0JM01858A]. *Journal of Materials Chemistry*, 20(41), 9089-9099.
- Nakum, K. J., Katariya, K. D., Jadeja, R. N., & Prajapati, A. K. (2019). Schiff base of 4-n-alkoxy-2-hydroxy benzaldehyde with 4-amino acetophenone and their Cu(II) complexes: synthesis, characterization and mesomorphic behavior. *Molecular Crystals and Liquid Crystals*, 690(1), 1-13.
- Nandi, R., Singh, H. K., Singh, S. K., Rao, D. S. S., Prasad, S. K., Singh, B., & Singh, R. K. (2017). Investigation of liquid crystalline property of a new calamitic liquid crystalline system methyl 4-(4'-(4''-(decyloxy)benzyloxy)benzylideneamino)benzoate. *Liquid Crystals*, 44(7), 1185-1193.
- Naoum, M. M., Fahmi, A. A., Abaza, A. H., & Saad, G. R. (2014). Effect of exchange of terminal substituents on the mesophase behaviour of some azo/ester compounds. *Liquid Crystals*, 41(11), 1559-1568.
- Naoum, M. M., Fahmi, A. A., Ahmed, N. H. S., & Saad, G. R. (2015a). The effect of lateral methyl substitution on the mesophase behaviour of aryl 4-alkoxyphenylazo benzoates. *Liquid Crystals*, 42(11), 1627-1637.
- Naoum, M. M., Fahmi, A. A., Alaasar, M. A., & Ahmed, N. H. S. (2011). Effect of exchange of terminal substituents on the mesophase behavior of laterally methyl substituted phenyl azo benzoates in pure and mixed systems. *Thermochimica Acta*, 525(1), 78-86.
- Naoum, M. M., Metwally, N. H., Abd eltawab, M. M., & Ahmed, H. A. (2015b). Polarity and steric effect of the lateral substituent on the mesophase behaviour of some newly prepared liquid crystals. *Liquid Crystals*, 42(10), 1351-1369.
- Nath, R. K., Sarkar, D. D., Shankar Rao, D. S., & Nandiraju, V. S. R. (2012). Influence of polar substituents on the mesomorphism of non-symmetrical achiral four-ring bent-core compounds: synthesis and characterisation. *Liquid Crystals*, 39(7), 889-902.
- Negrini, R., Fong, W.-K., Boyd, B. J., & Mezzenga, R. (2015). pH-responsive lyotropic liquid crystals and their potential therapeutic role in cancer treatment [10.1039/C4CC10274F]. *Chemical Communications*, 51(30), 6671-6674.
- Niezgoda, I., Pocięcha, D., & Galewski, Z. (2014). Monotropic or enantiotropic mesophases? Liquid-crystalline and solid state polymorphism 4-Chloro-1,3-phenylene bis-[4-(4-alkyloxyphenylazo)benzoates. *Thermochimica Acta*, 587, 59-66.

- Niori, T., Sekine, T., Watanabe, J., Furukawa, T., & Takezoe, H. (1996). Distinct ferroelectric smectic liquid crystals consisting of banana shaped achiral molecules [10.1039/JM9960601231]. *Journal of Materials Chemistry*, 6(7), 1231-1233.
- Niu, X., Luo, D., Chen, R., Wang, F., Sun, X., & Dai, H. (2016). Optical biosensor based on liquid crystal droplets for detection of cholic acid. *Optics Communications*, 381, 286-291.
- Ong, L.-K., Ha, S.-T., Yeap, G.-Y., & Lin, H.-C. (2018). Heterocyclic pyridine-based liquid crystals: synthesis and mesomorphic properties. *Liquid Crystals*, 45(11), 1574-1584.
- Patel, R. V., Panchal, J. G., Rana, V. A., & Menon, S. K. (2010). Liquid crystals based on calix[4]arene Schiff bases. *Journal of Inclusion Phenomena and Macrocyclic Chemistry*, 66(3), 285-295.
- Perju, E., Cozan, V., Timpu, D., & Bruma, M. (2017). The influence of methoxy side groups and halogen nature on the mesomorphic and optical properties of symmetrical azomethines. *Liquid Crystals*, 44(5), 798-808.
- Petsch, S., Rix, R., Reith, P., Khatri, B., Schuhladen, S., Ruh, D., Zentel, R., & Zappe, H. (2014). A thermotropic liquid crystal elastomer micro-actuator with integrated deformable micro-heater. 2014 IEEE 27th International Conference on Micro Electro Mechanical Systems (MEMS)
- Popov, N., Honaker, L. W., Popova, M., Usol'tseva, N., Mann, E. K., Jákli, A., & Popov, P. (2018). Thermotropic Liquid Crystal-Assisted Chemical and Biological Sensors. *Materials*, 11(1), 20.
- Popov, P., Honaker, L. W., Kooijman, E. E., Mann, E. K., & Jákli, A. I. (2016). A liquid crystal biosensor for specific detection of antigens. *Sensing and Bio-Sensing Research*, 8, 31-35.
- Popov, P., Mann, E. K., & Jákli, A. (2017). Thermotropic liquid crystal films for biosensors and beyond [10.1039/C7TB00809K]. *Journal of Materials Chemistry B*, 5(26), 5061-5078.
- Prakash, J., Parveen, A., Mishra, Y. K., & Kaushik, A. (2020). Nanotechnology-assisted liquid crystals-based biosensors: Towards fundamental to advanced applications. *Biosensors and Bioelectronics*, 168, 112562.
- Preusse, R. S., George, E. R., Aghvami, S. A., Otchy, T. M., & Gharbi, M. A. (2020). Hierarchical assembly of smectic liquid crystal defects at undulated interfaces [10.1039/D0SM01112F]. *Soft Matter*, 16(36), 8352-8358.

- Rathgeber, C., Schmit, H., Miró, L., Cabeza, L. F., Gutierrez, A., Ushak, S., Hiebler, S., & Hauer, A. (2015). *Analysis of supercooling of phase change materials with increased sample size – Comparison of measurements via DSC, T-History and at pilot plant scale.*
- Reinitzer, F. (1888). Beiträge zur Kenntniss des Cholesterins. *Monatshefte für Chemie und verwandte Teile anderer Wissenschaften*, 9(1), 421-441.
- Saad, G. R., Ahmed, N. H. S., Fahmi, A. A., Kaddah, M. M., & Naoum, M. M. (2019). Influence of lateral methyl and terminal substituents on the mesophase behaviour of four rings azo-ester liquid crystal compounds. *Liquid Crystals*, 46(8), 1285-1297.
- Sai, D. V., Zuhail, K. P., Sarkar, R., & Dhara, S. (2015). Structure–property correlation of bicyclohexane nematic liquid crystals. *Liquid Crystals*, 42(3), 328-333.
- Sakurai, Y., Takenaka, S., Miyake, H., Morita, H., & Ikemoto, T. (1989). Molecular structure and smectic properties. Part 1. The effect of linkages on smectic a thermal stability in three aromatic ring compounds linked by ester groups [10.1039/P29890001199]. *Journal of the Chemical Society, Perkin Transactions* 2(9), 1199-1204.
- Salamończyk, M., Vaupotič, N., Pocięcha, D., Walker, R., Storey, J. M. D., Imrie, C. T., Wang, C., Zhu, C., & Gorecka, E. (2019). Multi-level chirality in liquid crystals formed by achiral molecules [Article]. *Nature Communications*, 10(1), Article 1922.
- Sales, E. S., dos Santos, G. M., Mandle, R. J., Costa, W. C., Bechtold, I. H., Gonçalves, I. L., Eifler-Lima, V. L., & Merlo, A. A. (2020). Insight into Out-of-Layer Fluctuations in the Smectic A Stability of 3,5-Diarylisoxazole Liquid Crystals. *ChemPhysChem*, 21(13), 1408-1419.
- Sardon, S. N. F., Rahman, N. M. M. A., Karim, M. R., Zahid, N. I., & Salleh, N. M. (2021). Effects of lateral methyl and terminal substituents on thermal, mesomorphic and optical properties of azo-ester mesogens. *Journal of Molecular Structure*, 1225, 129112.
- Sastry, P. S., Pardhasaradhi, P., Srinivasu, C., Pisipati, V. G. K. M., & Datta Prasad, P. V. (2016). Synthesis, characterisation and phase transition studies in N-(4-ethoxybenzylidene)-4'-alkoxyanilines. *Liquid Crystals*, 43(5), 632-638.
- Seed, A. J., & Sampson, P. (2017). A review of self-organising 2,5- and 2,4-disubstituted 1,3-thiazole-containing materials: synthesis, mechanisms and tactics. *Liquid Crystals*, 44(12-13), 1894-1910.

- Selvarasu, C., & Kannan, P. (2015). Synthesis, characterization of azobenzene and cinnamate ester based calamitic liquid crystalline compounds and their photoresponsive properties. *Journal of Molecular Structure*, 1092, 176-186.
- Selvarasu, C., & Kannan, P. (2016). Effect of azo and ester linkages on rod shaped Schiff base liquid crystals and their photophysical investigations. *Journal of Molecular Structure*, 1125, 234-240.
- Selvarasu, C., & Kannan, P. (2017). Alkyloxy azo-cinnamate ester based thermotropic liquid crystals and their photophysical investigations. *Molecular Crystals and Liquid Crystals*, 648(1), 77-87.
- Seou, C.-K., Ha, S.-T., Lee, S.-L., Yeap, G.-Y., Lin, C.-M., Lin, H.-C., & Win, Y.-F. (2017). Synthesis and phase transition behaviours of laterally substituted liquid crystals containing methylhydroquinone: emerging of smectic C phase for higher homologues. *Phase Transitions*, 90(5), 449-464.
- Setia, S., Sidiq, S., De, J., Pani, I., & Pal, S. K. (2016). Applications of liquid crystals in biosensing and organic light-emitting devices: future aspects. *Liquid Crystals*, 43(13-15), 2009-2050.
- Sharma, V. S., Vekariya, R. H., Sharma, A. S., & Patel, R. B. (2017). Synthesis and mesomorphic properties of new chalconyl-ester based liquid crystals: The effect of tail group. *Molecular Crystals and Liquid Crystals*, 652(1), 10-22.
- Šmahel, M., Poryvai, A., Xiang, Y., Pocięcha, D., Troha, T., Novotná, V., Svoboda, J., & Kohout, M. (2020). Photosensitive bent-core nematic liquid crystals with various linking units in the side arms: Structure-properties relationships. *Journal of Molecular Liquids*, 306, 112743.
- Sperner, M., Tober, N., & Detert, H. (2019). Tris-triazolotriazines with Azobenzene Arms - Acidochromic Dyes and Discotic Liquid Crystals. *European Journal of Organic Chemistry*, 2019(29), 4688-4693.
- Spillmann, C. M., Naciri, J., Algar, W. R., Medintz, I. L., & Delehanty, J. B. (2014). Multifunctional liquid crystal nanoparticles for intracellular fluorescent imaging and drug delivery. *ACS Nano*, 8(7), 6986-6997.
- Srilekha, G., Pardhasaradhi, P., Madhav, B. T. P., Manepalli, R. K. N. R., & Rao, M. C. (2020). Design and analysis of 6CB nematic liquid crystal-based rectangular patch antenna for S-band and C-band applications. *Zeitschrift für Naturforschung A*, 75(10), 863-875.
- Srinivasa, H. T. (2019). Chiral liquid crystals: Synthesis and characterization for thermal and mesomorphic properties. *Molecular Crystals and Liquid Crystals*, 680(1), 10-19.

- Stegemeyer, H. (1989). Centenary of the discovery of liquid crystals. *Liquid Crystals*, 5(1), 5-6.
- Stephen, M. J., & Straley, J. P. (1974). Physics of liquid crystals. *Reviews of Modern Physics*, 46(4), 617-704.
- Subrao, M., Potukuchi, D. M., Sharada Ramachandra, G., Bhagavath, P., Bhat, S. G., & Maddasani, S. (2015). Novel biphenyl-substituted 1,2,4-oxadiazole ferroelectric liquid crystals: synthesis and characterization. *Beilstein Journal of Organic Chemistry*, 11, 233-241.
- Thakor, A., Dwivedi, D. J., Desai, V., Jadeja, U. H., Sharma, V. S., & Patel, R. B. (2021). Synthesis and characterization of biphenyl-based azo liquid crystals and its optical properties: effect of lateral and tail group. *Molecular Crystals and Liquid Crystals*, 1-19.
- Tiong, H., Ong, L.-K., Sivasothy, Y., Yeap, G.-Y., Lin, H.-C., Lee, S., Boey, P.-L., & Bonde, N. (2010). Mesogenic Schiff base esters with terminal chloro group: Synthesis, thermotropic properties and X-ray diffraction studies. *International journal of physical sciences*, 5.
- Trišović, N., Antanasijević, J., Tóth-Katona, T., Kohout, M., Salamonczyk, M., Sprunt, S., Jáklí, A., & Fodor-Csorba, K. (2015). Azo-containing asymmetric bent-core liquid crystals with modulated smectic phases [10.1039/C5RA09764A]. *RSC Advances*, 5(80), 64886-64891.
- Veerabhadraswamy, B. N., Rao, D. S. S., & Yelamaggad, C. V. (2018). Ferroelectric Liquid Crystals: Synthesis and Thermal Behavior of Optically Active, Three-Ring Schiff Bases and Salicylaldimines. *Chemistry – An Asian Journal*, 13(8), 1012-1023.
- Vícha, J., Novotný, J., Komorovsky, S., Straka, M., Kaupp, M., & Marek, R. (2020). Relativistic Heavy-Neighbor-Atom Effects on NMR Shifts: Concepts and Trends Across the Periodic Table. *Chemical Reviews*, 120(15), 7065-7103.
- Wang, K., Sprunt, S., & Twieg, R. J. (2019). The synthesis of [1,2,3]-triazole-based bent core liquid crystals via microwave-mediated 'Click Reaction' and their mesomorphic behaviour. *Liquid Crystals*, 46(2), 257-271.
- Wang, X., Li, Z., Zhao, H., & Chen, S. (2020). New azobenzene liquid crystal with dihydropyrazole heterocycle and photoisomerization studies. *Royal Society Open Science*, 7(7), 200474.
- Wheeler, S. E. (2013). Understanding Substituent Effects in Noncovalent Interactions Involving Aromatic Rings. *Accounts of Chemical Research*, 46(4), 1029-1038.

- Xie, P., & Zhang, R. (2005). Liquid crystal elastomers, networks and gels: advanced smart materials [10.1039/B413835J]. *Journal of Materials Chemistry*, 15(26), 2529-2550.
- Xiong, J.-F., Luo, S.-H., Huo, J.-P., Liu, J.-Y., Chen, S.-X., & Wang, Z.-Y. (2014). Design, Synthesis, and Characterization of 1,3,5-Tri(1H-benzo[d]imidazol-2-yl)benzene-Based Fluorescent Supramolecular Columnar Liquid Crystals with a Broad Mesomorphic Range. *The Journal of Organic Chemistry*, 79(17), 8366-8373.
- Xu, S., Held, I., Kempf, B., Mayr, H., Steglich, W., & Zipse, H. (2005). The DMAP-Catalyzed Acetylation of Alcohols—A Mechanistic Study (DMAP=4-(Dimethylamino)pyridine). *Chemistry – A European Journal*, 11(16), 4751-4757.
- Yang, X., Mo, L., Hu, M., Li, J., Li, J., Chen, R., & An, Z. (2018). New isothiocyanato liquid crystals containing thieno[3,2-b]thiophene central core. *Liquid Crystals*, 45(9), 1294-1302.
- Yeap, G.-Y., Ha, S.-T., Boey, P.-L., Mahmood, W. A. K., Ito, M. M., & Youhei, Y. (2006a). Synthesis and Characterization of Some New Mesogenic Schiff Base Esters N-[4-(4-n-Hexadecanoyloxybenzoyloxy)-Benzylidene]-4-Substituted Anilines. *Molecular Crystals and Liquid Crystals*, 452(1), 73-90.
- Yeap, G.-Y., Ha, S.-T., Ito, M. M., Boey, P.-L., & Mahmood, W. A. K. (2004). Synthesis, Fourier transform infrared, 1D and 2D NMR spectral studies on the conformation of two new cholesteryl 4-alkoxyphenyl-4' benzoates. *Journal of Molecular Structure*, 687(1), 57-64.
- Yeap, G.-Y., Osman, F., & Imrie, C. T. (2015). Non-symmetric dimers: effects of varying the mesogenic linking unit and terminal substituent. *Liquid Crystals*, 42(4), 543-554.
- Yeap, G. Y., Ha, S. T., Lim, P. L., Boey, P. L., Ito, M. M., Sanehisa, S., & Youhei, Y. (2006b). Synthesis, physical and mesomorphic properties of Schiff's base esters containing ortho-, meta- and para-substituents in benzylidene-4'-alkanoyloxyanilines. *Liquid Crystals*, 33(2), 205-211.
- Yuksel, F., Atilla, D., & Ahsen, V. (2007). Synthesis and characterization of liquid crystalline unsymmetrically substituted phthalocyanines. *Polyhedron*, 26(15), 4551-4556.
- Yuvaraj, A. R., Lee, W., & Kumar, S. (2021). Unconventional Liquid Crystals and Their Applications. In L. Wei & K. Sandeep (Eds.), *2 Unconventional liquid crystals: chemical aspects* (pp. 109-152). De Gruyter.

- Zakaria, M. A., Alazmi, M., Katariya, K. D., El Kilany, Y., El Ashry, E. S. H., Jaremko, M., Hagar, M., & Mohammady, S. Z. (2021). Mesomorphic Behaviour and DFT Insight of Arylidene Schiff Base Liquid Crystals and Their Pyridine Impact Investigation. *Crystals*, *11*(8), 978.
- Zhou, Y., Tsuji, T., & Chono, S. (2016). Fundamental study on the application of liquid crystals to actuator devices. *Applied Physics Letters*, *109*(1), 011902.
- Zhu, S., Chigan, J., Li, W., Yang, J., Chen, W., Zhang, W., Niu, X., Chen, X., & An, Z. (2019). The effect of intermolecular actions on the mesomorphic properties of alkenoxy biphenyl-based liquid crystals. *Journal of Molecular Liquids*, *296*, 111880.
- Zhu, X., Yin, F., Zhao, H., Chen, S., & Bian, Z. (2017). Some new azobenzene liquid crystals involving chalcone and ester linkages [10.1039/C7RA06958H]. *RSC Advances*, *7*(73), 46344-46353.
- Ali, G. Q., & Tomi, I. H. R. (2018). Synthesis and characterization of new mesogenic esters derived from 1,2,4-oxadiazole and study the effect of alkoxy chain length in their liquid crystalline properties. *Liquid Crystals*, *45*(3), 421-430.
- Goodby, J. W. (2011). The nanoscale engineering of nematic liquid crystals for displays. *Liquid Crystals*, *38*(11-12), 1363-1387.
- Ha, S. T., Lee, T. L., Lee, S. L., Yeap, G. Y., Win, Y. F., & Ong, S. T. (2012). Mesomorphic behaviour of new azomethine liquid crystals having terminal bromo substituent. *Chinese Chemical Letters*, *23*(2), 177-180.
- Kovářová, A., Kohout, M., Svoboda, J., & Novotná, V. (2014). New liquid crystal based on 2-phenylthiophene central core. *Liquid Crystals*, *41*(12), 1703-1718.
- Matharu, A. S., & Chambers-Asman, D. (2007). Structure–property investigation of 2- and 3-thienylacrylates bearing laterally fluorinated azobenzene moieties. *Liquid Crystals*, *34*(11), 1317-1336.
- Seed, A. J., & Sampson, P. (2017). A review of self-organising 2,5- and 2,4-disubstituted 1,3-thiazole-containing materials: synthesis, mechanisms and tactics. *Liquid Crystals*, *44*(12-13), 1894-1910.
- Subrao, M., Potukuchi, D. M., Sharada Ramachandra, G., Bhagavath, P., Bhat, S. G., & Maddasani, S. (2015). Novel biphenyl-substituted 1,2,4-oxadiazole ferroelectric liquid crystals: synthesis and characterization. *Beilstein Journal of Organic Chemistry*, *11*, 233-241.

- Thaker, B. T., Kanojiya, J. B., & Tandel, R. S. (2010). Effects of Different Terminal Substituents on the Mesomorphic Behavior of Some Azo-Schiff Base and Azo-Ester-Based Liquid Crystals. *Molecular Crystals and Liquid Crystals*, 528(1), 120-137.
- Tiong Ha, S., Ming Koh, T., Yeap, G. Y., Lin, H. C., Beh, J. K., Win, Y. F., & Boey, P. L. (2009). New mesogenic Schiff base esters comprising benzothiazole moiety: Synthesis and mesomorphic properties. *Chinese Chemical Letters*, 20(9), 1081-1084.
- Wang, X., Li, Z., Zhao, H., & Chen, S. (2020). New azobenzene liquid crystal with dihydropyrazole heterocycle and photoisomerization studies. *Royal Society Open Science*, 7(7), 200474.
- Yeap, G.-Y., Ha, S.-T., Boey, P.-L., Mahmood, W. A. K., Ito, M. M., & Youhei, Y. (2006). Synthesis and Characterization of Some New Mesogenic Schiff Base Esters N-[4-(4-n-Hexadecanoyloxybenzoyloxy)-Benzylidene]-4-Substituted Anilines. *Molecular Crystals and Liquid Crystals*, 452(1), 73-90.
- Zhu, X., Yin, F., Zhao, H., Chen, S., & Bian, Z. (2017). Some new azobenzene liquid crystals involving chalcone and ester linkages [10.1039/C7RA06958H]. *RSC Advances*, 7(73), 46344-46353.